# Spectral Hole-Burning Spectroscopy in Amorphous Molecular Solids and Proteins

R. Jankowiak, J. M. Hayes, and G. J. Small*

*Department of Chemistry and Ames Laboratory—USDOE, Iowa State University, Ames, Iowa 50011*

*Received December 11, 1992 (Revised Manuscript Received March 18, 1993)*

## Contents



## I. Introduction

Since the pioneering works of Kharlamov, Personov, and Bykovskaya[1] and Gorokhovskii, Kaarli, and Rebane[2] in 1974 on persistent spectral hole burning of molecular electronic transitions in crystalline and amorphous solids, the field has grown enormously, especially in the past decade. There are several reasons for this, including spectral hole burning is a powerful tool for probing the structural disorder and configurational tunneling dynamics of amorphous solids at low temperatures (indeed, glasses can be viewed as "life" that came in kicking and screaming with the cold); spectral hole burning provides an improvement in the resolution of the optical spectra of protein–chromophore (e.g., chlorophylls) complexes by 2–3 orders of magnitude; and spectral hole burning has long term potential for powerful information storage technologies. The first and third of these attributes are the subjects of a recent book.[3] The first attribute has also been the subject of a recent review in this journal.[4] The second attribute has been recently reviewed in three articles.[5-7] In addition, Volume 9, Numbers 5 and 6 of the *Journal of the Optical Society of America B* (1992) deal largely with the science and applications of hole burning and complementary techniques such as coherent time domain spectroscopies. Nevertheless, another review at this time would appear to be justified in view of the many developments that have occurred very recently.

Our review provides a rather broad coverage of the applications of spectral hole burning to fundamental and applied problems as the "Contents" indicates. In each section we have attempted to be reasonably complete in our referencing, especially with regard to seminal works, the most recent developments and earlier review articles of which there are many. Each section is more or less self-contained except for VI.1 on reaction center and antenna protein complexes which relies on the theory of hole profiles developed in section II.2 and assumes some exposure to the light-driven, physicochemical aspects of energy- and electron-transport in photosynthetic units. Sections III and V deal, respectively, with applications (e.g., information storage) and the utilization of hole burning with external fields, important and growing areas to which our group at Iowa State University has not contributed. Thus, these sections are briefer and perhaps more introductory than would be otherwise. Nevertheless, the reader is directed to the literature that provides more in depth treatments.

Sections II, IV, and VI on "Hole Profiles and Hole-Burning Mechanisms", "Manifestations of Two-Level System Relaxation in Amorphous Solids at Low Temperature", and "Applications of Spectral Hole Burning to the Photophysics of Biological Systems" cover problems and phenomena we have studied for several years now. Section II begins with an introduction to the underlying physics of hole burning and essential terminology such as site inhomogeneous broadening ($\Gamma_I$), the zero-phonon and phonon sideband holes, linear electron-phonon coupling, and vibronic satellite hole burning. It is the last of these that allows one to perform high-resolution molecular electronic spectroscopy in amorphous solids where $\Gamma_I$ is several hundred reciprocal centimeters. A simple but accurate theory for the overall hole profile is presented and illustrated with some model calculations which show that, even for strong electron-phonon coupling, the burn frequency

0009-2665/93/0793-1471$12.00/0 

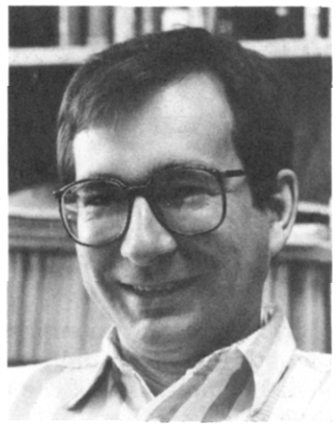

Ryszard Jankowiak is a scientist at Ames Laboratory—USDOE. He received his Ph.D. in physics from the Technical University in Gdańsk (Poland) in 1981 and was a research associate and visiting scientist at the Camerino University (Italy) (1981) and at Philipps University in Marburg (Germany) from 1981 to 1985. His research interests include molecular electronic spectroscopy, laser bioanalytical spectroscopy, chemical carcinogenesis and carcinogen metabolism, energy and electron transfer in photosynthesis, and structural disorder and tunneling in amorphous solids at very low temperatures and/or high pressures.

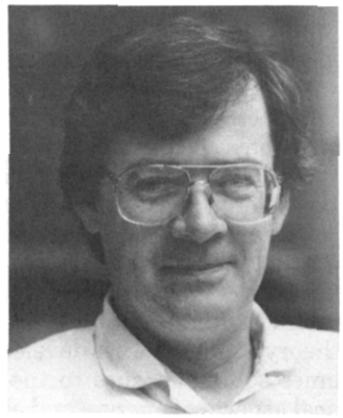

John M. Hayes is a chemist at Ames Laboratory—USDOE. He received his Ph.D. degree in physical chemistry from Boston University in 1974. After a 2-year stint as a post-doctoral fellow at the Ames Laboratory, he accepted a staff position there in 1976. His research interests include molecular electronic spectroscopy, laser analytical spectrometry, spectroscopic investigations of biochemical phenomena, including photosynthesis and chemical carcinogenesis, and the use of hole-burning spectroscopy to probe disorder and tunneling phenomena in amorphous solids.

($\omega_B$) dependence of the hole profile leads to a determination of $\Gamma_I$ and the coupling parameters. Such information is important for understanding energy- and electron-transfer dynamics in photosynthetic units and other amorphous solids. The above theory is applied to the special pair (dimer) or primary electron-donor absorption band of a bacterial reaction center in section VI.1. In section II.3 the original and current mechanisms for nonphotochemical hole burning (NPHB) in amorphous solids are discussed. Although the latter still invokes phonon-assisted tunneling of impurity–glass two-level systems (TLS) or asymmetric intermolecular double-well potentials, data are discussed that prove that the original standard tunnel model for NPHB is inadequate and indicate that the mechanism involves a hierarchy of constrained relaxation events.

The impurity–glass two-level system is often referred to as extrinsic, $TLS_{ext}$. The intrinsic bistable configurations of the glass itself are denoted by $TLS_{int}$. The standard $TLS_{int}$ tunnel model assumes that the disorder-induced bistable configurations of the glass can be approximated by a static distribution of TLS each defined, in part, by their asymmetry parameter $\Delta$ and a tunnel parameter $\lambda$ values. The tunnel state splitting is $E = [\Delta^2 + W^2]^{1/2}$ where $W = \omega_0 \exp(-\lambda)$ is the tunneling frequency. From the model one obtains a density, $\rho(E)$, of low-energy excitations not available to a perfect crystal and phonon-assisted relaxation between the tunnel states has been used to explain the anomalous magnitudes and temperature and/or time dependences of many properties at very low temperatures, e.g., specific heat, thermal conductivity, pure dephasing, and spectral diffusion of optical transitions. The standard tunnel model, as applied to $TLS_{ext}$, has been used to account for the dispersive kinetics of nonphotochemical hole growth and spontaneous hole filling. These topics are discussed in section IV where we emphasize the importance of using nonphenomenological TLS distribution functions for ensemble averaging in order to arrive at a consistent picture of all properties or, put another way, to stringently test the standard model. New results are presented on the interpretations of the temperature power law for pure dephasing and the time dependence of spectral diffusion.

As mentioned, spectral hole-burning spectroscopies (nonphotochemical, photochemical, and population bottleneck) have been applied to many photosynthetic antenna and reaction center protein–cofactor (e.g., chlorophyll) complexes and, we add, with very considerable success. The systems studied and what has been learned are reviewed in section VI.1. Attention is focused on two problems: the question of dispersive kinetics for the primary charge separation process arising from the glasslike disorder of proteins; and how one can use NPHB to probe exciton level structure and ultrafast interexciton level relaxation in antenna protein complexes possessing a unit cell that contains several strongly interacting chlorophylls. In the last section, VI.2, we consider an application of hole burning which

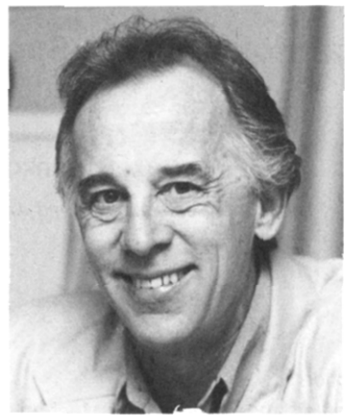

Gerald J. Small is a Distinguished Professor of Chemistry at Iowa State University and senior chemist at Ames Laboratory—USDOE. He received his Ph.D. in physical chemistry from the University of Pennsylvania in 1967. Following a 2-year appointment as a research fellow at the Australian National University, he joined the faculty of ISU in 1969. His research interests include molecular electronic spectroscopy, linear and nonlinear laser spectroscopies, energy and electron transfer in photosynthesis, carcinogen metabolism and cellular macromolecular damage, and structural disorder and tunneling in amorphous solids.

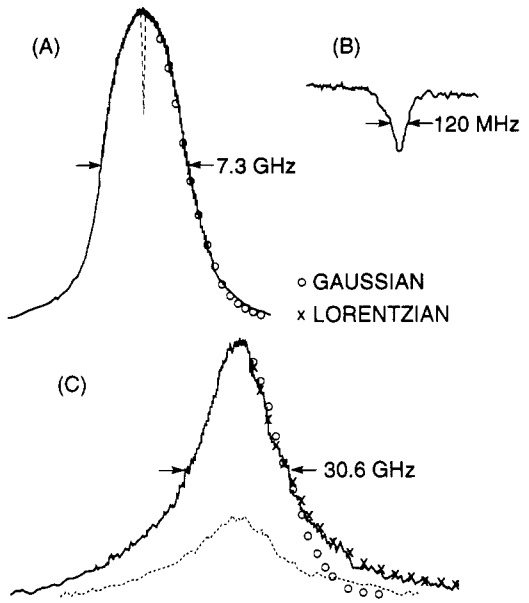


**Figure 1.** Absorption (photoexcitation) spectrum of (A) the origin and (C) a vibronic transition of dimethyl-*s*-tetrazine in durene at 2 K. The dotted spectra were obtained after 1-s laser burning in the origin and 5-min burning in the vibronic line (at the peak of the line). (B) High-resolution scan of the hole in the origin band. Reprinted from ref 8. Copyright 1976 American Physical Society.

is bound to receive much attention in the neat future; namely, configurational relaxation processes of proteins over a broad low-temperature regime.

## *II. Hole Profiles and Hole-Burning Mechanisms*

### 1. Inhomogeneous Broadening and Hole Profiles

Observation of spectral holes is dependent on three requirements: (1) a mechanism by which (electronic) excitation of a chromophore can alter the energy of the excitation; (2) a method of probing the original absorption during the persistence time of the energy alteration; and (3) the presence of an inhomogeneous broadening mechanism. In sections II.3 and 4, we will discuss requirements 1 and 2 in detail. In this section we will examine inhomogeneous broadening, its consequences for hole formation, and its influence on hole shape.

Although we will primarily be concerned with disordered systems, an example of hole burning in a crystalline system illustrates the necessity of inhomogeneous broadening for hole formation. This is shown in Figure 1 taken from an early hole-burning result of deVries and Wiersma.[8] Figure 1A shows the origin absorption band of dimethyl-*s*-tetrazine (DMST) in a durene host crystal obtained by photoexcitation at 2 K. This band is clearly Gaussian with a full width at half maximum (FWHM) of 7.3 GHz. In contrast, the lowest energy vibronic band shown in Figure 1C is a Lorentzian with a FWHM of 30.6 GHz. The line shapes suggest that while the origin is inhomogeneously broadened, the vibronic band is predominantly homogeneously broadened. DMST is photochemically unstable (hole-burning requirement 1) although at low-excitation intensity the absorption can be obtained by photoexcitation (requirement 2). Hence hole burning into the two bands provides a dramatic demonstration

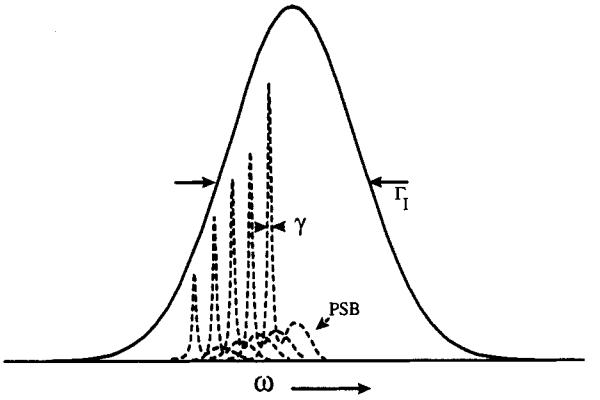


**Figure 2.** Schematic representation of homogeneous ($\gamma$) and inhomogeneous ($\Gamma_I$) broadening. Profiles of the zero-phonon lines (ZPL) and their associated sidebands (PSB) for specific sites at different frequencies have been enlarged compared to the inhomogeneous line to provide more detail. Reprinted from ref 7. Copyright 1992 Kluwer Academic Publishers.

of the necessity of inhomogeneous broadening for hole burning. As shown in Figure 1, part A (dotted line) and part B, narrow line excitation into the origin band produces a sharp hole with a FWHM of 120 MHz. (A subsequent measurement with a frequency- and intensity-stabilized source showed the homogeneous width as determined from the hole width to be 24 ± 5 MHz.[9]) The lifetime of the DMST excited state was determined by fluorescence to be 6 ns corresponding to a width of 25 MHz. Thus the 7.3 GHz absorption width is due to site inhomogeneous broadening; i.e., even in this crystalline host there is a distribution of environments which the chromophore can occupy. The dotted curve of Figure 1C shows that attempts to burn into the homogeneously broadened vibronic band produce only an overall decrease in band intensity with the band shape and bandwidth being preserved. Assuming that there is an inhomogeneous contribution to the vibronic band equal to 7.3 GHz, inhomogeneous broadening of the origin would give a true homogeneous width for the vibronic band of 28.8 GHz which corresponds to a lifetime of 5.5 ps. This lifetime was attributed to vibrational relaxation.

Although the DMST in durene system provides a dramatic example of the necessity of inhomogeneous broadening for hole burning, the extent of such broadening in crystalline hosts is minuscule ($\sim$1 cm$^{-1}$) compared to the amorphous (glassy) matrices in which much hole burning is done. Glassy matrices have been of interest to spectroscopists because numerous organic solvents and solvent mixtures which form glasses have been discovered, thus providing optically clear matrices for low-temperature spectroscopy of a wide variety of compounds.[10] The large degree of inhomogeneous broadening ($\sim$100–500 cm$^{-1}$), however, precluded obtaining the wealth of information available with even moderate spectroscopic resolution. Hole burning and related energy-selective spectroscopies reduce or eliminate the effects of inhomogeneous broadening while retaining the advantages of utilizing glassy matrices. Let us turn now to a detailed description of line shapes in glassy media. We present first a qualitative picture and then a mathematical description of the shapes.

Figure 2 depicts an inhomogeneously broadened origin or vibronic absorption band at low temperature. The sharp dashed bands are the zero-phonon lines

(ZPL) of the "guest" molecule occupying inequivalent sites. A zero-phonon transition is one for which no net change in the number of phonons accompanies the electronic transition. Building to higher energy on each ZPL is a broad phonon (lattice vibrational) wing or phonon sideband (PSB). Each single site ZPL carries a homogeneous line width, $\gamma$, which is determined by the total dephasing time $T_2$ of the optical transition (cf. section IV.3 for the interesting complications introduced by spectral diffusion):

$$\frac{1}{T_2} = \frac{1}{2T_1} + \frac{1}{T_2'} \quad (1)$$

where $T_1$ is the excited state lifetime and $T_2'$ is the pure dephasing time. The latter is best understood in terms of the density matrix formulation of spectroscopic transitions.[11,12] For now it suffices to say that $T_2'$ is due to the modulation of the single site transition frequency which results from the interaction of the excited state with the bath phonons (and other low-energy excitations in glasses[13]). This interaction does not lead to electronic relaxation of the excited state but rather to a decay of the phase coherence of the superposition state initially created by the photon. $\gamma = (\pi T_2 c)^{-1}$ (in $cm^{-1}$) where $c$ is the speed of light (in cm $s^{-1}$).

$\gamma$ determines the ultimate spectral resolution attainable by line narrowing techniques. A key point is that $T_2'$ is strongly temperature dependent. Pure dephasing theories are now well developed (see section IV.2), and photon echo and spectral hole burning (see same section) have been used to study the temperature dependence of $T_2'$ in a wide variety of glassy systems. At room temperature, the contribution to $\gamma$ from $T_2'$ is $\approx kT$, i.e., $\approx$200 $cm^{-1}$, which is comparable to $\Gamma_I$ for glasses. Line-narrowing spectroscopies cannot eliminate $\gamma$, which means that low temperatures are required to minimize the number of thermally populated low-frequency phonon and other excitations responsible for $\gamma$. For glass hosts it is now firmly established that the contribution to $\gamma$ from pure dephasing and/or spectral diffusion is $\leq$0.1 $cm^{-1}$ at 4.2 K, which is negligible relative to $\gamma$ = 5 $cm^{-1}$ from $T_1$ = 1 ps.

In the absorption spectrum shown in Figure 3A the burn frequency excites an isochromat in the (0,0) or origin band. However, the sites that contribute to the origin isochromat also contribute to the $(1_\alpha,0)$ and $(1_\beta,0)$ vibronic bands. Thus, a ZPH burnt at $\omega_L$ can be accompanied by higher energy vibronic satellite holes. Because the ZPL is accompanied by a PSB, the ZPH is accompanied by phonon sideband holes (PSBH). The PSBH to higher energy of the ZPH is readily understood and is referred to as the real-PSBH. The pseudo-PSBH is due to sites whose ZPL frequencies lie to lower energy of $\omega_L$ and which absorb the laser light by virtue of the PSB. The phonons excited rapidly relax to the zero-point level after which hole burning ensues.

In the same manner that the pseudo-PSBH can be produced, pseudo-vibronic hole structure can be generated. In Figure 3B the burn frequency ($\omega_L$) excites isochromats belonging to vibrations $\alpha$ and $\beta$. Since the time constant for hole burning is long relative to the vibrational relaxation time, the isochromats relax to their respective zero-point positions in the (0,0) band prior to hole burning. Two ZPH (at $(0,0)_A$ and $(0,0)_B$) are produced, which, in turn, lead to a ZPH at $\omega_L$. The relative intensities of the former two and the latter depend, in part, on the Franck–Condon factors for vibrations $\alpha$ and $\beta$.

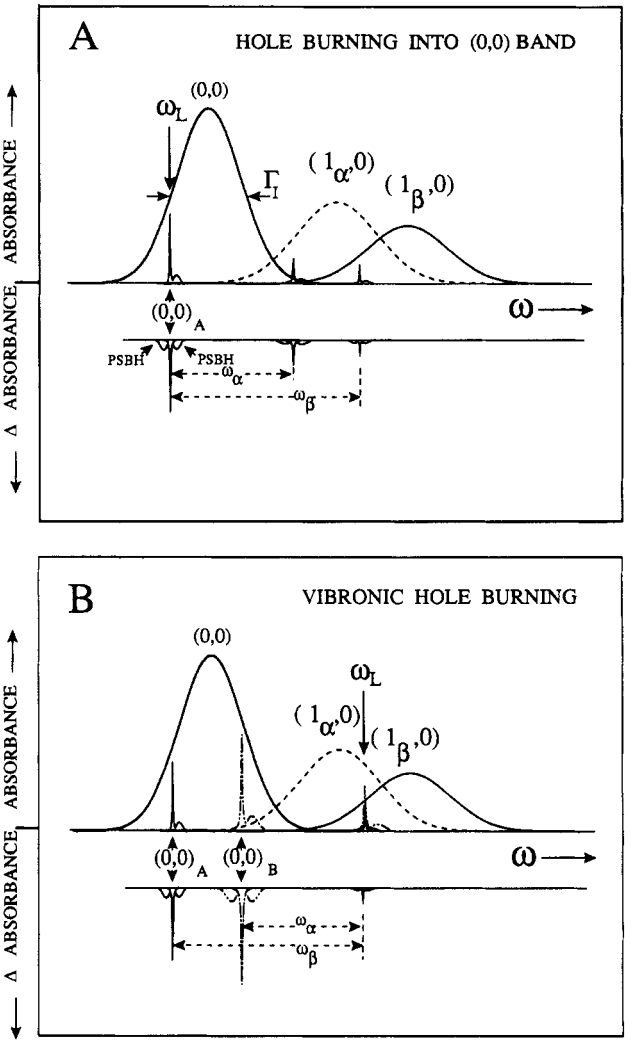


**Figure 3.** Schematic of hole burning (selective photobleaching) into origin band (A) and into vibronic region (B). Reprinted from ref 7. Copyright 1992 Kluwer Academic Publishers.

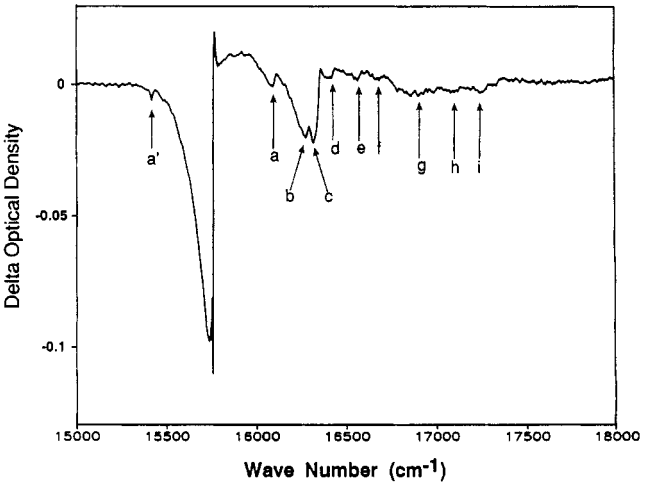


**Figure 4.** A hole spectrum for cresyl violet in poly(vinyl alcohol) burned at 15 837 $cm^{-1}$; $T_B$ = 1.6 K, $t_B$ = 20 min, $I_B$ = 30 mW/$cm^2$. Real vibronic satellite holes are labeled a–i. A weak pseudo-vibronic satellite hole (a') can be seen at $\omega_B$ −340 $cm^{-1}$. Reprinted from ref 152. Copyright 1992 Optical Society of America.

An example of these effects is shown in Figure 4. The figure shows the hole spectrum of a poly(vinyl alcohol) film doped with the dye, cresyl violet. Evident in the figures is the ZPH at $\omega_B$ (laser burn frequency) = 15 837 cm$^{-1}$, a broad pseudo-PSBH to lower energy, real vibronic satellite holes (a–i) and a weak pseudo-vibronic hole (a'). This spectrum is produced by nonphotochemical hole burning (see section II.3) as is evidenced by an antihole (increased absorption) at energies just above $\omega_B$.

## 2. Theory of Spectral Hole Profiles

The problem of understanding the interplay between the ZPH and PSBH and how the overall hole profile depends on the location of $\omega_B$ (laser burn frequency) within an absorption band whose width is contributed to by site inhomogeneity has been considered in considerable detail.[14-17] A summary of the theory developed in our laboratory is presented here.

The absorption profile of a single site with a ZPL frequency of $\nu$ can be written as

$$L(\Omega - \nu) = \prod_{j=1}^{N}\left[\sum_{r_j=0}^{\infty}\frac{e^{-S_j}S_j^{r_j}}{r_j!}\right]\sum_{r=0}^{\infty}\frac{e^{-S}S^r}{r!}\ell(\Omega - \nu - r\omega_m - \sum_{j=1}^{N} r_j\omega_j) \quad (2)$$

where $j$ runs over the discrete pseudolocalized or localized phonons[18] and, if necessary, the intramolecular modes. $S_j$ and $\omega_j$ are the Huang–Rhys factor, which is a measure of the electron–phonon coupling strength, and frequency for the $j$th mode. The sum over $r$ is isolated because it is meant to represent the contribution from the essentially continuous distribution of low frequency "phonons" of the disordered solid. The function $\ell$ is the line-shape function. For $r_j = 0$ and $r = 0$, then $L$ describes the ZPL associated with the total zero-point level of the excited electronic state. The ZPL is a Lorentzian with a homogeneous width we denote as $\gamma$. The sequential nonzero values of $r = 1$, 2, 3, etc. correspond to the one-, two-, etc. phonon profiles obtained by convolving the one-phonon profile with itself $r$ times. The width of the one-phonon profile centered at $\omega_m$ (relative to the ZPL) is defined as $\Gamma$. Guided by experimental data from the one-phonon profile in organic crystals, we have previously used Gaussian and Lorentzian line shapes for the low- and high-energy sides of the one-phonon profile rather than a symmetric and unphysical Gaussian profile which has been recently utilized by Middendorf et al.[19] Within the harmonic approximation, the phonon sidebands that build on the ZPLs associated with total zero-point and the discrete modes are identical.

Figures 5A and 6A show single-site absorption calculated with eq 2 for a single low-frequency mode and for the case of two low-frequency modes. In Figure 5A is a single-site absorption for $S = 1.8$, $\omega_m = 30$ cm$^{-1}$, $\Gamma = 43$ cm$^{-1}$, and $\gamma = 6$ cm$^{-1}$. The centroid of the PSB is, as expected, displaced to higher energy of the ZPL by $\sim S\omega_m$. The ratio of the integrated intensity of the ZPL to that of the entire absorption spectrum is exp ($-S$), which is a consequence of the fact that the sum over all the Franck–Condon factors in eq 2 equals unity. The single-mode case simulates the situation in which only coupling to phonon modes has an influence on the hole shape, i.e., Franck–Condon factors for low-frequency intramolecular vibrations are small. The two-mode calculation shown in Figure 6A is relevant when this is not so. This figure shows simulated spectra for the case where both the matrix phonons and a localized intermolecular mode couple linearly to the electronic transition. The frequency and Huang–Rhys factor of the latter are designated as $\omega_{sp}$ and $S_{sp}$ so that the total optical reorganization energy is $\sim S\omega_m + S_{sp}\omega_{sp}$. For the calculations we set $S_{sp} = 1.5$ and $\omega_{sp} = 125$ cm$^{-1}$, with the values of $\Gamma_I$ and the linear electron–phonon coupling parameters as given earlier. In addition, $\gamma$ for the one-quantum level of $\omega_{sp}(\omega_{sp}')$ was set equal to 50 cm$^{-1}$. The single-site absorption spectrum is shown in Figure 6A.

To obtain the absorption spectrum, the single-site profile is convolved with a Gaussian zero-phonon site excitation distribution function centered at $\nu_m$ with a FWHM of $\Gamma_I$:

$$A_0 = \int d\nu\, N_0(\nu - \nu_m)L(\Omega - \nu) \quad (3)$$

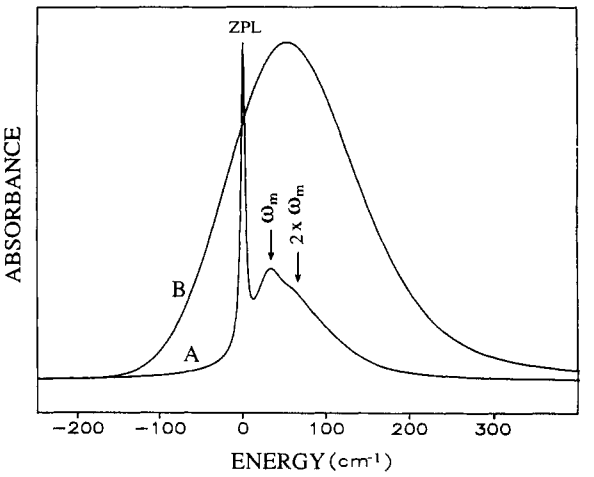


**Figure 5.** (A) Single-site absorption profile calculated according to eq 2 with $\omega_m = 30$ cm$^{-1}$, $S = 1.8$, $\gamma = 6$ cm$^{-1}$, and $\Gamma = 43$ cm$^{-1}$. ZPL = zero-phonon line. (B) Absorption profile calculated according to eq 3 with parameters of $A$ and $\Gamma_I = 130$ cm$^{-1}$. Reprinted from ref 7. Copyright 1992 Kluwer Academic Publishers.

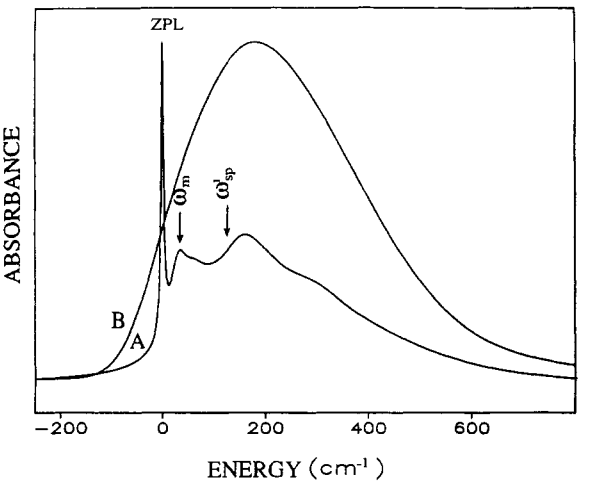


**Figure 6.** (A) Single-site absorption profile including coupling to the marker mode. Parameters as in Figure 5A with $S_{sp} = 1.5$ and $\omega_{sp} = 125$ cm$^{-1}$. $\omega_{sp}^1$ locates the position of the first overtone of the marker mode displaced 125 cm$^{-1}$ from the ZPL. (B) Absorption profile, including the marker mode, calculated as in Figure 5B. Reprinted from ref 7. Copyright 1992 Kluwer Academic Publishers.

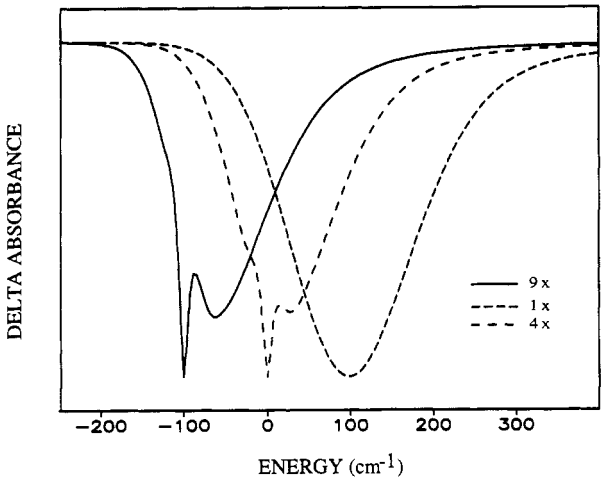


**Figure 7.** Three constant fluence hole-burned spectra calculated from eqs 4 and 3 with parameters of Figure 5. Holes burned (from left to right) −100, 0, and 200 $cm^{-1}$ relative to the site distribution function maximum, $\nu_m$. Inset refers to relative hole depths (i.e. the −100-$cm^{-1}$ burn is 9 times less intense than the 0-$cm^{-1}$ burn). Reprinted from ref 7. Copyright 1992 Kluwer Academic Publishers.

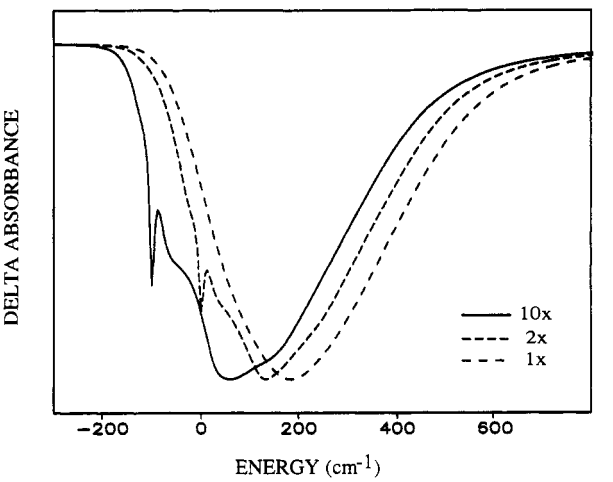


**Figure 8.** Three constant fluence hole-burned spectra calculated with the parameters of Figure 6. Reprinted from ref 7. Copyright 1992 Kluwer Academic Publishers.

where $N_0(\nu - \nu_m)/N$ is the probability of finding a site with a zero-phonon transition frequency equal to $\nu$. Figures 5B and 6B show the absorption spectra calculated with eq 3 for $\Gamma_I = 130$ $cm^{-1}$ and the same values for the other parameters used for Figure 5A and 6A. The fact that the calculated spectrum is not a symmetric Gaussian is due to the inclusion of the linear electron–phonon coupling. If a narrow band laser (i.e., laser line width $< \gamma$) is tuned to $\omega_B$ (the burn frequency) with an intensity $I$ for a time $\tau$, the number of sites that remain at frequency $\nu$ is given by $N_\tau(\nu - \nu_m) = N_0(\nu - \nu_m)$ exp $-[\sigma I \phi \tau L(\omega_B - \nu)]$, where $\sigma$ is the absorption cross section and $\phi$ is the hole-burning quantum yield. The absorption spectrum after burning is then

$$A_\tau = \int d\nu\, N_0(\nu - \nu_m)\, L(\Omega - \nu) \exp -[\sigma I \phi \tau L(\omega_B - \nu)] \quad (4)$$

The expression is valid for photochemical hole burning (PHB) and population bottleneck hole burning, but not nonphotochemical hole burning where the contribution to $A_\tau$ from the antihole must be taken into account. The hole-burned spectrum is defined as $A_\tau - A_0$.

Model calculations performed with eq 4 are shown in Figures 7 and 8 (for the parameter values used for Figures 5 and 6, respectively) for $\omega_B = \nu_m$ (center of the SDF distribution), $\omega_B = \nu_m + 200$ $cm^{-1}$ and $\omega_B = \nu_m - 100$ $cm^{-1}$ (constant fluence). As $\omega_B$ is tuned from lower to higher energy, two characteristics are evident. Firstly, the spectrum becomes much less structured. In fact the highest energy burn closely resembles the absorption spectrum while the lowest energy spectrum resembles the single site absorption spectrum. This is because as the burn frequency increases the probability of exciting multiphonon transitions increases. Secondly, the centroid of the hole shifts with burn frequency. This shift is approximately 150 $cm^{-1}$ and is directly related to the ratio of the total homogeneous broadening ($\Gamma_H$) to $\Gamma_I$.[16] As this ratio increases, it is observed that the shifting becomes less pronounced.

Comparison of the holes in Figure 8 for the two mode calculation with those of Figure 7 (single mode) reveals that the shifting of the centroid of the holes in Figure 8 ($\sim$70 $cm^{-1}$) has decreased. This is because the homogeneous broadening from electron–phonon coupling has increased, changing the $\Gamma_H$ to $\Gamma_I$ ratio (about 4.5 times greater than in the single mode case).

## 3. Hole-Burning Mechanisms

Implicit in the preceding discussion of hole shapes was the assumption that holes are formed due to loss of absorbers, i.e. that no new absorption results which interferes with the holes as described e.g. by eq 4. The degree to which this assumption is valid depends upon the mechanism of hole formation. In this section hole-burning mechanisms will be discussed, with particular attention to the influence of the mechanism on the observed hole shape. Although considerable overlap between them exists, three basic hole-burning mechanisms have been described. These are generally referred to as photochemical hole burning (PHB), nonphotochemical hole burning (NPHB), and population bottleneck hole burning.

PHB describes hole burning which results from a reaction initiated in an excited state of the chromophore. If the absorption spectra of the reaction products are well removed from $\omega_B$, then the hole shapes described previously will result with no spectral interference from product absorption. However, for photochemical reactions such as the much-studied inner proton tautomerization[20–24] of porphyrins, it has been shown[25] that in amorphous hosts the product absorption is distributed over a large range of frequency space including the vicinity of $\omega_B$. In such a case, the product absorption will overlap with the hole spectrum, causing distortion of the hole shape.

The term nonphotochemical hole burning was used originally[26,27] to denote a hole-burning process in which the chromophore is photochemically stable. NPHB occurs primarily in amorphous (glassy) matrices due to a rearrangement of the host environment about the chromophore, triggered by the electron–$TLS_{ext}$ coupling. The efficacy of NPHB in glasses stems from their intrinsic structural disorder which allows for the production of a probe–glass configuration, following completion of the ground to excited state and back to ground state cycle, which is different from and more or

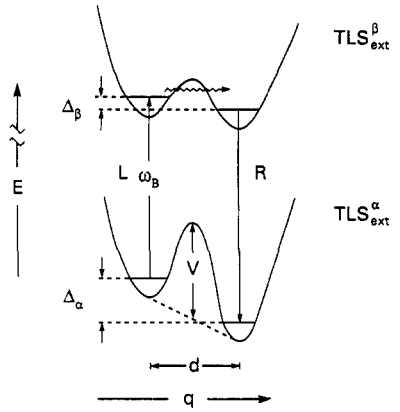


**Figure 9.** Potential energy diagrams for a TLS coupled to an impurity in its ground state ($\alpha$) and excited electronic state ($\beta$). $\Delta$ is the asymmetry parameter; $V$, the barrier height; and $q$, the intermolecular coordinate. $\omega_B$ is the laser frequency. Reprinted from ref 152. Copyright 1992 Optical Society of America.

less kinetically inaccessible to the preexcitation (preburn) configuration. Quantum yields for NPHB are generally low with the highest average value observed being $5 \times 10^{-3}$ for oxazine 720 in poly(vinyl alcohol).[28] (Structural disorder leads to dispersive kinetics, see section IV.4.) When measured against the $S_1$-state lifetime of oxazine 720, the average value of the NPHB rate constant is $1.9 \times 10^6$ s$^{-1}$. In sharp contrast, pure dephasing occurs with a rate that is about $10^{10}$ s$^{-1}$ at $\sim$4 K. This indicates that the configurational relaxation processes leading to dephasing and hole burning are distinct.[29,30] It is generally held that the "bistable" configurations or TLS responsible for NPHB are introduced by the probe, i.e. are extrinsic (ext), while those largely responsible for dephasing at sufficiently low temperatures are intrinsic (int) to the glass.

The standard two-level system (TLS) tunnel model has been extensively used for the interpretation of the anomalous thermal and acoustic properties of glasses at very low temperatures ($\lesssim$1 K),[31-33] the pure dephasing and spectral diffusion of optical transitions (see sections IV.2 and 3), the dispersive kinetics of NPHB (see section IV.4), and spontaneous hole filling (see section IV.5). In this model the tunneling configurations are approximated by a distribution of asymmetric intermolecular double-well potentials ($TLS_{int}$ or $TLS_{ext}$ depending on the problem at hand) with varying barrier height and asymmetry. The distribution is assumed to be temperature independent (static) and connectivity between TLS is neglected. Furthermore, it is assumed that both $TLS_{ext}$ and $TLS_{int}$ can be characterized by a single coordinate, $q_{ext}$ and $q_{int}$. When used with sufficiently accurate distribution functions (see section IV.1), the standard model can account for the temperature dependences of thermal properties and pure dephasing and the dispersive kinetics of NPHB and SPHF. Thus, certain types of measurements appear to be incapable of taking us beyond the standard model, which is an obvious oversimplification.

The standard $TLS_{ext}$ model for NPHB proposed by Small[34] and by Hayes and Small[27] is illustrated in Figure 9. The superscripts $\alpha$ and $\beta$ label the $TLS_{ext}$ for the ground and excited electronic state of the probe. In the figure, excitation of the zero-phonon transition is pictured as occurring on the left (L) with the critical L $\rightarrow$ R relaxation taking place in the excited electronic state ($\beta$). Note that the transition frequency of the absorber in the postburn configuration is higher than for the preburn configuration. The distribution of probe sites conforming to the energy-excitation scheme of Figure 9 would lead to a blue-shifted antihole. If instead, excitation corresponded to the R side, the antihole would be red-shifted. There are six more energy–excitation schemes including two that are obtained from Figure 9 with $\Delta_\alpha < \Delta_\beta$ and the relative energies of the R and L minima of $\alpha$ and $\beta$ still correlated. The remaining four correspond to the uncorrelated case. Of the eight schemes, four yield a blue-shifted antihole and four yield a red-shifted antihole. According to the mechanism of Hayes and Small, hole burning occurs at very low temperatures by phonon-assisted tunneling in state $\beta$ (the persistence of the hole being a consequence, for example, of a higher $TLS_{ext}$ barrier for state $\alpha$). In the $T_B \rightarrow 0$ K limit, hole burning must occur by phonon emission. Of the four schemes that conform to this scenario, only one corresponds to a blue-shifted antihole (see Figure 9). That is, the antihole should be predominantly red-shifted in the low-temperature limit provided the four schemes are equally probable. One further point is that one would expect to be able to burn only 50% of the ZPL (zero-phonon lines) at $\omega_B$ in the low-temperature limit provided all eight schemes are equally probable. In fact, a lesser degree of burning might be anticipated since equilibration between the tunnel states of $TLS^{\alpha}_{ext}$, which is rapid relative to the time scale of the experiments (seconds), could exist for a subset of the $TLS_{ext}$ at the burn temperature $T_B$.[35]

It was recently demonstrated for oxazine 720 in polyvinyl alcohol films and glycerol glasses, however, that essentially 100% of the ZPL could be burned for $1.6 \leq T_B \leq 7.0$ K (the range studied) and, furthermore, that the antihole of NPHB lies predominantly to the blue.[28] The same observations have been made for chlorophyll *a* in the light-harvesting complex of photosystem I.[36] The $S_1$ states of these probes are $\pi\pi^*$ and it has been noted that[37] the antihole from NPHB lies predominantly to the blue for all other $S_1(\pi\pi^*)$ states which have been studied, including those of tetracene in 2-methyltetrahydrofuran,[38] resorufin in poly(methyl methacrylate),[39] and perylene in poly(vinylbutyral), polymethane, and poly(vinyl chloride).[40] (To the best of our knowledge, NPHB has not been reported for an $^1n\pi^*$ state of any molecule.) The above two observations cannot be reconciled in terms of the standard $TLS_{ext}$ model of Hayes and Small[27] or that of Bogner and Schwarz[40] who proposed that NPHB is the result of barrier hopping in $TLS^{\alpha}_{ext}$ triggered by a nonequilibrium distribution of phonons localized at the probe following $S_1 \rightarrow S_0$ electronic relaxation. In light of these results, the early thermal annealing and burn-temperature-dependent data for tetracene in an ethanol/methanol glass[35] can be taken as evidence that the standard $TLS_{ext}$ model for NPHB is too simplistic.

The same results together with burn-temperature-dependent hole spectra (encompassing the zero-phonon hole (ZPH), phonon sideband holes (PSBH), and antihole) for cresyl violet (CV) in PVOH led recently to a new NPHB mechanism.[37] Like the aforementioned systems, CV/PVOH exhibits a broad and tailing blue-

shifted antihole and, furthermore, one that shifted further to the blue as $T_B$ was increased from 1.6 to 15 K. The change in shape of the antihole with $T_B$ showed that a substantial subset of the sites which yield stable (persistent) antihole sites when burned at 1.6 K do not yield the same stable antihole sites at higher burn temperatures. The data available on the linear electron–phonon coupling indicated that close to 100% of the ZPL could be burned at temperatures between 1.6 and 15 K. (One expects that at a sufficiently high burn temperature this would not be possible due to rapid spontaneous hole filling in the ground state.) The above mechanism retains the notion that at a given temperature there is a more or less well-defined $TLS_{ext}$ coordinate, $q_{ext}$. (From deuteration studies of resorufin in ethanol[29,41] and oxazine 720 in glycerol and PVOH[28] it is known that, at $T_B \approx 1.5$ K, $q_{ext}$ involves a large amplitude of motion of the hydroxyl proton of the host.) It was proposed that persistent NPHB occurs as a result of an outside-in hierarchy of dynamical events, which are triggered by electronic excitation, and result in an increase in the free volume of the probe for the postburn configuration. The free volume increase would explain the blue-shifted antihole since $^1\pi\pi^*$ states typically undergo a red-shift in going from the gas to the condensed phase. The free volume increase for the probe in its inner shell of host molecules was proposed to occur following relatively fast configurational relaxation processes in the outer shell which lead to a reduction in the excess free volume of the outer shell. With reference to Figure 9, the $TLS^{\delta}_{ext}$ shown, which leads to L → R relaxation by phonon emission (operative at 0 K), is viewed in the model as having evolved on a relatively long time scale (if it is not preformed).

Thus far it has been assumed that regardless of mechanism (i.e. photochemical or nonphotochemical) holes are persistent. The term "persistent" means that as long as the sample temperature is held at $T_B$, the burn temperature, the hole profile does not change. Exact retention of hole profiles is seldom observed, particularly in disordered media. Both spontaneous hole filling and broadening of the ZPH following termination of the burn (spectral diffusion) appear to be general phenomena. Both will be discussed in detail in section IV. In this section transient holes, i.e. holes with lifetimes $\sim 10^{-4}$–$10^{-2}$ s are discussed. Two transient hole-burning mechanisms are described: population bottleneck holes and reversible photochemical holes.

Population bottleneck hole burning is akin to the original solid-state hole burning reported by Szabo[42] in which a weak probe beam monitors the ground-state depletion induced by a strong burning beam. That experiment (on ruby) involved only two states: the ground state and the excited state. More generally, population bottleneck hole burning utilizes a third, longer-lived level to store the population depleted from the ground state. The technique was first described for $Pr^{3+}$ in a $LaF_3$ crystal in which nuclear hyperfine levels provided the bottleneck state.[43] That experiment, however, was also done utilizing two beams: a strong saturating beam and a weak probe. Both holes and antiholes were observed. A single beam technique taking advantage of the temporal resolution afforded by the bottleneck lifetime was first described for zinc porphine in *n*-octane.[44] In this system, the long-lived triplet level is used as a population reservoir to observe a hole in the $S_1 \leftarrow S_0$ transition. As expected the hole lifetime was shown to be the same as the triplet lifetime.

Transient photochemical hole burning differs from bottleneck hole burning only in so far as that, in the former case, the bottleneck state is an electronic state of the molecule A. In transient photochemistry, however, the analogous state is a product of the photochemical reaction of the excited state. The photoproduct can however revert to the initial material A with a rate $k$. Thus, holes can be observed if the A absorption is monitored on a time scale of $k^{-1}$. An example of a transient photochemical hole is hole burning of bacterial photosynthetic reaction centers. For isolated reaction centers (RC) at low-temperature photoexcitation of the primary electron donor, P, results in electron transfer from P* to one or more electron acceptors. In functioning photosynthetic systems, this initial charge transfer ultimately leads to charge return to the primary donor. Although the electron transfer from P* occurs on a picosecond timescale, return of the electron to P* typically requires milliseconds. Thus, a hole in the absorption of P can be observed if the spectrum is probed within milliseconds of narrow-line excitation of P. Section VI will deal with hole burning of various photosynthetic complexes in greater detail.

## *III. A Sampling of Hole-Burning Applications*

In a previous review of NPHB,[13] a section entitled "Survey of NPHB Systems" was included. That survey discussed from a mechanistic viewpoint various systems for which NPHB had been reported. All of those systems had in common a photochemically stable material dissolved in a disordered medium. The various disordered media were hydrogen-bonded crystals, amorphous films, organic and inorganic glasses, and polymers. A similar section, "Photochemical Systems and Mechanisms" was included in a review of PHB[45] in the same source. A comprehensive list of pertinent hole-burning systems is also available.[46]

The list cited above contains some 150 entries, published through mid-1986. In the time period since that list was prepared, hole-burning research has continued to grow to such an extent that a comprehensive discussion of hole-burning papers in the past five years is beyond the scope of a single review. A further reason for eschewing a list of hole-burning systems in the present case is that, although new hole-burning materials have been reported, these materials for the most part are typical of the systems previously described.[13]

Thus in this section rather than summarizing hole-burning materials, we will focus on recent applications of hole burning. Table I summarizes recent advances in hole-burning research taken from the programs of two recent meetings on this topic.[47,48] To adequately review the current status of each of these areas is also beyond the scope of a single article. Thus in sections IV and VI, we treat in detail only a narrow range of applications, primarily in areas where our own contributions to the field have been made. In this section, we briefly treat other areas as indicated in Table I. Certain areas listed in the tables have recently been reviewed by others, and the interested reader is referred to those papers for a more comprehensive treatment.

**Table I. Areas of Recent Advances in Hole-Burning Research**

| area | ref(s) |
|---|---|
| spectral diffusion | section IV.3 |
| line widths and relaxation, spectral diffusion, line shapes, dephasing | section IV.2 |
| mechanisms | section II.3 |
| time domain | ref 4 |
| high temperature and photon-gating | section III.2 |
| external fields | section V |
| optical processing and holography | section III.1 |
| single molecule detection | section III.3 |
| novel spectroscopies and systems | section III.4 |

## 1. Information Storage, Holography, and Optical Computing

The prospect of high-density storage available by exploiting the frequency variable has made optical information storage the most active area of applied hole-burning research. Both data storage and image storage have been proposed as HB applications. Data storage involves recording digital data on micrometer-sized spots utilizing the frequency dimension to increase the storage density. Storage densities as high as $10^{12}$ bits $cm^{-2}$ have been projected.[49] Using an electric field in conjunction with hole burning adds a further dimension which can provide an additional increase in density.[50,51] Moerner et al. have discussed all the requirements for a practical frequency domain optical storage (FDOS) system.[52]

While data storage utilizes micrometer-sized spots image storage records a large number of bits (on the order of $10^{12}$ $cm^{-3}$) simultaneously in an area of a few square millimeters by means of holography.[53] As in the case of data storage specific images are indexed by the appropriate combination of laser frequency and electric field. Storage of as many as 50 holograms in a 5-mm diameter spot has been achieved.[54,55] Similar techniques have also been used to perform logical operations AND and XOR by interferences of holograms.[56,57] By such operations hole burning can, in principle, become the basis of a molecular computing system.[58]

## 2. High Temperature and Photon Gating

Research on new materials for hole burning has focused primarily on two areas: (photon) gated hole burning and high-temperature persistent hole burning. A rigorous analysis by Moerner and Levenson of the properties (hole-burning efficiency, absorption cross section, concentration, etc.) needed of a hole-burning medium for data storage has shown that all materials studied thus far in which burning occurs by a one-photon mechanism fall far short of meeting the requirements.[59] One requirement which greatly restricted the acceptable range of photophysical properties is the necessity of being able to perform multiple reads (>1000) without needing to refresh the data. In a one-photon hole burning mechanism which has no threshold for hole burning, multiple data reads tend to burn holes thus requiring frequent data refresh except for a very narrow range of photophysical parameters. This conclusion spurred research on gated hole-burning mechanisms in which an external field, in addition to the photon field at the burn frequency, is needed. Such an external field establishes a threshold for burning thereby enabling multiple reads with low refresh rates. Although the use of electrical or magnetic fields as the gating field are possible, most research has focused on the use of a second light source, i.e. photon gating. Photon-gating schemes based on photoionization,[60,61] photodissociation,[62,63] and donor–acceptor electron transfer[64,65] have all been demonstrated.

The search for high-temperature hole-burning systems is motivated by the desirability of simplifying the cryogenic apparatus required for frequency domain optical storage. Although the hole widths attainable at ambient temperatures would probably preclude the development of practical room temperature FDOS devices, the widths potentially achievable in the 80–100-K region present a reasonable compromise between storage density and system complexity. Even if high-temperature burning is not feasible, it would be desirable to be able to cycle materials from their operating temperature to higher temperatures without erasing stored data. Among organic materials, hole burning up to 80 K has been realized in certain polymers doped with tetraphenylporphine derivatives.[66] For inorganic materials, hole burning up to room temperature has been reported for $Sm^{+2}$ in disordered alkaline earth halides[67] and for neutron-irradiated sapphire.[68] These materials are photon gated; however, the ratio of inhomogeneous to homogeneous width is ~10, thus precluding high-density FDOS. Nevertheless, an understanding of high-temperature hole burning in these materials is an important milestone in the development of practical FDOS devices.

## 3. Sensitive Detection

For a practical FDOS system it is necessary not only to burn a hole in a short time but also to be able to quickly read that hole with high signal to noise ratio (SNR). Methods of achieving high SNR readout of holes which have been demonstrated fall primarily into four categories: modulation techniques, holographic techniques, polarization techniques, and fluorescence detection.

Holographic detection of holes utilizes two beams overlapped at the sample in the hole-burning process. The interference pattern thus produced forms a spatial grating in the medium. For readout one tunable beam is used and diffraction of that beam by the spatial grating is detected.[69,53] Holographic detection is a zero-background technique, thus explaining its high sensitivity. Application of the technique to image storage has been demonstrated.[53-58]

Polarization detection methods utilize the transmission of a probe beam through a sample placed between crossed polarizers. Before burning, the polarizers are adjusted for zero transmission, thus compensating for any strain induced birefringence in either cryostat or sample. Hole burning with a polarized beam now induces a polarization anisotropy at the frequencies of spectral holes.[70] Thus, this is also a zero background technique capable of high resolution. The technique has been demonstrated by application to the detection of vibronic satellite holes.[71]

The ultimate in sensitivity, single-molecule detection has been achieved by Moerner and co-workers[72-78] and by Bernard and Orrit.[79-81] The Moerner group[72,73]

initially used two different double modulation techniques to directly measure absorption of pentacene in *p*-terphenyl. Far in the wings of the absorption, absorption due to single molecules was detected by combining frequency modulation spectroscopy with either Stark or ultrasonic modulation. In common with holographic and polarization techniques, frequency modulation is also a zero-background technique.

Fluorescence detection, on the other hand is not a zero-background method. Nevertheless by optimizing signal while minimizing noise contributions, fluorescence excitation spectra of single molecules of pentacene in *p*-terphenyl were reported by Bernard and Orrit[79] and by Ambrose and Moerner.[74] The former authors reported sudden drops and surges in some emission peaks which they interpreted as single molecule hole burning.[79,80] Moerner and Ambrose,[75] however, showed that such drops and surges were not laser driven and hence were examples of spectral diffusion (see section IV.3), not hole burning. Fluorescence excitation detection of absorption of single molecules was subsequently extended to polymer systems by Basché et al.[77,78] In this case both light-independent and light-induced changes in absorption frequency were seen. The former changes were ascribed to spectral diffusion while the latter were described as hole burning. In the hole-burning case, both reversible and irreversible burning was observed.

### 4. Novel Systems

Apart from the search for materials for high-temperature hole burning, the hole-burning phenomenon has also been used to study dye–matrix interactions in a variety of materials. As described in section II, the requirements for hole burning are the presence of an inhomogeneous distribution and a mechanism for frequency-selective alteration of that distribution. Both photochemical and nonphotochemical mechanisms have been proposed for the various novel systems discussed in this section. Because its mechanism depends on the inherent structural disorder of amorphous hosts, NPHB is a more versatile probe of dye–matrix (amorphous) interactions.

Hole burning has been reported for a number of dye–surface systems.[82–86] A nonphotochemical hole-burning mechanism involving surface TLS has been proposed.[82,85] The inhomogeneity is thought to arise from disorder among surface hydroxyl groups which are involved in binding the dye to the surface. Hole widths for quinizarin chemisorbed on $\gamma$-alumina are comparable to the widths observed for hole burning in organic glasses.[83] For physisorbed dyes, however, hole widths are considerably broader.[82,86] For the quinizarin/$\gamma$-alumina system hole widths were measured as a function of temperature.[83,85] For 1.0 K < $T$ < 10 K the width was found to be described by a combination of a $T^{\alpha}$ law with $\alpha$ = 1.0 with an additional contribution due to a thermally activated process. The activation energy was 12 cm$^{-1}$, but the mode involved was not identified. High-temperature hole burning has been reported for this system.[84] Over the range 1.6 K < $T$ < 77 K, a similar behavior of the width was seen, but in this case the activation energy was 87 cm$^{-1}$, which corresponds to the energy of a weak mode seen in line-narrowed fluorescence spectra. For molecules on surfaces, Pack and Fayer[87] have shown that the reduction in dimensionality may lead to non-Lorentzian hole shapes.

Hole burning of aggregates of pseudoisocyanine (PIC) salts has been reported by Hirschmann et al.[88–91] and by DeBoer et al.[92] In concentrated solutions of these materials, a relatively narrow, red-shifted absorption band appears that is due to excitation delocalized over a large aggregate. Hole burning was first reported for the bromide salt by DeBoer et al.[92] The inhomogeneity of the absorption was explained as being due to the occurrence of a distribution of aggregate lengths (such as has also been proposed to explain inhomogeneity and hole burning in polysilanes[93,94]). For the PIC bromide the hole burning was thought to be due to photoionization.[92] For the chloride and iodide, however, Hirschmann et al. proposed that the inhomogeneity arises from a conformational distribution[88] and from aggregate–solvent interactions[91] with the hole burning being due to a conformational change of the aggregate.[88]

Arnold et al.[95,96] have introduced a truly unique hole-burning medium, dye-coated microparticles, in which the inhomogeneity arises from the distribution of particle sizes. These microparticles produce morphology-dependent resonances associated with photon confinement by the particle's dielectric potential. This system is of interest as a room temperature hole burning system since the holewidths are primarily determined by the photon confinement efficiency, $Q$, which is virtually temperature independent. On the other hand the inhomogeneous width is associated only with the size distribution. Thus in a simple model of noninteracting particles, hole widths comparable to those observed at cryogenic temperatures are predicted. The observed line widths, however, are several orders of magnitude broader, apparently due to intraparticle absorption.[96] Nevertheless, the observed widths at room temperature ($\sim$0.1 Å) are considerably narrower than widths observed in other high-temperature hole-burning materials.

## *IV. Manifestations of Two-Level System Relaxation in Amorphous Solids at Low Temperatures*

As discussed in the Introduction, the magnitudes and temperature dependencies of a wide variety of physical properties such as thermal conductivity, specific heat, and ultrasound absorption are anomalous in glasses at very low temperatures, $T \lesssim 1$ K. This is also true for the pure dephasing of impurity electronic transitions. The standard tunnel model, which is based on a static distribution of bistable configurations of the glass ($TLS_{int}$) and impurity–glass ($TLS_{ext}$), has been extensively used to account for the anomalous behaviors. Within this model the immense structural disorder provides for a very broad distribution of TLS relaxation times, from picoseconds to hours, which leads to the phenomenon of spectral diffusion and dispersive kinetics for nonphotochemical hole growth and spontaneous hole filling. For many years progress toward a unified understanding of the low-temperature behaviors was hampered by the unavailability of accurate nonphenomenological distribution functions for the TLS required for ensemble averaging. In this regard, we will attempt, in this section, to show that significant

progress has been made with the distribution functions of Jankowiak, Small, and Athreya (JSA).[97]

### 1. TLS Distribution Functions and Ensemble Averaging

Many of the phenomenological distribution functions proposed up to 1985 are reviewed in refs 13 and 97. The simplest and best-known of these is due to Anderson et al.[31] and Phillips;[32] $P(\Delta,\lambda) = \bar{P}$ (constant) for $\lambda_{min} \leq \lambda \leq \lambda_{max}$ and $\Delta_{min} \leq \Delta \leq \Delta_{max}$ and zero otherwise, where $\lambda$ and $\Delta$ are the tunnel and asymmetry parameters, cf. section II.3. This distribution function leads to a density of states $\rho(E) \approx \rho_0$ (constant), where $E$ is the tunnel state splitting equal to $(\Delta^2 + W^2)^{1/2}$ with $W = \omega_0 \exp(-\lambda)$ the tunneling frequency. The prefactor, $\omega_0$, is the harmonic frequency of the wells of the TLS. With the constancy of the density of low-energy excitations, the near linear and quadratic dependences of the specific heat and thermal conductivity could be qualitatively understood. However, a quantitative understanding is not possible as will be discussed. It should be noted that an absence of correlation between $\lambda(W)$ and $\Delta$ is most often assumed.

The JSA distribution functions are based on Gaussians for $\Delta$ and $\lambda$ with mean values and variances $\Delta_0, \sigma_\Delta^2$ and $\lambda_0, \lambda^2$. The physical basis for this choice is discussed elsewhere.[97,98] Utilization of a Gaussian for $\lambda$ requires that $\lambda_0^2/2\sigma_\lambda \gg 1$ in order to avoid unphysical negative values for $\lambda$. In the absence of correlation, distribution functions for the reduced variables $\tilde{\Delta}^2$ and $\tilde{W}^2$ are easily obtained (e.g., $\tilde{\Delta} = \Delta/\omega_0$):

$$f_{\tilde{\Delta}^2}(Y) = \lambda_1 Y^{-1/2} \exp(\alpha Y) \cosh(\beta Y^{1/2}) \quad (5)$$

with $\lambda_1 = ([2\pi]^{1/2}\tilde{\sigma}_\Delta)^{-1} \exp[-Y_0/2\tilde{\sigma}_\Delta^2]$, $\alpha = -(2\tilde{\sigma}_\Delta^2)^{-1}$, $\beta = Y_0^{1/2}/\tilde{\sigma}_\Delta^2$. Here $\tilde{\sigma}_\Delta = \sigma_\Delta/\omega_0$ and $Y = \tilde{\Delta}^2$, and

$$f_{\tilde{W}^2}(Z) = \lambda_2 Z^{\theta-1} \exp[\gamma(\ln Z)^2] \quad (6)$$

where $Z \equiv \tilde{W}^2$, $\gamma = -(8\sigma_\lambda^2)^{-1}$, $\theta = -\lambda_0(2\sigma_\lambda^2)^{-1}$, and $\lambda_2 = [2(2\pi)^{1/2}\sigma_\lambda]^{-1} \exp[-\lambda_0^2/2\sigma_\lambda^2]$. For the variable $X = \tilde{E}^2$ one has

$$f_{\tilde{E}^2}(X) = \int_0^X f_{\tilde{\Delta}^2}(Y) f_{\tilde{W}^2}(X - Y)\, dY \quad (7)$$

from which the TLS density of states $\rho(E)$ follows,

$$\rho(\tilde{E}) \sim 2x \int_0^{x^2} f_{\tilde{\Delta}^2}(Y) f_{\tilde{W}^2}(X - Y)\, dY \quad (8)$$

where $x \equiv \tilde{E}$.

If, for example, one is interested in the average value of the asymmetry parameter $\langle\tilde{\Delta}\rangle_{\tilde{E}}$ then

$$\langle\tilde{\Delta}\rangle_{\tilde{E}}(x) = 2x \int_0^{x^2} Y^{1/2} f_{\tilde{\Delta}^2}(Y) f_{\tilde{W}^2}(X - Y)\, dY \quad (9)$$

It is important to realize that the $T$ dependence of a physical property generally depends on a quantity $\langle g(\tilde{\Delta},\tilde{W})\rangle_{\tilde{E}}$ and that the temperature scale is set by $\tilde{E}$, i.e., the value of $\omega_0$ since $\tilde{E} = E/\omega_0$, cf. following subsection.

In our published works in which the JSA distribution functions were applied to several properties, the emphasis was on the derivation of analytic expressions that govern the temperature and/or time dependence. As a result, the expressions appear at first sight to be quite formidable. In this review they will not be reproduced since all pertinent integrals can be evaluated numerically using readily available software.

### 2. The $T^{\sim 1.3}$ Power Law of Pure Dephasing for Impurity Molecules in Amorphous Solids

One of the photophysical properties of organic molecules and inorganic ions whose behavior, at low temperatures ($\lesssim$10 K for molecules), is markedly different in amorphous solids than in crystalline hosts is the pure dephasing of their electronic transitions. Interest in this problem began in the late 1970s as a result of resonant fluorescent line narrowing studies of $4f^n$ transitions of rare earth ions in inorganic glasses[99-102] and nonphotochemical hole burning (NPHB) experiments on the $S_1 \leftarrow S_0$ transition of aromatic molecules in alcohol glasses.[35,103] The anomalous behavior of the homogeneous width of the zero-phonon line (ZPL) was quickly linked[99,35,103-106] to the bistable configurations (asymmetric intermolecular double well potentials or two-level systems, TLS) of amorphous solids which had been invoked earlier to explain the anomalous behaviors of specific heat, thermal conductivity, and ultrasound absorption in inorganic glasses.[31-33,107] The TLS together with phonon-assisted tunneling between their tunnel states constitute what is often referred to as the standard tunnel model. Several recent reviews of the applications of this model to pure dephasing are available.[13,108,109]

We wish to consider the origin of the well-known[110] $T^{\sim 1.3}$ power law for the homogeneous width of the ZPL observed for organic molecules in glasses and amorphous polymers[110] and even proteins[111] for $T \lesssim 10$ K. Initially, photochemical and nonphotochemical hole burning (long time scale experiments) were used for the $T$-dependent studies. Recently, it has become clear that, in addition to the pure dephasing contribution to the hole width, there is a contribution from spectral diffusion (for a review see ref 4). The spectral diffusion is a consequence of the inherent structural disorder of the glass which leads to a broad distribution of TLS relaxation times, from picoseconds to hours. The problem of spectral diffusion is now attracting considerable attention. However, we will be concerned in this subsection only with the temperature power law for the pure dephasing ($T_2^{*-1}$). Importantly, Fayer and co-workers[4,112-115] have recently applied the 2-pulse photon echo to several systems and showed that the $T^{\sim 1.3}$ power law holds for $T_2^{*-1}$ dictated by the impurity–TLS interaction. This is fortunate since the $T^{\sim 1.3}$ power law for pure dephasing was the stimulus for the development of theories prior to the decisive 2-pulse photon echo experiments.

The starting point for the theories of pure dephasing in glasses is the impurity–TLS interaction

$$H_{12} = \sum_{\rho=\alpha,\beta} \left[ \frac{V_\rho \Delta}{E} (|1\rangle\langle 1| - |2\rangle\langle 2|) + \frac{V_\rho W}{E} (|1\rangle\langle 2| + |2\rangle\langle 1|) \right] |\rho\rangle\langle\rho| \quad (10)$$

where $|1\rangle$ and $|2\rangle$ are the lower and higher energy tunnel states of the TLS and $\Delta$, $W$, and $E$ are its asymmetry, tunneling frequency, and tunnel state splitting, vide supra. The ground and excited electronic states of the

impurity correspond to $\rho = \alpha$ and $\beta$. The term $V_\rho = 1/2(V_{\ell\rho} - V_{u\rho})$ represents the difference in the interaction between the impurity (in state $\rho$) and the lower ($\ell$) and upper (u) localized oscillator states of the TLS. Theories which ascribe the dephasing to the first[99,104,106] and second[35,103,105] terms of $H_{12}$ are referred to as diagonal and off-diagonal, respectively. It is generally held that the diagonal modulation mechanism, investigated in detail by Lyo,[106,116] is the dominant one. Lyo argued that weak interactions between the impurity and a "sea" of distant (outer shell and beyond) intrinsic TLS ($TLS_{int}$) of the glass host should dominate the interaction from a nearby TLS of the inner shell, e.g., the extrinsic TLS ($TLS_{ext}$) which is intimately associated with the impurity and responsible for nonphotochemical hole burning (NPHB). Support for this model comes, in part, from studies of the dependence of the NPHB efficiency and pure dephasing of dye molecules in alcohol glasses on deuteration of the hydroxyl proton.[28,29,41] Whereas the NPHB efficiency undergoes a marked decrease, the pure dephasing is unaffected which means that the $TLS_{ext}$ and $TLS_{int}$ coordinates involve large and small amplitudes of motion for the proton, respectively. Implicit in the complete theory are the assumptions of weak TLS–phonon coupling and that the effects of electronic excitation on the TLS parameters $\omega_0$, $\lambda$, and $\Delta$ are negligible. For a single interacting TLS the contribution to the homogeneous line width is[99,117]

$$\Delta\omega = \frac{V'^2}{\hbar^2}\,\mathrm{sech}^2(E/2kT)\frac{\tau}{1 + (V'\tau/\hbar)^2} \qquad (11)$$

where $V' = |V_\beta - V_\alpha|\Delta/E$ and $\tau$ is the inverse of the TLS relaxation rate

$$\tau^{-1} = AW^2E\,\mathrm{ctnh}(E/2kT) \qquad (12)$$

where $A$ depends on the square of the deformation potential associated with the TLS–phonon interaction. As mentioned, weak impurity–TLS coupling is assumed ($V' < E$). Since motional narrowing of $\Delta\omega$ with increasing temperature has never been observed, one may safely assume that the slow modulation limit, $V' > \tau^{-1}$, is applicable. In this limit eq 11 simplifies to

$$\langle\langle\Delta\omega\rangle\rangle(T) = \langle\langle\mathrm{sech}^2(E/2kT)\tau^{-1}\rangle\rangle \qquad (13)$$

for a sea of $TLS_{int}$, where the double brackets indicate a double averaging. First, one must sum over all $TLS_{int}$ of a given $E$ subject to the constraint that $V' > \tau^{-1}$ and then, having determined quantities such as $\langle\Delta\rangle_E$, etc., integrate over $E$ from 0 to $E_{max}$ to obtain the $T$ dependence.

Until 1986[118,119] the averaging procedures used were too crude for a convincing explanation of slight deviation from linearity of the temperature power law for pure dephasing. Utilization of phenomenological distribution functions necessitated additional assumptions for a determination of the $T$ power law of pure dephasing which, in the case of diagonal modulation, led to a $T^{1+\mu}$ power law for pure dephasing when the impurity–TLS interaction is of the dipole–dipole type. Here, $\mu$ is the exponent of $\rho(E) = \rho_0E^\mu$. Since specific heat measurements had indicated (for $T \lesssim 1$ K) that $\rho(E)$ is a slowly increasing function of $E$ with $\mu \approx 0.2$–$0.3$,[120] i.e., the above distribution function is not quite right, it was not so unreasonable to assume that the $T^{\sim 1.3}$ power law for pure dephasing is associated with the $\mu \approx 0.3$ of the specific heat even though specific heat measurements had not established that $\rho(E) \propto E^{\sim 0.3}$ holds for $T > \sim 1$ K. In refs 118 and 119 in which the JSA functions are used, it was concluded that the above association appears to be unjustified.

Nevertheless, this conclusion has, for the most part, been ignored.[110] In the slow modulation limit the impurity–TLS interaction $V'$ does not appear in the expression for the line width, eq 13. However, it reenters the problem via the spatial integration associated with summing over the TLS that interact with the impurity subject to the constraint of slow modulation, $V' = |V_\beta - V_\alpha|\Delta E^{-1} > \tau^{-1}$. Writing $|V_\beta - V_\alpha| = b/r^s$, where $r$ is the impurity–TLS distance, allows one to determine the cutoff radius, $r_c$ from

$$\tau^{-1} = \frac{b\Delta}{r_c^{\,s}E} \qquad (14)$$

for each value of the tunnel splitting $E$. It is instructive to briefly review the procedure utilized by Lyo[106,116] and others[117] for a uniform spatial distribution of TLS with a number density of $n$. It involves two assumptions: namely, that only TLS with $W \ll E$ are important so that $\Delta/E \approx 1$ and eq 10 reduces to $\tau^{-1} = b/r_c^{\,s}$; and that $\langle W^2\rangle_E/E^2$ is a constant so that from eq 7, $\tau^{-1} \propto E^3$. With these assumptions the spatial integration is trivial, yielding $v_c n\rho(E)$ where $v_c = 4\pi r_c^{\,3}/3$ and $\rho(E)$ is the TLS density of states. For $s = 3$ (dipole–dipole interaction), the case of interest here, it follows that

$$\langle\langle\Delta\omega\rangle\rangle(T) \propto \int_0^{E_{max}}\rho(E)\,\mathrm{sech}^2(E/2kT) \qquad (15)$$

which in the low-temperature limit for $\rho(E) = \rho_0E^\mu$ yields $\langle\langle\Delta\omega\rangle\rangle \propto T^{1+\mu}$. That is, the temperature power law is determined by the density of states as noted earlier.

The above assumptions need not be made provided that reliable TLS distribution functions for $\Delta$ and $\lambda$ are available. One starts with[119]

$$\langle r_c^{\,s}\rangle_{\tilde{E}} = \frac{b\langle\tilde{\Delta}\rangle_{\tilde{E}}}{\langle\tau^{-1}\rangle_{\tilde{E}}\tilde{E}} \qquad (16)$$

where $\tilde{E} \equiv E/\hbar\omega_0$ is introduced for calculative purposes ($\omega_0$ is the harmonic circular frequency of the TLS wells). The $\langle\ \rangle_{\tilde{E}}$ indicates average value for a given $\tilde{E}$. Performing the spatial integration as above leads directly to

$$\langle\langle\Delta\omega\rangle\rangle(T) \propto \int_0^{\tilde{E}_{max}}\langle\tilde{\Delta}\rangle_{\tilde{E}}^{3/s}\,\tilde{E}^{-3/s}\langle\tau^{-1}\rangle_{\tilde{E}}^{1-3/s} \times \mathrm{sech}^2(\tilde{E}/2\tilde{k}T)\,\mathrm{d}\tilde{E} \qquad (17)$$

which, for a dipole–dipole interaction ($s = 3$), simplifies to

$$\langle\langle\Delta\omega\rangle\rangle(T) \propto \int_0^{\tilde{E}_{max}}\langle\tilde{\Delta}\rangle_{\tilde{E}}\,\tilde{E}^{-1}\mathrm{sech}^2(\tilde{E}/2\tilde{k}T)\,\mathrm{d}\tilde{E} \qquad (18)$$

that is, the TLS relaxation rate cancels out of the problem. Equation 18 establishes that it is the average value of the asymmetry parameter $\tilde{\Delta}$ and not the TLS density of states that figures importantly for the T dependence of $\Delta\omega$. Anticipating that $\langle\tilde{\Delta}\rangle_{\tilde{E}} \propto \tilde{E}^{\mu_\Delta}$ (where $\mu_\Delta$ is the average slope of log $\langle\Delta\rangle$ versus log $E$, see e.g., Figure 11) over a suitable temperature range, one sees from eq 18 that in the low-temperature limit for $s = 3$, $\Delta\omega \propto T^{\mu_\Delta}$.

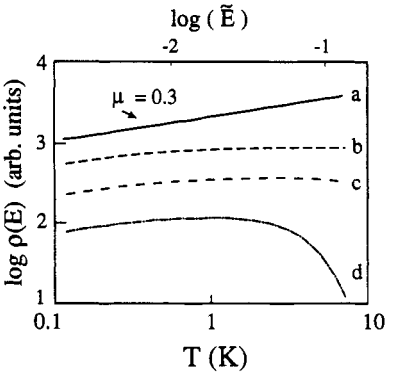


**Figure 10.** The density of states, $\rho(E)$, of the two-level systems ($TLS_{int}$) calculated with $\lambda_0 = 7$, $\Delta_0 = 0$, $\sigma_\lambda = 2.5$, and different $\tilde{\sigma}_\Delta$ values; $\tilde{\sigma}_\Delta = 0.4$ (curve b), $\tilde{\sigma}_\Delta = 0.2$ (curve c), and $\tilde{\sigma}_\Delta = 0.05$ (curve d). Curve a is a line with slope 0.3. $\sigma_\Delta = \tilde{\sigma}_\Delta(\hbar\omega_0)$ and $\hbar\omega_0 = 4.96 \times 10^{-3}$ eV (40 $cm^{-1}$).

The JSA distribution functions have been applied to the problem of the temperature dependence for specific heat,[121] pure dephasing from diagonal[118] and off-diagonal[119] modulation, and thermal conductivity.[122] Monte Carlo type calculations of the TLS density of states have also been reported.[98] Particularly relevant to the present work is ref 122 in which the JSA distribution functions were used to explain why the power law for thermal conductivity for most glasses ($T \lesssim 1$ K) deviates from $T^{2-\mu}$ when $\rho(E) \propto E^\mu$ and $C_V \propto T^{1+\mu}$. The $T^{2-\mu}$ power law is a prediction that emerges from the standard tunnel model when approximations of the type discussed above are made in averaging over the TLS parameters. In ref 122, values of $\lambda_0 \approx 7$, $\sigma_\lambda \approx 3$, $\Delta_0 \approx 0$, $\tilde{\sigma}_\Delta \approx 0.1$ and $\omega_0 = 20$ $cm^{-1}$ for the $TLS_{int}$ could account for the deviations from $T^{2-\mu}$ behavior. Indeed, the above works and the results that follow in this and the following subsection indicate that the above values for $\lambda_0$ and $\sigma_\lambda$ are consistent with the low-temperature behaviors of a wide variety of physical properties.

Curves b–d of Figure 10 are the $TLS_{int}$ density of states obtained by numerical evaluation of the distribution for $\tilde{E}^2$, ($\rho(E) \propto E f_{E^2}(E^2)$) with $\lambda_0 = 7.0$, $\sigma_\lambda = 2.5$, $\Delta_0 = 0$, and $\tilde{\sigma}_\Delta = 0.4$, 0.2, and 0.05 (the latter corresponding to variances of 16, 8, and 2 $cm^{-1}$), respectively. For comparison, curve a is a line with slope 0.3. The results are consistent with those obtained by a Monte Carlo type procedure.[98] For $0.1 \lesssim T \lesssim 0.6$ K, the b–d density of states can be described as lines with slopes approaching 0.3. For $T > 1$ K concave curvature in log $\rho(E)$ sets in and for b and c there is a near constant density of states between 1 and 5–6 K. In curve d the turn down at ~5 K (log $\tilde{E} \approx -1$) marks the onset of the decline of the density of states to zero. The onset shifts to lower temperature as the width of the $\Delta$ distribution is narrowed ($\tilde{\sigma}_\Delta$ decreased), as is apparent from curve d, and the results of ref 98. In ref 98 $\rho(E)$ is calculated down to lower log $\tilde{E}$ values (~−4) so that the gap at very low temperatures, which is indicated by specific heat measurements[123,124] was revealed. From the results of ref 122, we estimate that this gap for curve c would onset at ~50 mK. Because of convergence problems in the numerical integration for log $\tilde{E} <$ ~−2.8, we restricted ourselves to $T \gtrsim 0.1$ K, which is the region of interest here.

Figure 11 shows the results obtained for $\langle\tilde{\Delta}\rangle_{\tilde{E}}$ with the same three sets of parameter values used in Figure 10 (b–d) plus $\lambda_0 = 7$, $\sigma_\lambda = 3$, and $\tilde{\sigma}_\Delta = 0.2$ (curve e). Curve a is a line with slope 1.3. Focusing on b ($\tilde{\sigma}_\Delta = 0.4$) and c ($\tilde{\sigma}_\Delta = 0.2$), one observes that their curvatures are significantly less than those of b and c in Figure 10 and, furthermore, that they are well approximated by lines with essentially identical slopes approaching 1.3 for $T \lesssim 5$ K. Figure 12 provides a clearer picture of the extent to which $\langle\Delta\rangle_{\tilde{E}}$ provides the better accounting of the T dependence of pure dephasing up to ~5 K which, of course, should be expected from eq 14 in the low-temperature limit. We have confirmed that the low-temperature limit for eq 14 is valid for the parameter values used to calculate curves b, c, and e ($T \lesssim 7$ K). We note that recent 2-pulse photon echo experiments have established that an additional dephasing mechanism in organic systems onsets at about ~6 K.[4] Furthermore, the uncertainty in the 1.3 exponent of the $T$ power law determined experimentally is no better than ±0.05. Thus, we have made no attempt to *fine* tune the parameter values to yield a value for $\mu_\Delta$ of exactly 1.3.

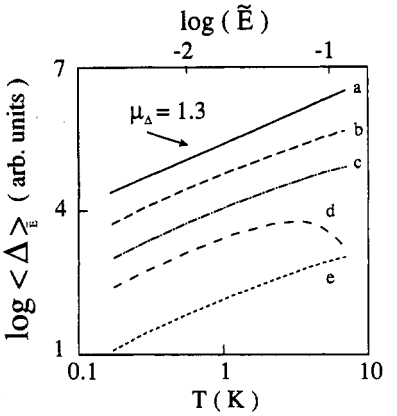


**Figure 11.** Average value of $\langle\Delta\rangle_{\tilde{E}}$ as a function of reduced energy $\tilde{E} = E/\hbar\omega_0$ (and $T$) for $\hbar\omega_0 = 4.96 \times 10^{-3}$ eV (40 $cm^{-1}$) obtained for $\lambda_0 = 7$, $\Delta_0 = 0$, $\sigma_\lambda = 2.5$ and different values of $\tilde{\sigma}_\Delta$: $\tilde{\sigma}_\Delta = 0.4$ (curve b); $\tilde{\sigma}_\Delta = 0.2$ (curve c); $\tilde{\sigma}_\Delta = 0.05$ (curve d), respectively. Curve e was obtained for $(\lambda_0,\Delta_0,\sigma_\lambda,\tilde{\sigma}_\Delta) = (7,0,3,0.2)$. Curve a is a line with slope $\mu_\Delta = 1.3$.

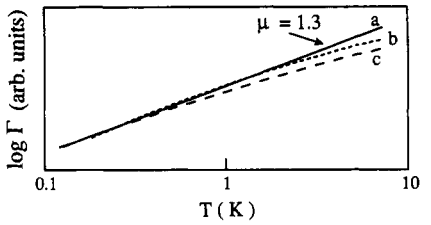


**Figure 12.** Temperature dependence of pure dephasing. Curve a is a line with slope $\mu = 1.3$. Curves b and c were calculated for $\Delta_0 = 0$, $\lambda_0 = 7$, $\sigma_\lambda = 2.5$, $\tilde{\sigma}_\Delta = 0.2$, and $\hbar\omega_0 = 4.96 \times 10^{-3}$ eV. Curve b is the plot of $\langle\Delta\rangle_{\tilde{E}}$ while curve c is the plot of $\tilde{E}\rho(\tilde{E})$ which yields $T^{1+\mu}$ only for $T <$ ~0.7 K.

We turn now to a discussion of the parameter values used in the calculations. Since the reduced tunnel state splitting $\tilde{E} = E/\hbar\omega_0$, the value of the TLS harmonic frequency $\omega_0$ sets the temperature scale. The value of 40 $cm^{-1}$ ($7.6 \times 10^{12}$ $s^{-1}$) used is within the ~20–80-$cm^{-1}$ range of values typically used for $TLS_{int}$. Theoretical modeling for amorphous silica has indicated that $\omega_0$ in the range 20–40 $cm^{-1}$ is reasonable[124] (see also ref 125). For the present work the mean asymmetry parameter ($\Delta_0$) was set equal to zero as in our previous studies. It has been argued that such an assumption is justified.[97,126]

Relaxation of this assumption would be of no consequence provided $\Delta_0 \ll \sigma_\Delta$ which, for example, equals 8 $cm^{-1}$ for $\tilde{\sigma}_\Delta = 0.2$ and $\omega_0 = 40$ $cm^{-1}$. As mentioned, our previous studies of specific heat and thermal conductivity and, most recently, time-dependent spectral diffusion (cf., following subsection) have led to the finding that $\lambda_0 \approx 7$ and $\sigma_\lambda \approx 3$ are appropriate values for $TLS_{int}$. The present work provides additional support for such values. As discussed in ref 122, modest and correlated changes in a set of $(\lambda_0, \sigma_\lambda)$ values can lead to the same value of $\mu$ in $\rho(E) \approx E^\mu$ for $T < \sim 1$ K. (The value of $\mu$ is quite insensitive to significant variations in $\tilde{\sigma}_\Delta$ which do, however, affect the temperature of onset for the gap in $\rho(E)$.[98] However, one cannot vary $\lambda_0$ and $\sigma_\lambda$ too much. For example for $(\lambda_0,\sigma_\lambda) = (12,2)$, $\mu \approx 0$ for $0.01 \lesssim T \lesssim 1$ K.[98] For $(\lambda_0,\sigma_\lambda) = (7,2.5)$, $\mu \approx 0.25$.

In the calculations values of 0.4, 0.2, and 0.05 for $\tilde{\sigma}_\Delta$ were used. The values of $\sigma_\lambda$ employed here are sufficiently small to have $2\tilde{\sigma}_\Delta$ determine the temperature (tunnel splitting) at which $\rho(E)$ begins its decline to zero, i.e., $2\tilde{\sigma}_\Delta \approx \tilde{E}_{max}$, eq 18. For $\tilde{\sigma}_\Delta = 0.2$ and 0.4, cf. Figure 11, and $\omega_0 = 40$ $cm^{-1}$, $E_{max} \approx 16$ and 32 $cm^{-1}$. We believe these to be physically reasonable values. On the other hand, the value of $\tilde{\sigma}_\Delta = 0.05$ is probably too short. In order to experimentally determine values for $\tilde{\sigma}_\Delta$ it is necessary, in part, to probe the $TLS_{int}$ at high temperatures. This, of course, is a difficult task since additional mechanisms generally enter into play at high temperatures. It is also the case that time-dependent spectral diffusion and specific heat measurements provide no information on the $\Delta$ distribution for weak TLS–phonon coupling. However, Kassner and Silbey[127] and Kassner[128] have recently reemphasized that the common assumption of weak coupling is suspect. This is interesting because for strong coupling the distribution function for TLS relaxation rates is dependent on $\tilde{\sigma}_\Delta$ as we shall see in the following subsection on spectral diffusion.

### 3. Spectral Diffusion of Electronic Transitions in Amorphous Solids

Thermal cycling–hole burning experiments had proven early on that[129,130] broadening of the zero-phonon hole (ZPH) occurs by spectral diffusion induced by slow thermally assisted, irreversible glass relaxation processes with the impurity in its *ground* state. However, it has only been recently[4,112–114,131,132] that the question of the contribution of spectral diffusion to persistent nonphotochemical, photochemical, and transient population bottleneck ZPHs produced under normal protocol has been actively pursued. The term "normal" means that the burn and read temperatures $(T_B,T_R)$ are the same. In the thermal cycle experiment the hole is burned and read at $T_B$, the sample temperature raised to $T > T_B$, then lowered to $T_B$ and the hole read again. The resulting partial thermal annealing of the hole is accompanied by broadening.[130,133] Given the result from thermal cycling, that the longitudinal (depopulation) relaxation time ($\tau_1$) of the typical probe molecule is short, a few nanoseconds, and the time dependence of the specific heat,[133–135] it would be reasonable to expect a contribution to the ZPH width from spectral diffusion when the waiting and reading times ($t_W$, $t_R$) are long. In a series of beautiful 2-pulse photon echo and NPHB experiments with resorufin and cresyl violet in alcohol (ethanol, glycerol) glasses Fayer and co-workers[4,112–115] determined that the homogeneous width of the ZPL determined by photon echo is substantially narrower (~6×) than that determined by NPHB for $T \lesssim 8$ K. They ascribed the difference to spectral diffusion. Although later NPHB experiments on the same systems by Völker and co-workers[110,136,137] led to some controversy concerning the magnitude and temperature dependence of the spectral diffusion reported by Fayer and co-workers, very recent 2-pulse photon echo and fast ($\gtrsim 10$ $\mu$s) hole-burning experiments by Littau and Fayer[113] and Littau et al.[114,115] on cresyl violet in ethanol glass, stimulated photon echo experiments by Meijers and Wiersma[138] on zinc porphin in ethanol glass, and fast population bottleneck hole-burning experiments on bacteriochlorophyll *a* in triethylamine and ethanol glasses by Wannemacher et al.[139] have further established that spectral diffusion *does occur* in organic systems on a time scale ranging from several nanoseconds to minutes (see also refs 113 and 140). In addition, the *single*-molecule experiments of Basché and Moerner[77,78] on perylene in amorphous poly(ethylene) have revealed intriguing optical transition frequency excursions of *single* molecules on a long time scale.

In what follows we investigate the time-dependent spectral diffusion data of Littau and Fayer[113] within the framework of weak and strong TLS–phonon coupling and with the JSA TLS distribution functions. The time-dependent hole burning data of Littau and Fayer[113] extend from ~10 $\mu$s to 1000 s and indicate there are two (faster and slower relaxing) TLS distributions that contribute to the spectral diffusion. We had shown earlier that[141] the log of the normal distribution for the slower relaxation rates used by Littau et al.[113] follows from the JSA distribution function for $\lambda$, vide infra. Furthermore, it was noted, in passing, that the parameter values required to fit the data are similar to those used to describe spontaneous filling of nonphotochemical holes.[142] NPHB and spontaneous hole filling are associated with the $TLS_{ext}$, sections IV.5 and 6. With the temporally extended data sets one is better able to assess this connection, to determine whether a log of the normal distribution for the faster relaxing TLS is also appropriate and, if so, whether the parameter values for this distribution correspond to those for the $TLS_{int}$ connected with pure dephasing and other observables. Of particular interest is the effect of strong TLS–phonon coupling on spectral diffusion.

A description of spectral diffusion requires distribution functions for the TLS relaxation rates (cf. eq 22). For weak TLS–phonon coupling the rate for the $k$th TLS is

$$R^k_{WC} = A W_k^2 E_k \coth(E_k/2kT) \qquad (19)$$

where $A$ depends on the square of the TLS deformation potentials. Very recently Kassner and Silbey[127] (see also refs 128 and 143) have reemphasized that the common assumption of weak coupling is questionable on the basis of existing experimental data.[144] Using methods from polaron theory, they treated the problem of phonons dressed with TLS and vice versa and concluded that, to a good approximation, the relaxation rate for strong coupling is

$$R^k_{SC} = \exp[-G(\Delta_k/E_k)^2]R^k_{WC} \quad (20)$$

for temperatures below several Kelvin. Here $G$ is a function of the TLS deformation potentials from which they estimate $G \approx 175$ for organic glasses. One anticipates from eq 20 that the main effect of strong coupling will be to produce a distribution of relaxation rates, $P(R)_{SC}$, that is significantly different from $P(R)_{WC}$ for the slower relaxation rates, i.e., $P(R)_{SC}$ should have an extended tail for such rates. We note that the unitary transformation employed by Kassner and Silbey only includes the diagonal part of the TLS–phonon interaction.

The distribution function for $W^2$, eq 6, leads to a log of the normal distribution for $P(R)_{WC}$[140]

$$P(R)_{WC}R_{WC} = (\sigma\sqrt{2\pi})^{-1} \exp-[\{\ln(R/R_0)\}^2/2\sigma^2] \quad (21)$$

where $\sigma = 2\sigma_\lambda$, $R_0 = \Omega_0 \exp(-2\lambda_0)$, with $\lambda_0$ the mean value of $\lambda$, and $\Omega_0 \approx \omega_0$. Littau et al.[113] found that their spectral diffusion data for $t \gtrsim 1$ ms were well explained in terms of the above distribution function.

The distribution function for strong coupling has recently been derived.[145] With $P(R)_{SC} = P(y)/R_{SC}$,

$$P(y) = \alpha_1 \exp(\alpha_2) \exp[\beta(y)] \int_0^\infty \frac{dt}{\sqrt{t}} \times \exp[-(t + \gamma(y))^2/8\sigma_\lambda^2] \quad (22)$$

with $\alpha_1 = (4\pi\sigma_\lambda\sigma_\Delta\sqrt{C})^{-1}$, $\alpha_2 = \sigma_\lambda^2/8\sigma_\Delta{}^4C^2$, $\beta(y) = (y-\mu)/2\sigma_\Delta{}^2C$, $\gamma(y) = y - \mu + 2\sigma_\lambda{}^2/\sigma_\Delta{}^2C$, $C = G/E^2$. The parameter $\mu$ is the mean value of the normal Gaussian distribution of $\ln R_{WC}$, i.e., $\ln R_0$.

Following the work of Hu and Walker,[146] Bai and Fayer[112] used the four-point correlation function formalism of Mukamel[147] and Mukamel and Loring[148] to derive, for the spectral diffusion contribution to the optical line width,

$$\Gamma_{SD} \propto \int P(R)\,[1 - \exp(-Rt_W)]\,dR \quad (23)$$

where $P(R)$ is the distribution function for the TLS relaxation rate (for weak (WC) or strong (SC) TLS–phonon coupling) and $t_W$ is the waiting time. In the stimulated echo experiment the three pulses are applied at times 0, $\tau$, and $\tau + t_W$, i.e., $t_W = 0$ corresponds to the 2-pulse photon echo which yields the homogeneous width of the optical transition (as operationally defined by Fayer and co-workers). For $t_W = 0$, $\Gamma_{SD}$ is zero. Hole burning is the Fourier transform of the stimulated echo and so the waiting time can be viewed in time-dependent hole burning as the time of burning and reading of the hole. In the highest resolution ($\sim$10 $\mu$s) time-dependent hole burning experiments reported a population bottleneck via the lowest triplet state has been employed,[113] as in the 3-pulse stimulated echo experiments.[138,140] Equation 23 is obtained following spatial averaging over the TLS interacting with the chromophore. The interaction, if dipole–dipole, leads to a Lorentzian hole shape, as is generally observed. As written, eq 23 is applicable to a given temperature. Elsewhere we will examine the $T$ dependence of spectral diffusion.[149]

With eqs 20 and 22 and noting again that $y = \ln R_{SC}$, one obtains

$$\Gamma_{SD}(t_W)_{SC} \propto \int_{-y_{min}}^{y_{max}} P(y)[1 - \exp\{-\exp(y)t_W\}]\,dy... \quad (24)$$

for strong TLS-phonon coupling. The expression used to calculate $\Gamma_{SD}(t_W)_{WC}$ follows directly from eqs 19 and 23. Integrations were performed numerically.

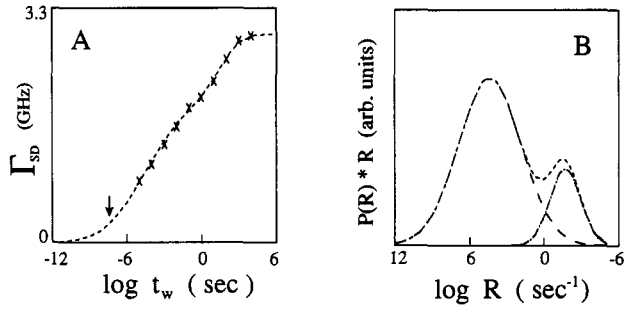


**Figure 13.** (A) Spectral diffusion contribution ($\Gamma_{SD}$) versus log ($t_W$) for cresyl violet in ethanol-$d$ glass at $T = 1.2$ K. Crosses correspond to the data from ref 113 (only a few points are shown), when the contribution from pure dephasing was subtracted. The dashed line is the fit obtained with the two distribution functions shown in part B. The arrow locates the excited state lifetime ($\tau$). $\Gamma_{SD}$ (for log $t_W$ = log $\tau$) = 120 MHz (see text for details). (B) Plot of the relaxation rate distributions $P(R)$ (weak TLS–phonon coupling) for $TLS_{int}$ ($\lambda_0 = 9.8$, $\sigma_\lambda = 2.9$; the left-most distribution) and $TLS_{ext}$ ($\lambda_0 = 16.8$, $\sigma_\lambda = 1.4$), used to fit the data in Figure 13A. The short-dashed line is the resultant of the log of two normal distributions. Reprinted from ref 145. Copyright 1993 American Physical Society.

When the pure dephasing and lifetime contributions are subtracted out, the actual data of Littau and Fayer appear as in Figure 13A. The dashed line is the fit for weak coupling obtained with the two distribution functions of Figure 13B. The $\lambda_0$ and $\sigma_\lambda$ values for the right-most distribution are $\lambda_0 = 16.8$ and $\sigma_\lambda = 1.4$. To be consistent with our earlier work, cf. also preceding subsection, we have used $\Omega_0 = 7.6 \times 10^{12}$ s$^{-1}$ (40 cm$^{-1}$) in the relaxation rate expression $R = \Omega_0 \exp(-2\lambda) \propto W^2$. The parameter values for the distribution of faster relaxation rates are $\lambda_0 = 9.8$ and $\sigma_\lambda = 2.9$. The fit in the region of the data points is comparable to that of Littau and Fayer who invoke a $P(R)$ distribution of $1/R$[113,114] for log $R \gtrsim 0.6$ and a log of the normal distribution for the slower rates, with the result that there is essentially a forbidden gap in the region around log $R = 0.6$. For log $t_W$ equal to the excited state lifetime (solid arrow), $\Gamma_{SD} = 120$ MHz. The tail of the calculated curve to the left of the arrow indicates that spectral diffusion might be observable for 100 ps $\lesssim t_W \lesssim$ excited-state lifetime. Interestingly, Narasimhan et al.[150] have recently obtained 3-pulse stimulated photon echo data for rhodamine 101 in the PMMA polymer at 1.35 K that show a $\sim$100-MHz contribution from spectral diffusion to the line width at $t_W = 3.4$ ns (excited-state lifetime). Also of interest is that the results show that the $P(R) \propto 1/R$ approximation is poor for short $t_W$'s. This may be of consequence to the question of nonexponentiality of 3-pulse stimulated echo decays at short (less than or similar to the lifetime) $t_W$'s.[150] From our studies of the dispersive kinetics of nonphotochemical hole growth,[28,151] cf. section IV.4, it is very clear that the often invoked $1/R$ distribution (which stems from the TLS distribution function of Anderson et al. and Phillips, vide supra) is accurate only in the intermediate time regime. It is more physically reasonable to use the log of two normal distribution functions to fit the data of Littau and Fayer especially if their $\lambda_0$,$\sigma_\lambda$ values can be related to those of other

physical properties, cf. discussion at the end of this section.

Next we examine the consequences of strong TLS–phonon coupling on spectral diffusion (the effect on pure dephasing is currently being investigated). Now the distribution function for the asymmetry parameter comes into play, cf. eq 22. As discussed by Kassner and Silbey[127] and Kassner[128] the experimental evidence for strong coupling for $TLS_{int}$ is quite convincing. Later we associate the faster and slower distributions of relaxation rates with the $TLS_{int}$ and $TLS_{ext}$, respectively. We assume strong coupling for the $TLS_{ext}$. In part A of Figure 14 curve c is a fit to the data with the a and b curves, respectively, the contributions from the faster and slower relaxing distributions which are shown in part B. The distribution function parameters $(\tilde{\sigma}_\Delta,\sigma_\lambda,\lambda_0)$ are (0.20,2.3,7.3) and (0.02,0.82,16.2), respectively, where $\tilde{\sigma}_\Delta = \sigma_\Delta/\Omega_0$ and $\Omega_0 = 40\ cm^{-1}$. A value of 175[127] for $G$, the TLS–phonon coupling parameter, was used. Comparing the distributions of Figures 13 and 14 one observes that strong coupling leads to pronounced tailing to slower relaxation rates and that the tailing for the right-most distribution leads to the prediction that spectral diffusion should continue to times much longer than $\sim 10^4$ s. However, the assumption of strong coupling for this distribution may be questionable. It is obvious that a comparably good fit to the data could be obtained with strong and weak coupling for the distributions of faster and slower relaxation rates, respectively. Two further points are that strong coupling significantly reduces the value of $\lambda_0$, e.g., from 9.8 to 7.25 for the distribution of faster relaxation rates, and reduces the probability for the fastest relaxation rates ($\gtrsim$(lifetime)$^{-1}$).

Spectral diffusion can be understood (within the confines of the current model of spectral diffusion) in terms of the JSA TLS distribution functions under the assumption of either weak or strong TLS phonon coupling. For weak coupling, the log of normal functions for the distributions of the faster and slower relaxing TLS account well for the data. This is important because the JSA distribution functions have a physical basis. Thus, it is not necessary to utilize the phenomenological $P(R) \propto 1/R$ distribution function which cannot be expected to be sufficiently accurate at the extremes of the distribution. It has been emphasized that the JSA functions provide a vehicle for systematic testing of the standard tunneling model against data from a wide variety of measurements including specific heat,[121] thermal conductivity,[122] the gap in the $TLS_{int}$ density of states at very low temperatures,[98] the pure dephasing of impurity transitions,[122,119] NPHB growth kinetics,[28,151] and spontaneous hole filling.[151] Spectral diffusion can now be added to the list. The question is then whether the JSA distribution function parameter values determined here for spectral diffusion correlate with those of other physical properties. We consider first the distribution of slower relaxation rates, which for cresyl violet in ethanol-$d$ at 1.2 K $(\lambda_0,\sigma_\lambda) = (16.8,1.4)$. The large and relatively small values of $\lambda_0$ and $\sigma_\lambda$, respectively correlate well with those determined for spontaneous (in the dark) filling of nonphotochemical holes in three similar systems at comparable temperatures.[142,151] For example, $(\lambda_0,\sigma_\lambda) = (17.6,1.3)$ for cresyl violet in a poly(vinyl alcohol) (PVOH) film at 1.6 K[151]

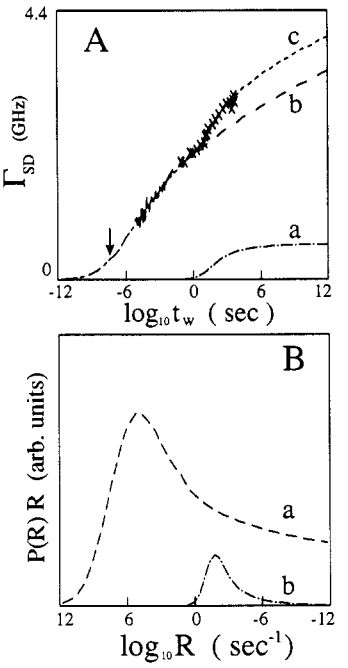


**Figure 14.** (A) Fit (curve c) to the experimental data of $\Gamma_{SD}$ (GHz) (of Littau and Fayer[113]) within the strong TLS–phonon coupling approximation with the faster ($TLS_{int}$; curve b) and slower ($TLS_{ext}$; curve a) distributions of relaxation rate. The arrow locates the excited-state lifetime. (B) $P(R)R$ versus log $R$ for strong TLS–phonon coupling. The distribution function parameters $(\tilde{\sigma}_\Delta,\sigma_\lambda,\lambda_0)$ are (0.2,2.3,7.3) and (0.02,0.82,16.2) for $TLS_{int}$ (curve a) and $TLS_{ext}$ (curve b), respectively. $G = 175$, $\Delta_0 = 0$ and $\Omega_0 = 7.6 \times 10^{12}\ s^{-1}$. Reprinted from ref 145. Copyright 1993 American Physical Society.

and $(\lambda_0,\sigma_\lambda) = (19,1.5)$ for oxazine 720 in glycerol at 1.6 K.[28] From refs 151 and 28 it is clear that for the efficient NPHB systems, cresyl violet in ethanol and PVOH, and oxazine 720 in glycerol and PVOH, that the above $\lambda_0$ values are far too high to be correlated with nonphotochemical hole growth (where $\lambda_0 \approx 9$–10) which involves phonon-assisted tunneling of the $TLS_{ext}$ triggered by electronic excitation of the chromophore. Spontaneous hole filling is most reasonably ascribed to $TLS_{ext}$ relaxation processes which occur with the chromophore in its *ground* state. It is important to note that the $TLS_{ext}$ coordinate(s) responsible for NPHB and hole filling is associated with a relatively strong interaction between the chromophore and the inner shell of hydrogen binding solvent molecules and, for the above systems, that it involves considerable amplitude of motion of the hydroxyl proton of the host. The latter follows from the fact that deuteration of the hydroxyl proton leads to a reduction of the average quantum yield for NPHB of well over 1 order of magnitude.[41,151] In sharp contrast, the pure dephasing is unaffected by deuteration[4] which strongly suggests that the $TLS_{int}$ coordinate(s) are due to spatially extended hydrogen-bonding networks of the host molecules occupying mainly the outer shell. This provides support for the diagonal modulation theory of Lyo[106,116] in which the pure dephasing is due to weak interactions of the chromophore with a sea of $TLS_{int}$.

In the earlier mentioned work on several physical properties, whose $T$ dependencies are dictated by *intrinsic* TLS, $\lambda_0$ and $\sigma_\lambda$ values in the range $\sim$6–7 and $\sim$3, respectively, were utilized for the $TLS_{int}$. As one example, it proved possible to understand, for several

inorganic glasses, why the temperature dependence ($T < 1$ K) of the thermal conductivity deviates from $T^{2-\mu}$ when the $TLS_{int}$ density of states is $\rho(E) = \rho_0 E^{\mu}$ (and the power law for specific heat is $T^{1+\mu}$).[28,122] The $T^{2-\mu}$ prediction of the standard tunneling model is a consequence of approximate averaging; e.g., the assumption that $\langle W^2 \rangle_E / E^2$ is independent of $E$. We note that the values of ($\lambda_0$, $\sigma_\lambda$, $\tilde{\sigma}_\Delta$) found to be suitable in ref 122 lead to $\mu \approx 0.2$–$0.3$ over about two decades of temperature $\lesssim 1$ K. Above $\approx 1$ K the density of states begins to decrease.

From the spectral diffusion data for cresyl violet in ethanol-*d* pertaining to the distribution of faster relaxing TLS it is found, for weak and strong coupling, that ($\lambda_0$,$\sigma_\lambda$) = (9.8,2.9) and (7.3,2.3), respectively, with $\tilde{\sigma}_\Delta = 0.20$ for strong coupling. These $\sigma_\lambda$ values are consistent with those determined earlier for $TLS_{int}$. (The fact that they are considerably larger than those for $TLS_{ext}$ is qualitatively understandable given the stronger interaction between the chromophore and inner shell solvent molecules.) For strong coupling, especially, the $\lambda_0$ value is similar to those determined earlier for $TLS_{int}$. We consider it reasonable, therefore, to assign the faster relaxing TLS as mainly $TLS_{int}$.

Finally we point out that the applicability of the basic equation used, eq 23, for spectral diffusion is limited to waiting times $t_W > 10\ \tau$,[4] where $\tau$ can be viewed as the total dephasing time $T_2$. For the systems studied then this means $t_W \gtrsim 10$ ns. Thus, our spectral diffusion results for shorter waiting times should only be considered as indicative.

## 4. Dispersive Nonphotochemical Hole Growth Kinetics

In this section we derive the expression, $D(t)$, which can be used to describe the dispersive kinetics of nonphotochemical zero-phonon hole growth.[28,151] As discussed in section II.3, the mechanism for NPHB recently proposed by Shu and Small[37,152] retains an essential idea of the earlier model.[26,27,34] It is that the rate-determining step for hole formation is phonon-assisted tunneling of $TLS_{ext}^{\beta}$ ($\beta$ denotes the impurity excited electronic state) and that the intrinsic disorder of the glass leads to a distribution of tunneling frequencies. However, the new model asserts that the tunneling is strongly biased toward processes that involve phonon emission.[37] That is, the excited-state energy (as well as the ground state) of the probe molecule for the postburn configuration is lower than that for the preburn configuration. The excited-state energy difference will be denoted by $E$. For a single $TLS_{ext}^{\beta}$ the downward phonon-assisted relaxation rate is[13,107]

$$R = (3f^2W^2E/16\pi\rho c^5\hbar^5)(\langle n_E \rangle_T + 1) \qquad (25)$$

where $E^2 = \Delta^2 + W^2$, $\Delta$ and $W$ are the asymmetry parameter and tunneling frequency, $\rho$ is the sample density and $c$ is an average sound velocity. The phonon thermal occupation number $\langle n_E \rangle_T = (\exp(E/kT) - 1)^{-1}$. The $f$ parameter is related to the $TLS_{ext}$ deformation potential.[13,107]

For the case where the antihole is significantly shifted away from the ZPL which are burned, the tunnel splitting $E$ may be replaced by $\Delta$, i.e. $\Delta \gg W$. It is generally assumed that $f$, $W$, and $\Delta$ are not correlated and that an average value for $f^2$ in eq 25 can be used.[13] Because the tunneling frequency w depends exponentially on the tunnel parameter $\lambda$, $W = \omega_0 \exp(-\lambda)$, and $\lambda$ depends on several parameters subject to statistical fluctuations due to disorder, it is reasonable to assume that the distribution of relaxation rates ($R$) should derive mainly from the distribution function for $W^2$.[118,119,153] Thus, we write

$$R = \Omega_0 \exp(-2\lambda) \qquad (26)$$

where $\Omega_0 = 3\langle f^2 \Delta \rangle \omega_0^2 / 16\pi\rho c^5 \hbar^5$. It has been argued that $\Omega_0 \approx \omega_0$ and that $\omega_0 \approx 20$–$80$ cm$^{-1}$ is a reasonable estimate, cf. section IV.3. Because $\lambda \geq 0$, $R_{max} = \Omega_0$. We define $f(R)$ as the normalized distribution function for the $TLS_{ext}$ relaxation rate so that with

$$D(t) = \int_0^{\Omega_0} dR\, f(R) \exp(-\sigma P \phi(R) t) \qquad (27)$$

$1 - D(t)$ is the fractional ZPH depth following a burn for time $t$ with a burn photon flux $P$. Here $\sigma$ is the peak absorption cross section for the ZPL and $\phi(R) = R/(R + k)$ is the NPHB quantum yield for a probe excited state lifetime of $k^{-1}$ (a few nanoseconds for laser dyes). Equation 27 is valid for a burn laser with frequency width much narrower than the homogeneous line width of the ZPL. A form for $f(R)$ is obtainable from the distribution function for $W^2$ (eq 6) which, in turn, is derivable from the distribution function for $\lambda$.

For the simulations it is convenient to employ a particular form for $D(t)$ which is equivalent to eq 27. Starting with

$$D(t) = [(\sqrt{2\pi})\sigma_2]^{-1} \int_{+\infty}^{-\infty} d\lambda \exp[-(\lambda - \lambda_0)^2/\sigma_2^2] \times \exp[-P\sigma\phi(\lambda)t] \qquad (28)$$

and defining $x = (\lambda - \lambda_0)/\sigma_2$, it is easy to show that

$$D(t) = (2\pi)^{-1/2} \int_{-\infty}^{+\infty} dx \exp(-x^2/2) \exp(-\Sigma_0\, \xi(x) t) \qquad (29)$$

where $\Sigma_0 \equiv P\sigma\Omega_0/k$ and $\xi(x) = \exp[-2(\lambda_0 - \sigma_\lambda x)]$. In deriving this equation it was assumed that for the majority of the $TLS_{ext}$,

$$\phi(R) = R/(R + k) \approx R/k \ll 1 \qquad (30)$$

This assumption, based on earlier studies which showed that average NPHB quantum yields are low ($<10^{-4}$ [142,153]), is readily tested by the experimental data.

Equation 29 has been successfully utilized for the simulations of the hole growth curves.[28,151] However, eq 29 neglects the contribution to dispersive growth associated with the utilization of linearly polarized burn and read beams.[154] Therefore, the effect of orientational averaging on the hole-growth kinetics, depending on burn and probe beams polarization, needs to be considered. In ref 28 it was demonstrated that the orientational averaging (the effect of polarization) has a weak effect on the hole-growth kinetic during the initial stages of burning (hole depth less than $\approx 50\%$ of the saturated depth). Its primary effect is to alter slightly the value of $\lambda_0$.[28]

From the fit of eq 29 to the experimental data (see below) the distribution parameters $\lambda_0$ and $\sigma_2$ are obtained and consequently the average value $\langle R \rangle = \Omega_0 \exp(-2\lambda_0) \exp(2\sigma_2^2)$. The dispersion provides an amplification for $\langle R \rangle$ over $R_0 = \Omega_0 \exp(-2\lambda_0)$, which is the relaxation frequency for a nondispersive system.[142] It

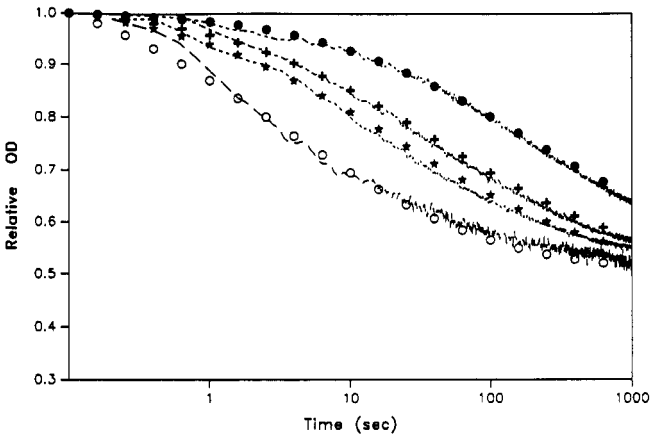


**Figure 15.** Hole growth curves of cresyl violet in PVOH at 1.6 K for different burn intensities, $I_B$ = 3, 15, 30, and 200 $\mu W/cm^2$ (from top to bottom). The dots, crosses, stars, and circles represent theoretical fits. For all simulations, a single set of parameters, $\lambda_0 = 9.85$, $\sigma_2 = 1.3$, $\Omega_0 = 10^{12}\ s^{-1}$, $\sigma = 2 \times 10^{-11}\ cm^2$, and $S = 0.7$, were used. The OD of sample is ~0.35 (at 632.8 nm, He–Ne line). Reprinted from ref 151. Copyright 1992 Optical Society of America.

also is instructive to consider $\langle R \rangle$ as a function of the fractional hole depth $\xi$, $\langle R \rangle_\xi$. A convenient formula for $\langle R \rangle_\xi$ is given in ref 28.

The expression for the fractional ZPH depth $1 - D(t)$, with $D(t)$ given by eq 29, does not take into account the linear electron–phonon coupling. The modifications necessary to do so are quite straightforward and include incorporation of the single-site absorption profile (ZPL plus one- and multi-phonon sidebands) and site excitation distribution function. For strong coupling ($S > 1$), the only reliable approach to the characterization of the dispersive kinetics would involve monitoring of the entire hole profile (ZPH plus phonon sideband holes). Interference from the antihole would have to be taken into account.[17] Furthermore, it would be necessary to study hole growth as a function of $\omega_B$ within the inhomogeneously broadened profile. Obviously, it is far simpler to study systems characterized by weak coupling. For such systems, the ZPH is not significantly interfered with by the phonon sideband holes up to the point of its saturation. An independent measurement of $S$ allows for the determination of the ZPL Franck–Condon factor $\exp(-S)$ (accurate for $\omega_B$ located on the low-energy side of the absorption origin profile[16]). In the absence of gross heterogeneity this factor is the maximum fractional ZPH depth. The Franck–Condon factor must also be taken into account in the calculation of the peak absorption cross section of the ZPL. Thus, knowledge of $S$ enables the relatively simple expression for $D(t)$ given by eq 29 to be utilized. The reader is referred to ref 28 for details and a lengthy description of the double-beam laser system used to obtain the growth kinetics.

As one example of the data obtained, Figure 15 shows hole-growth curves of cresyl violet in a poly(vinyl alcohol) film at 1.6 K from ref 150 for four laser burn intensities. The relative hole depth is the optical density difference, ΔOD, divided by the preburn OD; e.g., 0.6 corresponds to a 40% OD change. The symbols represent the theoretical simulations obtained with eq 3. As was pointed out by Kenney et al.,[28] knowledge of the Huang–Rhys factor $S$ is essential for such simulations, since the fraction of the absorption at $\omega_B$ (located on the low-energy side of the origin absorption band) is $\sim\exp(-S)$. From an analysis of the real phonon sideband hole we determined that $S$ = 0.5–1.0. The bottom growth curve of Figure 15 indicates that the ZPH saturates at a relative OD of ~0.5, which corresponds to an $S$ value of 0.7. Thus, for the simulations an $S$ value of 0.7 was used along with a value for $\sigma$ of $2.0 \times 10^{-11}\ cm^2$ at 1.6 K for which determination is described in ref 151. The value of $\lambda_0 = 9.9$ reported in this reference is for $\Omega_0 = 10^{12}\ s^{-1}$. Since a value of $\Omega_0 = 7.6 \times 10^{12}\ s^{-1}$ (40 $cm^{-1}$) was used in the two preceding subsections we note that for this value, $\lambda_0 = 10.9$ with $\sigma_\lambda = 1.3$ unaffected. With the same value for $\Omega_0$ the average value for the NPHB quantum yield is $4.6 \times 10^{-4}$.

Readers interested in the temperature dependence of the quantum yield and its connection with the NPHB mechanism of Shu and Small[37] are referred to ref 152.

## 5. Spontaneous Hole Filling (SPHF)

In this section we discuss the time-dependence of the filling of holes that occurs when the sample is maintained at the burn temperature for extended periods. The rate of filling is generally quite slow which explains why this phenomenon has received relatively little attention. In the reports which have appeared two types of behavior have been observed: (a) the holes decay logarithmically with time and broaden as they decay[45,129,154,155] and (b) the holes decay nonlogarithmically with time and hole widths not changing during the decay process.[28,151,156,157] The former behavior has been observed for both PHB (quinizarin in EtOH/MeOH)[45,29] and for NPHB (tetracene in EtOH/MeOH),[155] while the latter behavior has only been reported for NPHB systems (tetracene in MTHF,[156] Rh640, $Nd^{3+}$, $Pr^{3+}$, OX720, and CV in poly(vinyl alcohol) films[157,28,151]). At the end of this section we will return to a discussion of the two types of behavior observed. For now we concentrate on type b hole recovery.

The theory of dispersive kinetics used in the previous section to describe hole growth, has also been shown to be applicable to spontaneous hole filling (SPHF).[151] In this case, however, eq 29 becomes

$$D(t) = 2\pi^{-1/2} \int_{-\infty}^{\infty} dx \exp(-x^2/2) \exp[-\Omega_0 \xi(x) t] \quad (31)$$

with $1 - D(t)$ being the fractional filling at time $t$ following hole burning. As in section IV.2, $x = (\lambda - \lambda_0)/\sigma_\lambda$, but here $\lambda_0$ and $\sigma_\lambda$ are to be associated only with $TLS^{\alpha}_{ext}$ (where $\alpha$ indicates the ground state of the probe).

Elschner and Bässler[156] for tetracene in methyltetrahydrofuran reported that the hole-filling rate decreased with increasing hole depth. As pointed out by Shu and Small[151] this is clearly unsatisfactory as it would lead to $\lambda_0$ and $\sigma_\lambda$ being dependent upon the hole depth also. However, as Shu and Small showed, this phenomenon is dependent upon the method of data analysis. If relative hole filling is analyzed (i.e., $\Delta OD_{filling}/\Delta OD_{original}$), then indeed the observed rate is dependent upon hole depth due to correlation between the hole-burning rate and the hole-filling rate. Thus at short burn times (shallow holes) the sites burnt are those with the fastest rates, and due to correlation these

will also be the fastest to refill. Elimination of this artifact requires that the data be analyzed in terms of absolute hole filling (i.e., $\Delta OD_{filling}/\Delta OD_{100\%\ hole}$). Note that while it is not necessary to burn a 100% hole, it is necessary to know the strength of the electron–phonon coupling so that the depth of a 100% hole can be calculated. However, so that a large portion of the $TLS_{ext}^{\alpha}$ involved in hole refilling are sampled deeper holes provide a more reliable data set.

Having determined the appropriate manner of analyzing SPHF data, Shu and Small compared the values for $\lambda_0$ and $\sigma_\lambda$ determined for SPHF with those relevant to hole growth for cresyl violet in poly(vinyl alcohol). For hole growth they found $\lambda_0 = 9.9$ and $\sigma_\lambda = 1.3$ using a Huang–Rhys coupling factor, $S = 0.7$ (see section IV.4). These values lead to an average rate, $\langle R \rangle = 7.4 \times 10^4\ s^{-1}$ and an average quantum yield, $\langle \phi \rangle_{NPHB} = 4.6 \times 10^{-4}$. For SHF, fitting the data to eq 31 gives $\lambda_0 = 20.9$ and $\sigma_\lambda = 3.8$ which leads to $\langle R \rangle = 2 \times 10^6\ s^{-1}$, more than an order of magnitude larger than the value for NPHB! Such a discrepancy is not reconcilable within the standard $TLS_{ext}$ model for NPHB. However, if it is assumed that not all burned sites necessarily revert to absorption at the preburn frequency, then using $\sigma_\lambda$ (SPHF) = $\sigma_\lambda$ (NPHB) leads to $\lambda_0$ for SPHF equal to 16.6 and only 20% of burned sites capable of reverting to frequencies within the hole. Under these conditions $\langle R \rangle_{SPHF} = 0.1\ s^{-1}$.

It is noteworthy that burning of single molecule absorption lines has shown similar behavior, i.e., some burnt molecules spontaneously revert to their original absorption energy while others are not observed to return within the experimental time scale.[77,78]

Finally we conclude this section with some remarks on the differences between the results of Friedrich and Haarer et al.[129,154,155] and those of the Small[28,151,157] and Bässler[156] groups. The former have reported both for PHB (of quinizarin) and for NPHP (tetracene in ethanol/methanol) that hole filling occurs logarithmically with time and is accompanied by hole broadening. The latter two groups, on the other hand, report that the kinetics is dispersive and that the widths are constant. The primary experimental difference between these various reports are the time scales of the measurements. Friedrich and Haarer et al. have reported their results over a range of times from a few minutes up to $10^4$ min. Bässler's and Small's results have ranged from ~1 s up to ~$10^3$ or $10^4$ s. The absence of data for the shortest times (fastest rates) most likely obscures the dispersion in the data of Friedrich and Haarer, while the absence of data at very long times in the Small/Bässler data does not reveal hole broadening. Note that the data of ref 155 would be inconclusive regarding broadening if the data were truncated at 400 min, particularly for protonated tetracene.

### 6. Laser-Induced Hole Filling

The phenomenon of laser- or light-induced hole filling, LIHF, has received less attention than spontaneous hole filling. Two cases have been distinguished: that for which the secondary irradiation is at a frequency, $\omega_s$, which is not absorbed by the impurity and lies in the infrared[158,159] and that for which $\omega_s$ lies in the same electronic absorption band used for hole burning. These two types have been referred to as $LIHF_v$ and $LIHF_e$, respectively, with the subscript denoting (host) vibrational excitation and (probe) electronic excitation.[160] Here we focus primarily on $LIHF_e$, as it is this phenomenon that is most relevant to the concept of a well-defined $TLS_{ext}$ and to the mechanism of NPHB.

The most detailed previous study was that of Fearey et al.,[161] who reported on hole filling for the origin band of rhodamine 640 in PVOH at 1.6 K. It was found that the extent of filling for $\omega_s > \omega_B$ and that for either case the filling was essentially independent of the variation of optical density across the absorption band. In that paper, a mechanism involving global spectral diffusion of ZPLs produced primarily by $\omega_s$ excitation of sites not involved in the primary burn was proposed. However, this mechanism did not in any obvious way explain the independence of filling efficiency on optical density for $\omega_s > \omega_B$ or $\omega_s < \omega_B$. The possibility of an additional mechanism becoming operative for $\omega_s > \omega_B$ was not discounted.

More recently Shu and Small[160] presented a detailed study of LIHF for cresyl violet in PVOH. Two types of experiments were reported: a two-laser experiment for continuous monitoring of the filling of ZPH at $\omega_B$; and an experiment utilizing a Fourier transform spectrometer for probing of the total absorption at various times following hole burning at $\omega_B$ and $\omega_s$. The latter experiment had poorer time resolution but facilitated separating interference between ZPH filling and, e.g., decrease of absorption at $\omega_B$ due to overlap of the pseudo-phonon sideband hole associated with $\omega_s$. The following four observations were made by Shu and Small:[160] (i) filling of the ZPH at $\omega_B$ depends linearly on the fluence at $\omega_s$; (ii) filling is significantly more efficient for $\omega_s > \omega_B$ than for $\omega_s < \omega_B$; (iii) for both $\omega_s < \omega_B$ and $\omega_s > \omega_B$, filling efficiency is independent of $\omega_s$; and (iv) the ZPH at $\omega_B$ and its associated pseudo-PSBH fill in concert.

Coupled with the above observations was detailed information regarding the antihole for cresyl violet in poly(vinyl alcohol).[152] This antihole extends ~1000 $cm^{-1}$ to the blue of $\omega_B$. The width of the antihole, coupled with moderately intense real vibronic holes necessitates integrating the hole spectrum out to 5000 $cm^{-1}$ to the blue of $\omega_B$ in order to determine that overall absorption intensity is conserved in NPHB. Being spread over such a broad range makes the antihole difficult to observe except for hard burns. However, for chlorophyll *a* in the core antenna of photosystem I[36] the antihole is much narrower. Data for this system showed that as hole filling occurs, a corresponding diminution of the antihole intensity takes place.

All of these data lead to the following explanation for the increased LIHF efficiency for $\omega_s > \omega_B$. The hole filling is caused by electronic excitation of antihole sites by (primarily) phonon sideband transitions; i.e., sites not involved in the initial burn at $\omega_B$ are of no consequence. Hole filling is thus due to light-induced antihole reversion. Excitation of antihole sites through their phonon wing is a necessary condition of the model as a consideration of only antihole sites with ZPL coincident with $\omega_s$ would lead only to excitation of a small fraction of the total antihole sites. Within this model the increased filling at $\omega_s > \omega_B$ is a consequence of the antihole being blue-shifted from $\omega_B$ as observed

and explained in refs 37 and 152. Additionally, the width of the antihole[152] explains the absence of a strong dependence of the hole-burning efficiency on $\omega_s$. The observation that $\omega_s$ excitation of antihole sites leads to their being red-shifted (thereby filling the ZPH and PSBH) but that excitation of virgin sites leads to a blue-shifted antihole shows that antihole sites retain at least a partial memory of their preburn configuration. This suggests that the notion of a more-or-less well-defined extrinsic relaxation coordinate, $q_{ext}$, at a given burn temperature can be retained in hole-burning models that go beyond the standard $TLS_{ext}$ model.

We conclude this section with a consideration of the LIHF for $\omega_s < \omega_B$. In this region there is at most a weak dependence on $\omega_s$, even for excitation into the edge of the low-energy tail of the absorption. Since in this region there is no evidence for antihole sites, it has been suggested that the filling is due to optical excitation of high energy overtone and combination bands of the host.[161] Such bands would provide a weak, more-or-less uniform background absorption in the region of the probe's electronic absorption band.

## V. Hole Burning in External Fields

In this section we briefly discuss how the marriage of spectral hole burning with external electric (Stark) or magnetic (Zeeman) fields, hydrostatic pressure, ultrasound, and high frequency acoustic phonons can provide important information on the properties of the probe molecule, the probe–inner shell matrix interactions, microscopic compressibility, and new approaches for detection of the ZPH. Owing to the very narrow ZPH widths attainable at low temperatures, the ZPH enhances the effects of external fields by several orders of magnitude.

### 1. Electric Field Effects

The principles of Stark hole-burning spectroscopy of optical transitions of impurity centers were recently reviewed by Maier.[162] Detailed descriptions of experimental data and model calculations of electric field effects on persistent spectral holes have been presented for a variety of dye molecules in amorphous polymers.[54,162-174] In general, an electric field induces a frequency shift, $\Delta\nu$, of a line (Stark effect[162,169,175,176]) in the electronic spectrum of a molecule due to its interaction with the dipole moments and polarizabilities of the ground and excited states. The frequency shift is given by[162,169,171,175]

$$\Delta\nu(\vec{E}) = (1/h)(f\Delta\vec{\mu}_m\cdot\vec{E} + {}^1/_2 f^2\vec{E}\cdot\Delta\hat{\alpha}\cdot\vec{E}) \qquad (32)$$

where $\Delta\vec{\mu}_m = \vec{\mu}_e - \vec{\mu}_g$ is the difference of the permanent dipole moment vectors of the excited (e) and ground (g) states and $\Delta\hat{\alpha}$ is the difference of the polarizability tensors of the two states. The external field is given by $\vec{E}$. In eq 32 $f$ is the Lorentz local field correction given by $f = (\epsilon + 2)/3$, where $\epsilon$ is the dielectric constant. In an amorphous host with isotropic orientation of the impurity molecules, the Stark effect depends on the dipole moments and polarizabilities averaged over all possible molecular orientations.[162,164] Filling, broadening, and/or splitting of the ZPH may be observed experimentally, depending, in part, on the senses of the vectors associated with the external field and polarizations of the burn and read beams, vide infra.[162,163]

**Table II. Examples of Experimental Results for the Electric Dipole Moment Difference $|\Delta\vec{\mu}_m|$, the Effective Matrix-Induced Electric Dipole Moment Differences $|\Delta\vec{\mu}_{ind}|$, and the Angle $\gamma$, between $|\Delta\vec{\mu}_m|$ and the Transition Dipole Moment $\mu_{ge}$ of Several Guest Molecules in Amorphous Matrices from Hole-Burning Experiments at Low-Temperature (See Also Ref 179)**

| guest molecule | matrix | $\lvert\Delta\vec{\mu}_m\rvert$ (D) | $\gamma$ (deg) | $\lvert\Delta\vec{\mu}_{ind}\rvert$ (D) | ref(s) |
|---|---|---|---|---|---|
| resorufin | | 0.42 | 90 | 0.13 | 164, 165 |
| | | 0.2 | | | 179 |
| oxazine-4 | PVB[a] | 0.66 | 90 | 0.28 | 164 |
| cresyl violet | PVB | 2.1 | 28 | 0.9 | 164 |
| chlorin | PVB | 0.28 | | 0.10 | 166 |
| perylene[b] | PVB without $H_2O$ | | | 0.27 | 164, 167 |
| perylene[b] | PVB | | | 0.31 | 167 |
| perylene[b] | cellulose nitrate | | | 0.46 | 167 |
| tetracene | benzophenone | | | 0.35–1.2 | 176 |
| isobacteriochlorin | *n*-octane | 1.62 | | | 176 |
| chlorophyll *a* | PVB | | | 0.22 | 179 |

[a] PVB = poly(vinylbutyral). [b] For perylene, since the molecule has no electric dipole moment in the ground or excited states, a linear Stark effect is observed due to matrix induced electronic level shifts.[168]

In all measurements in amorphous solids reported to date (irrespective of molecular symmetry), a linear dependence of the electronic level shifts of the molecules on the electric field strength has been found. Thus, the second term in eq 32 will not be considered in what follows. For molecules with inversion symmetry the Stark effect has been attributed to the influence of the host matrix.[168] In this case, since the dipole moment is matrix induced, it is assumed that the transition dipole $\vec{\mu}_{ge}$ and the change in the dipole moment $\Delta\vec{\mu}_{ind}$ are not correlated.[172] However, correlation has to be considered for noncentrosymmetric molecules. Different types of correlation have been considered.[45,171,173] Changes of spectral holes of amorphous host–guests have been calculated for various combinations of senses for $\vec{E}$ and the wave vectors and polarization vectors of the burn and read light of the hole-burning laser light field, the probing laser light field, and the external electric beams.[173] When $|\Delta\vec{\mu}_m|$ dominates $|\Delta\vec{\mu}_{ind}|$, the spectral hole broadens or splits into two holes in the electric field, depending on the angle $\gamma$ between $|\Delta\vec{\mu}_m|$ and the transition dipole moment $\vec{\mu}_{ge}$ and the just mentioned field, wave vector, and polarization senses.[162,164,173] When $|\Delta\vec{\mu}_{ind}|$ dominates, the spectral hole broadens in the electric field and reduces in depth. In this case, the spectral hole shape and width are independent of the polarization directions of the light fields.[167,173] From an analysis of the dependence of the ZPH profile on the external electric field strength $|\Delta\vec{\mu}_m|$, the angle $\gamma$, as well as matrix-induced contribution $|\Delta\vec{\mu}_{ind}|$ can be determined.[164] Values of these three quantities determined from Stark hole-burning profiles and theoretical simulations for several systems are presented in Table II.

Kanaan et al.[167] demonstrated that the electric field effect for centrosymmetric dye molecules, like perylene, embedded in a complex matrix, e.g. in Langmuir–Blodgett films, can be used as a sensitive probe to get information on the effective matrix-induced electric dipole moment differences for different host matrices.

Table III. Pressure Shift and Pressure Broadening[a] of the ZPH with Increasing Pressure in Amorphous Solids ($T$ = 1.5 K)

| | | experiment | | | theory | | $\gamma^b$ | | |
|---|---|---|---|---|---|---|---|---|---|
| guest molecules | host matrix | $\delta$ (cm$^{-1}$/MPa) | $s$ (cm$^{-1}$/MPa) | ref | $s$ (cm$^{-1}$/MPa) | ref | exp | theory | ref |
| $H_2PC$ | PS | −0.22 ± 0.01 | 0.12 ± 0.01 | 190 | 0.12 ± 0.02 | 195 | 2.43 ± 0.22 | 1.97 ± 0.40 | 195 |
| | | −0.22 ± 0.01 | 0.12 ± 0.01 | 183 | | | (ref 190) | | |
| $H_2PC$ | PMMA | −0.17 ± 0.01 | 0.09 ± 0.01 | 183 | | | | | |
| $H_2PC$ | PE | −0.18 ± 0.01 | 0.06 ± 0.01 | 190 | | | 3.67 ± 0.69 | 4 ± 1 | 195 |
| | | | | | | | (ref 190) | | |

[a] Pressure shift $s = \Delta\Gamma(\Delta_p)/|\Delta p|$; pressure broadening $\delta = \Delta\nu(\Delta p)/\Delta p$; PE = polyethylene, PS = polystyrene, PMMA = poly(methyl methacrylate). [b] $\gamma = \Delta\Gamma(\Delta p)/\Gamma_s\kappa\Delta p$ describes the pressure broadening ratio.[192] $\kappa$ is the bulk isothermal compressibility of the solvent and $\Gamma_s$ is the experimentally measured full-width half maximum (FWHM) of the inhomogeneously broadened line.

Electric field effects have also found applications in optical storage (for hole readout).[52,170] It is also believed that the molecular systems with large Stark shifts and narrow hole widths are interesting candidates for frequency- and field-sensitive holographic storage devices.[54,174] Recently, Maier et al.[162] and Schwoerer et al.[177] have demonstrated a hybrid optical bistable device which is based on voltage-controlled changes of the absorption in the center of a persistent spectral hole. Finally, voltage-induced changes of spectral holes have already been used for pulse forming[170] and modulation of the laser light.[170,178]

## 2. Hydrostatic Pressure Effects

Spectroscopy at high pressures has also proven to be a very useful tool for the study of intermolecular interactions in the condensed phase.[180,181] Pioneering work by Drickamer and co-workers[181] showed that the investigation of electronic transitions as a function of pressure provides, e.g., information about the relative stabilization/destabilization of electronic states by intermolecular interactions, and the pressure dependence of vibrational transitions can reveal the perturbation of the vibrational potential of the electronic ground state by intermolecular interactions.

In the past the bulk of experimental and theoretical efforts has been directed to study the pressure induced red shifts (of the order of 0.2–0.6 cm$^{-1}$/MPa[180–182] of electronic transitions of the entire absorption band. More recently,[183–187] using high-resolution HB spectroscopy, inhomogeneous solvent effects may be studied in a more sensitive way.

Inhomogeneous broadening (see section II.1) is an indicator of the degree of structural disorder present in the system under study. HB and FLN spectroscopies belong to the most sensitive techniques for elucidating the influence of the environment on electronic transitions in impurities.[3,188,189] In high-pressure HB spectroscopy two types of experiments are in general performed. In the first type, after the hole is burned the external hydrostatic pressure is changed;[183,190,191] the second involves burning and recording the spectral holes under the same fixed physical conditions.[184] In the first case spectral holes exposed to hydrostatic pressures experience a line shift and a broadening.[186–188,191] In the second case, narrowing of spectral holes by nearly a factor of 2 at 510 MPa (for chlorin molecules embedded in PS matrix) and an incomplete restoration of the widths ($\Gamma_{hom}$) of the holes burned at normal pressure after pressure cycling was observed.[184]

The above hole-burning experiments provide more sensitive probes of the pressure dependence of inhomogeneous solvent effects than studies which focused on the pressure dependence of the entire band, for several reasons.[190,192,193] First, because of the narrow hole widths (~$10^{-2}$ cm$^{-1}$), the pressure necessary to produce detectable changes may be orders of magnitude smaller[190] than the pressure necessary to shift detectably the entire inhomogeneously broadened absorption band.[187,188] Second, the degree to which the holes are broadened is a good indication of the degree of microscopic disorder in the amorphous structure and provides information that is not obtainable from the previous studies.[192] A simple theory, which predicted a pressure dependence of the frequency shift of the spectral holes and their broadening in reasonable agreement with the experimental data was described by Haarer and co-workers.[183,190] A fully statistical microscopic theory of pressure effects on spectral holes and of the inhomogeneous line shape itself, was recently developed by Laird and Skinner.[195,196] Their theory predicted that the pressure induced hole width is frequency dependent, i.e., that it depends on where in the inhomogeneous line the hole is burned.[195,196] In addition, the theory[195] predicts that both the inhomogeneous line shape and the hole shape after a pressure change will be Gaussian, in qualitative agreement with experiment. Experimental data for the pressure broadening parameter $\gamma$ for $H_2Pc$ molecule in PS and PE matrices,[190] which are 2.43 ± 0.22 and 3.67 ± 0.69, respectively, are compared in Table III with the theoretical values which are 1.97 ± 0.40 and 4 ± 1, respectively.[195] In addition, Table III provides pressure shift ($s$) and pressure broadening ($\delta$) of the ZPH with increasing pressure for $H_2PC$ in several host matrices (e.g., PS, PE and PMMA). Comparison of the experimental results with theoretical calculations for $s$ and $\gamma$ (see Table III) demonstrates that the theory of Laird and Skinner is general enough to predict the results of the pressure-tuning experiments, as well as the inhomogeneous line shape itself.[190,195] The theory of Laird–Skinner has been recently extended by Kador[197] beyond the Gaussian approximation. In his model, Kador calculated pressure effects on hole-burning spectra in glasses in a semianalytical fashion without using this approximation. It turned out that not only the pressure shift but also the pressure broadening of HB spectra increases from the blue to the red of the absorption band. Moreover, HB spectra are predicted to become asymmetric when the sample is exposed to hydrostatic pressure. Although experimental studies are in good agreement with the Gaussian approximation, more experimental data is required to test these predictions.

However, for sufficiently high pressures (≳500 MPa) depending on the prepressure, i.e., the pressure applied

to the polymer sample before hole burning, the changes in hole width may be irreversible.[184] This could indicate that in soft polymeric matrices irreversible or post-pressure effects may be present. Possible mechanism(s) of recently observed line narrowing of the spectral holes burned at high pressure as compared with the results obtained at normal pressure are discussed in ref 184. Very recently, nonlinear color effects in the pressure-induced broadening of a spectral hole burned into resorufin-doped alcohol glasses were also observed.[186,187] These observations were explained in terms of correlation between dispersive and electrostatic forces.

Although, more studies on different host polymer/(and/or glass/)guest molecule systems are necessary to establish the physical mechanisms of the pressure effects reported so far, it has been already established that pressure tuning of spectral holes can provide a more detailed insight into the microscopic interactions between a probe and its surroundings and can yield information on structural disorder.[183,184,186-188,190-193,195-197] The study of a physical property as a function of pressure and temperature, rather than temperature alone, should provide the data required for a better understanding of the molecular dynamics in disordered solids. It is also believed that application of high-pressure hole-burning spectroscopy to proteins and/or macromolecules will become a very valuable method for investigation of many biochemical problems at the molecular level. For example, very recently, the compressibility and volume fluctuations in proteins (e.g., horseradish peroxidase and myoglobin) were measured by hole-burning spectroscopy.[192,193]

### 3. Other Field Effects

Magnetic effects, utilizing hole-burning spectroscopy, have been studied in various crystalline[198] and organic amorphous systems (for reviews, see refs 52 and 162). From the shift of spectral holes due to the quadratic Zeeman effect the matrix element of the angular momentum operator $L_z$ between the excited singlet states can be derived. In organic glasses where the orientation of the molecules with respect to the magnetic fields is random, in addition to shift a broadening phenomenon is observed.[199,200] The small shifts are visible, due to the high resolution of HB, where a sharp ZPH serves as a frequency marker in the broad absorption band. From the hole shape in magnetic fields, the change in magnetic susceptibility of the molecule in a magnetic field on excitation to its lowest excited singlet state, and the matrix element $\Lambda = |\langle S_1|L_z|S_2\rangle|$ of the effective orbital angular momentum between two lowest excited singlet states $S_1$ and $S_2$, could be determined.[201,202] In general, Zeeman shifts of the order of $10^{-4}$ to $10^{-3}$ of $\Gamma_{inh}$ are not observed. It has been shown, for example, that the change of magnetic susceptibility $^1/_2\,\chi^{z'z'}$ of free-base porphin in polyethylene is 60.6 MHz/$T^2$,[203] in good agreement with the value previously found for the same molecule in a crystalline host.[203] From

$$\chi^{z'z'} = 2\beta^2\Lambda^2/(E_2 - E_1) + \chi_D \qquad (33)$$

where $\beta$ is the Bohr magneton and $\chi_D = -17 \pm 5$ MHz/$T^2$ [203] is the diamagnetic effect resulting from the Larmor precession of the electrons in the field, one can easily obtain the value of $\Lambda = 5.64 \pm 0.06$.[202] It has been shown that magnetooptical studies provide valuable information on the magnetooptical properties, and the interaction between the lowest excited singlet states of complex molecules not only in single crystal hosts but also in disordered materials.[199] For example, Ulitskii et al.[204] have analyzed the hole profile and its dependence on an external magnetic field for molecules with a doubly degenerate $S_1$ level. From these measurements the static magnetic moment in the degenerate $S_1$ state (for zinc phthalocyanine (Zn-Pc) in poly(vinylbutyral) (PVB)) at $T = 4.2$ K was obtained. Magnetic field hole-burning experiments also allow determination of an average value of the relatively small Jahn-Teller splitting[204] which otherwise cannot be observed in disordered systems due to the large inhomogeneous broadening.

Spectral holes can be also detected using phase-sensitive ultrasonic modulation.[194] This method, developed by Moerner and Huston, offers zero background and the potential for high-speed detection with sensitivity near the quantum limit. It also has been demonstrated that prolonged exposure to ultrasound causes erasing and modulation of holes. Thus, an optical measurement of the hole depth provided a method of monitoring the ultrasound in solids.[205]

Investigations of the influence of phonons on spectral holes were also carried out, by either heating the sample or generating phonons with a heat-pulse technique.[206] Two types of phonon detection have been demonstrated, real-time phonon detection[206] and phonon memory.[207] In the first type, the filling of the persistent spectral holes is by heat-pulse phonons which are radiated to the sample simultaneously with the detecting laser light. The phonons give rise to changes of the spectral hole depth which follow instantaneously the changes of the phonon pulses with time. This method is used for real-time broad band phonon detection which is comparable to phonon detection by a bolometer.[203] In the second type of experiment a heat pulse generates phonons in the dark pause between laser pulses causing a partial filling of the spectral holes. Since, after phonon irradiation the hole does not recover to its original value, information on the effect of the phonons can be stored and detected later by switching on the laser and measuring the hole depth. Phonon-induced filling of the spectral holes has been explained by phonon processes in which barriers of the double-well potentials are crossed.[207]

## VI. Applications of Spectral Hole Burning to the Photophysics of Biological Systems

During the past decade it has become apparent that laser-based line-narrowing spectroscopies are generally applicable to proteins and nucleic acids containing bound chromophores. In this section we will review some of the more recent applications of hole burning to antenna and reaction center complexes of the photosynthetic unit and hemeproteins. Readers interested in the application of the companion technique, fluorescence line narrowing, to the problem of DNA damage from covalent binding to carcinogenic metabolites, such as those from the infamous chimney sweep carcinogen benzo[a]pyrene, can refer to a recent review article by Jankowiak and Small.[189] Covalent binding

**Table IV. Recent Applications of Hole Burning to Primary Donor State of Reaction Centers**

| major results | ref(s) |
|---|---|
| Purple Bacteria (*Rps. viridis, Rb. sphaeroides*) | |
| large absorption width of P870/P960 due to $\Gamma_I$ and strong electron–phonon coupling ($\Gamma_{ep}$) | 16 |
| observation of weak ZPH for P870/P960 yields $P^*$ lifetimes in agreement with time domain values; no ultrafast electronic relaxation (<100 fs) of $P^*$; thermalization of relevant phonons precedes charge separation | 220,221 |
| observation of special pair intermolecular marker mode progression ($\omega_{sp}$ = 115/135 cm$^{-1}$; $S_{sp}$ = 1.5/1.1): significant geometry change for special pair in $P_-$ state. | 222 |
| moderately strong coupling of P870*/P960* to protein phonons ($\omega_m \sim$ 25–30 cm$^{-1}$, $S \approx 2$) | 223 |
| marker mode and protein phonons of $\omega_m \approx$ 25–30 cm$^{-1}$ must be important contributors to reorganization energies of primary charge separation | 7 |
| Photosystem I | |
| broad ($\sim$300 cm$^{-1}$) hole for P700 with no intrinsic structure, no ZPH | 224 |
| $\lambda_B$-dependent spectra yield $\Gamma_I \approx$ 100 cm$^{-1}$, $S \approx$ 4–6 for $\omega_m \approx$ 35–50 cm$^{-1}$ (strong coupling) | 224 |
| zero-point level of P700* at $\sim$710 nm, 1.6 K; predicted fluorescence maximum at $\sim$718 nm, 1.6 K | 224 |
| strong linear electron–phonon coupling for P700* is strong evidence for P700 being a special pair | 224 |
| Photosystem II | |
| P680 yields structured hole profile with resolved ZPH and phonon sideband holes ($\omega_m$ = 20 cm$^{-1}$, $S \approx 1$, $\Gamma_I \approx$ 105 cm$^{-1}$) | 225 |
| P680* lifetime is 1.9 ± 0.2 ps at 4.2 K (with and without TX-100 in glass) | 225,226 |
| absorption and hole spectra for Seibert and Yocum preparations are very similar | 227 |
| special pair marker mode progression not resolved for P680; needs further study | 225 |

**Table V. Recent Applications of Hole Burning to Accessory Pigments of Reaction Centers**

| major results | ref(s) |
|---|---|
| Purple Bacteria (*Rps. viridis, Rb. sphaeroides*) | |
| low-energy shoulder of BChl monomer absorption band is $P_+$ of special pair | 223,7 |
| $Q_y$ bands of BChl and BPheo monomers largely homogeneously broadened due to $\sim$30 fs downward energy transfer, 4.2 K | 222 |
| Photosystem II | |
| Chl $a$* lifetime due to energy transfer is 12 ps, 1.6 K | 227 |
| active Pheo $a$* lifetime is 50 ps at 1.6 K (due, presumably to energy transfer to P680) | 227 |
| zero-point level of Pheo $a$* lies only $\sim$25 cm$^{-1}$ above that of P680* at 4.2 K | 227 |
| TX-100 disrupts downward energy transfer from accessory Chl $a$ | 226 |
| electron–phonon coupling for accessory pigments is weak ($S < 1$), $\Gamma_I \approx$ 100 cm$^{-1}$ | 225 |

is the first critical step in mutagenesis and carcinogenesis and fluorescence line narrowing is now the most powerful tool available for detailed studies of macromolecular DNA–carcinogen adducts. Fluorescence line narrowing has also been used by Vanderkooi and co-workers[208–211] to provide detailed vibronic structural data on porphyrins in heme proteins.

## 1. Reaction Center and Antenna Protein Complexes

The structure that underlies the broad ($\sim$100–500 cm$^{-1}$ at 4.2 K) absorption profiles of the photocatalytic excited state ($Q_y$) of chlorophylls and pheophytins is relevant to the energy- and electron-transfer dynamics of photosynthetic units, e.g., temperature dependence, dispersive kinetics, coherence effects. Spectral hole burning has proven to be an important and versatile tool for the determination of such structure (for recent reviews, see refs 5–7). The burn wavelength dependence of the hole profile yields the magnitudes of the site inhomogeneous broadening ($\Gamma_I$) and homogeneous broadening ($\Gamma_H$) contributions to the $Q_y$ absorption profile. Studies of many protein complexes have yielded $\Gamma_I \approx$ 50–200 cm$^{-1}$, depending on the complex and $Q_y$ band. Given the normal glasslike heterogeneity of the protein,[212,213] most of $\Gamma_I$ is intrinsic, rather than solvent- or detergent-induced. That is, it is the existence of a large number of conformational substates of the protein[214] that leads to a broad distribution of transition frequencies. An important contributor to $\Gamma_H$ is the linear electron–phonon coupling ($\Gamma_{sp}$). On the basis of hole burning studies on complexes of purple bacteria, cyanobacteria, green algae, and photosystem I and II of green plants it is clear that coupling to a broad distribution of protein phonons with a mean frequency of $\omega_m$ = 20–30 cm$^{-1}$ is ubiquitous.[6,7] Furthermore, the coupling strength is weak ($S < 1$) for antenna chlorophylls and moderately strong ($S \approx 2$) for the special pair or primary donor state of reaction centers. For antenna protein complexes characterized by structural subunits containing strongly exciton-coupled chlorophylls, the contribution to $\Gamma_H$ from exciton level structure/ultrafast inter-exciton level relaxation can be very significant,[215–219] vide infra. Tables IV–VI summarize the protein complexes that have been recently studied along with principal findings.

To illustrate the power of hole burning we will first present very recent photochemical hole-burned spectra of the bacteriochlorophyll (BChl) special pair or primary electron donor state $Q_y$ band, P870, of *Rhodobacter sphaeroides*.

The two BChl monomers of the special pair (P) are closely juxtaposed with their pyrrole rings (I) overlapping at an average macrocycle separation of $\sim$3.3–3.5 Å. Rings I of the two monomers are essentially perfectly overlapped with the $Q_y$-transition dipoles making an angle of 139°. It is the lowest excited $\pi\pi^*(Q_y)$ state of P,P*, that is the primary electron donor state. This state is also designated as $P_-$ because the structure of the special pair mandates that it is the antisymmetric linear combination of the localized excitations, $P_MP_L^*$ and $P_M^*P_L$, within the excitonic dimer model. The

**Table VI. Recent Applications of Hole Burning to Antenna Protein Complexes**

| major results | ref(s) |
|---|---|
| Base-Plate Complex of *P. aestuarii* | |
| structured absorption spectrum's resolved bands ($Q_y$) are connected (communicate) via excitonic interactions of 7 BChl *a* molecules in subunit; upper exciton levels undergo ultrafast downward scattering via Davydov mechanism | 228 |
| improved $\lambda_B$-dependent hole spectra identify 8 $Q_y$ states: excited state electronic structure must be interpreted in terms of a $C_3$ trimer of subunits | 219 |
| upper exciton levels decay in ~100 fs | 219 |
| Antenna Complex of *Rb. sphaeroides* | |
| B800 of B800–850 complex largely inhomogeneously broadened, $\Gamma_I \approx 170$ cm$^{-1}$, coupling to protein phonons weak ($S \leq 0.5$) | 229,218 |
| B800* lifetime at 1.6 K is 2.4 ps | 229,218 |
| above lifetime due to B800 → B850 Förster transfer (750 cm$^{-1}$ vibration most important) | 218 |
| B850 and B875 largely homogeneously broadened due to exciton level structure and ultrafast inter-exciton level scattering, $\Gamma_H \approx \Gamma_{ex} \approx 200$ cm$^{-1}$: temperature-dependence of B800 → B850 ET explained | 215 |
| "shuttle" states B870 and B896 identified and assigned as the lowest (weakly absorbing) exciton levels of the B850 and B875 exciton bands; B896 undergoes dephasing in ~3 ps at 4.2 K due to exciton-defect (from heterogeneity) scattering | 217 |
| strongest vibronic absorption band corresponds to the 750-cm$^{-1}$ mode with a Franck–Condon factor of 0.05 (others also measured) | 216 |
| Core and PSI-200 Complexes of Photosystem I | |
| high-resolution frequency and Franck–Condon factor analysis of intramolecular vibrations for Chl *a* and Chl *b* | 36 |
| absorption bands severely inhomogeneously broadened, $\Gamma_I \approx 200$ cm$^{-1}$, weak electron–phonon coupling ($S \approx 0.8$, $\omega_m \approx 20$ cm$^{-1}$) | 36 |
| no obvious manifestations of excitonic effects in hole spectra | 36 |
| exceedingly narrow ZPH (~0.03–0.06 cm$^{-1}$) with TX-100 in the glass: energy transfer at 1.6 K markedly slower than at room temperature (effect of TX-100?); needs further study | 36 |
| Phycobilosomes (of *Mastigocladus laminosus*) | |
| sharp ZPH (1–2 cm$^{-1}$) for phycocyanin (PC), ~16-ps decay due to downward energy transfer at 4.2 K | 231 |
| broad low-energy satellite holes observed for phychoerythrocyanin and allophycocyanin absorption bands for excitation of PC: broadness is the result of inhomogeneous broadening and uncorrelated energy | 231 |

**Table VII. Structure of P870 and P960[a,b]**

| | $\omega_{sp}/S_{sp}$[c] | $\omega_m/S$ | $\Gamma$ | $\Gamma_I$ |
|---|---|---|---|---|
| P960 | 135/1.1 | 25/2.1 | 40 | 120 |
| P870 | 115/1.5 | 30/2.2 | 30 | 170 |

[a] From ref 238. [b] Units of $\omega_{sp}$, $\omega_m$, $\Gamma$, and $\Gamma_I$ are in cm$^{-1}$. [c] Homogeneous width of the ZPL for the marker mode level $\omega_{sp}$ is 50 cm$^{-1}$ and $j \times$ (50 cm$^{-1}$) for the $\omega_{sp}^j$ ($j \geq 2$) levels. [d] One-phonon profile on low- and high-energy sides is a Gaussian and Lorentzian, respectively, cf. ref 238.

upper dimer component is then $P_+$. The subscripts M and L designate protein subunits. The RC possesses a pseudo-$C_2$ symmetry axis that extends from P to the nonheme Fe. The other cofactors are, in order of proximity to P, $BChl_M$ and $BChl_L$, then $BPheo_M$ and $BPheo_L$ and, finally, the two quinones ($Q_{M/L}$). The results were obtained with a new apparatus that has resulted in a 20-fold improvement in signal to noise ratio relative to previously reported spectra. The main objectives of the studies were to further test certain assumptions and the values of the theoretical parameters used in previous work and simulations of the hole spectra and to generate data pertinent to the question of dispersive kinetics for the primary charge-separation process.[232]

Earlier studies, which are reviewed in ref 7, established that the absorption transition to P870* (asterisk denoting lowest excited $Q_y$-dimer state of the special pair, i.e., the primary electron-donor state) couples quite strongly to a ~120 cm$^{-1}$ mode with an $S$ value of 1.5. This mode was assigned as an *intermolecular* mode of the special pair since the largest $S$ value for the *intramolecular* modes of Chl monomers is ~0.05.[36] In the uppermost row of Table VII the frequency and $S$ value are denoted as $\omega_{sp}$ and $S_{sp}$ (sp means special pair intermolecular "marker" mode). For the protein phonons, $\omega_m = 30$ cm$^{-1}$ and $S = 2.2$. The values for P960*, the analogous state for *Rhodopseudomonas viridis*, are given in the second row of Table VII. Some of the dynamical implications of these results are reviewed in ref 7. For example, it was argued that, along with the ~30 cm$^{-1}$ phonons, the marker mode should be an important contributor to the reorganization energy associated with the initial phase of charge separation as well as the temperature dependence[233] of this separation. On the other hand, it was suggested that the marker mode is not a *promoting* mode for charge separation since, if it were, it would lead to a ctnh($\hbar\omega_{sp}/2kT$) dependence for the kinetics, in sharp contrast to the findings that[233] the kinetics for *Rb. sphaeroides* and *Rps. viridis* speed up by a factor of 2 and 4 as the temperature is reduced from room temperature to 10 K. Another finding was that[220] the zero-phonon hole (ZPH) widths of P870 and P960 yielded P870* and P960* decay times equal, within experimental uncertainty (±0.2 ps), to those measured in the time domain in the low-temperature limit.[233] This is important because the ZPH measures decay from the total zero-point level of P*, whereas, in the time domain measurements, it is the marker and phonon modes that are predominantly initially excited. The agreement in the decay rates indicates that thermalization of the relevant low frequency modes precedes charge separation, an assumption in most of the widely used electron-transfer theories.[234]

Until recently,[232] the data from hole burning had not been used to theoretically address any facet of charge separation. Hayes et al. simplified the usual nonadiabatic expression for the electron-transfer rate to a form valid in the strong electron–phonon coupling limit. As a result, they were able to study the effect of a distribution of values (stemming from normal glasslike structural heterogeneity) for the relevant P*-charge-separated state energy gap on the $T$ dependence of primary charge separation. Their work also examined

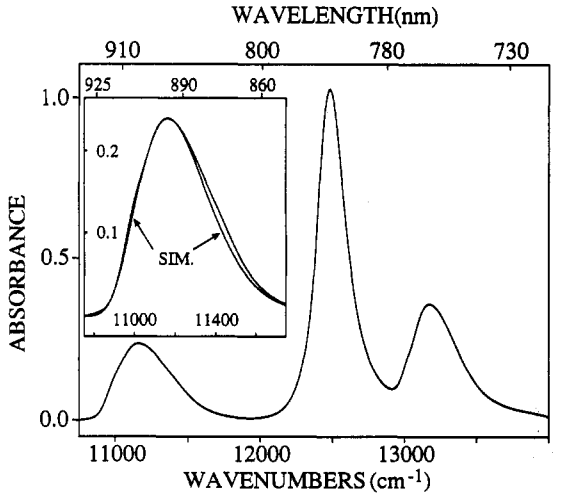


**Figure 16.** Absorption spectrum at 4.2 K of the $Q_y$ region of protonated RC of *Rb. sphaeroides* (R-26 strain). Inset shows simulation of P870 (FWHM = 437 $cm^{-1}$) with parameter values listed in Table VIII. Reprinted from ref 238. Copyright 1992 American Chemical Society.

whether or not the distribution was sufficiently broad, relative to the "homogeneous width" of the phonon nuclear factor associated with electron–phonon coupling, to yield P* decay kinetics sufficiently dispersive to account for the nonexponential kinetics recently reported for P870* at room temperature.[235,236] With regard to the last question they concluded that it was not. It was suggested that perhaps a distribution of values for the pure electronic coupling matrix element $V$ is responsible for the nonexponentiality. The improved quality of our photochemical hole-burned spectra have allowed us to explore this possibility.[237,238] In these works burn irradiation (line width = 0.03 $cm^{-1}$) was provided by a Coherent 899 Ti:Sapphire CW ring laser pumped by 15 W of the visible multiline output of a Coherent Innova $Ar^+$ laser. Typical output at 870 nm was 200 mW, which was reduced to 10 $mW/cm^2$ with a variable neutral density filter to keep bleaching of the P870 band maximum at 4.2 K below 20%. Bleaching of up to 60% was possible with higher intensities. Absorption and photochemical hole-burned spectra over the range 8 750–24 000 $cm^{-1}$ were taken at 2-$cm^{-1}$ resolution with a Bruker IFS 120 high resolution Fourier transform (FT) spectrometer. Hole spectra are defined as the difference in absorbance with the burn laser on and off.

Figure 16 shows a 4.2 K absorption spectrum of the $Q_y$ transition region of the *Rb. sphaeroides* reaction center (R26) for a high quality sample. The FWHM of P870 (the lowest energy band) is 440 $cm^{-1}$ which is about 40 $cm^{-1}$ sharper than in the highest quality spectra previously reported. Figure 17 shows 3 of the 10 PHB spectra obtained with $\omega_B$ values that span the entire inhomogeneous distribution of ZPL transition frequencies. The slightly smoother spectra marked with an $S$ are simulated using the theory described in section II.2. The 10 PHB spectra and the absorption profile of P870 were fit simultaneously which led to the values given in Table VIII for the theoretical variables (results for the deuterated reaction center are also given). From the spectra, see inset of Figure 17, one sees that it is the region in the vicinity of the quite highly Franck–Condon-forbidden ZPH that presents the greatest difficulty. Lyle et al.[238] conclude that this is due to the

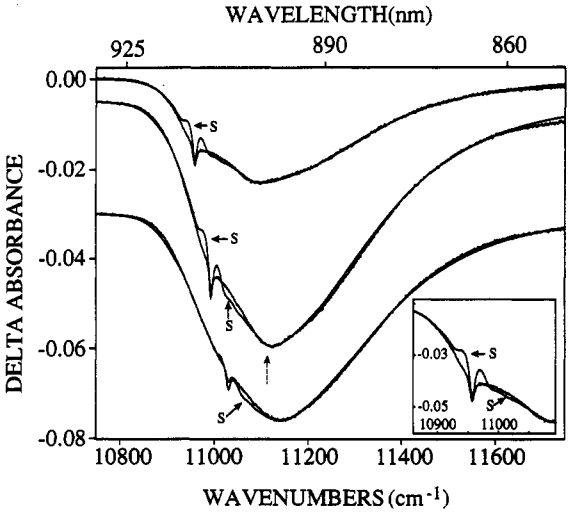


**Figure 17.** PHB spectra of P870 (protonated, R-26) for $\omega_B$ = 10 921, 10 992, and 11 039 $cm^{-1}$ (top to bottom), $T$ = 4.2 K. Simulations (S) of these spectra were obtained with the parameter values of Table VIII. The dashed arrow indicates the position where the satellite ZPH of $\omega_{sp}{}^1$ would occur if the marker mode were not damped, cf. text. The inset is a blowup of the region around the ZPH for the upper spectrum. Reprinted from ref 238. Copyright 1993 American Chemical Society.

**Table VIII. Structure of P870[a]**

| P870 | $\omega_{sp}/S_{sp}$[b] | $\omega_m/S$ | $\Gamma$[c] | $\Gamma_1$ | $\nu_m$ | $\Gamma_{ZPH}$ |
|---|---|---|---|---|---|---|
| protonated | 120/1.5 | 30/1.8 | 42.5 | 150 | 10992 | 11.5 ± 1.0 |
| deuterated | 115/1.5 | 30/2.0 | 42.5 | 130 | 10992 | 11.5 ± 1.0 |

[a] Units of $\omega_{sp}$, $\omega_m$, $\Gamma$, $\Gamma_1$, $\nu_m$, and $\Gamma_{ZPH}$ (zero-phonon hole width) are in $cm^{-1}$. [b] Homogeneous width of the ZPL for the marker mode level $\omega_{sp}$ is 50 $cm^{-1}$. Widths for the $\omega_{sp}{}^j$ ($j \geq 2$) are $j \times$ (50 $cm^{-1}$) [a Fermi–Golden rule prediction with cubic anharmonicity]. [c] One-phonon profile on low- and high-energy sides is a Gaussian (half-width = 15 $cm^{-1}$) and Lorentzian (half-width = 27.5 $cm^{-1}$), respectively.

existence of anomalous low frequency protein modes which are disorder induced. We note that the dashed arrow in the middle spectrum locates where the $\omega_{sp}'$ satellite hole would appear if the damping of the marker mode level was sufficiently reduced below 50 $cm^{-1}$, cf. Table VIII.

For the protonated and deuterated RCs, P870 ZPH widths were measured at 4.2 K for 10 and 9 $\omega_B$ values that spanned the range 10 921–11 049 and 10 921–11 068 $cm^{-1}$, respectively. From Table VIII it can be seen that these ranges encompass the distribution of ZPL excitation frequencies for the total zero-point level. For all $\omega_B$ values the quality of the spectra was comparable to those of the spectra in Figure 17. Examples of the ZPH profiles used for analysis are given in Figure 18. For both the protonated and deuterated RC the ZPH width did not show any dependence on $\omega_B$; the widths for both are 11.5 ± 1.0 $cm^{-1}$, corresponding to a P870* lifetime of 0.93 ± 0.10 ps at 4.2 K. Thus, primary charge separation is not affected by deuteration. It was also shown that the P870* lifetime is independent of temperature between 1.8 and ~10 K. On the basis of the time domain measurements of the temperature dependence of the P870* lifetime (10 K to room temperature)[223] and theoretical analyses[232,239] one would expect a weak (at best) dependence for $T$ < 10 K. Nonetheless, the results of ref 227 are the first to establish that this is the case.

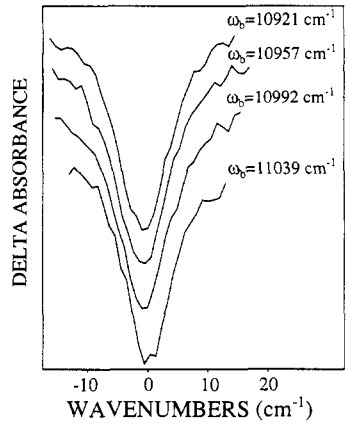


**Figure 18.** Four representative ZPH profiles for the protonated RC, $T = 4.2$ K. These profiles plus six others yielded a ZPH width of 11.5 ± 1.0 cm$^{-1}$ (95% confidence limit). The fits to the profiles are not shown as they would be indistinguishable from the experimental profiles. Reprinted from ref 238. Copyright 1993 American Chemical Society.

The invariance of the P870* lifetime to excitation frequency within the inhomogeneous distribution of ZPL frequencies cannot, by itself, be interpreted as meaning that nonexponential decay kinetics for P* could not arise from a distribution of values for the coupling matrix element $V$. The reason is that the inhomogeneous ZPL absorption frequency distribution depends on the distribution functions for the ground- and excited-state energies ($E$,$E^*$) of the special pair, $f_P(E)$ and $f_P(E^*)$, and the extent/type of correlation between them.[240] Noting that at any given value of $E$ of $P$ there is a high degree of accidental degeneracy, an absence of correlation means that $\Gamma_I$ of P870 is the width of $f_P(E^*)$ and, furthermore, that at any excitation frequency one essentially samples the entire ensemble of RCs, i.e., all possible $V$ values. At the other extreme there is perfect positive or negative correlation. In this case the width of $f_P(E^*) < \Gamma_I$ of P870 and, also, different excitation frequencies would sample different subsets of the RC ensemble and, therefore, also different parts of the $V$ value distribution. The actual situation may lie between these two extremes. However, the above negative result, when viewed in concert with two other recent findings, leads to the conclusion that a distribution of $V$ values is unlikely to be the source of the nonexponential decay of P870*. The first finding, from $\omega_B$-dependent PHB spectra of the RCs from *Rps. viridis* and *Rb. sphaeroides*, is that the site excitation energies of $P^*$($P_-$) and $P_+$ (the upper excitonic dimer component of the special pair) are *positively correlated*.[223] The second finding is a very recent one,[241] and it is that a significant, persistent photoinduced structural transformation of the special pair has been observed that shifts the upper and lower dimer components to the blue and red, respectively, by ~150 cm$^{-1}$ in *Rps. viridis*. This *negative correlation* is consistent with the simple excitonic dimer model. Thus, the above positive correlation establishes that the inhomogeneous broadening of P870 (P960) is due primarily to statistical fluctuations in protein structure around the cofactors rather than a distribution of special pair structures. Noting also that the dimer splitting is *large*, ~1300 cm$^{-1}$, while $\Gamma_I$ for P870 is small, 130 cm$^{-1}$, it is clear that variations in the structure of the special pair from RC to RC in the ensemble are very small. One can reasonably assert, therefore, that the structure of the special pair and the two neighboring BChl monomers is also extremely well defined and, as a consequence, that the distribution of $V$ values is very narrow.

We conclude this discussion by emphasizing that PHB studies of the primary donor state absorption profiles of reaction centers have shown that spectral hole burning can provide valuable insights on the underlying structure of the profile even for the case of strong linear electron–phonon coupling.

We turn next to a discussion of how hole burning can be used to study the excited electronic state structure and energy-transfer dynamics of antenna protein complexes.

Excitons and their role in optical excitation transfer (ET) in photosynthetic antenna protein–chlorophyll complexes have long been subjects of interest.[242-246] However, our understanding of excitonic effects in such complexes, in contrast with aromatic molecular crystals, is quite poor. To put our level of understanding in perspective, we note that the following have been subjects of thorough experimental and theoretical study in organic crystals: unit-cell exciton level (Davydov) and exciton band structure;[247-254] inter-exciton level relaxation via scattering of phonons;[255-258] and coherent and incoherent exciton (wavepacket) transport.[259] These works illustrate that one cannot adequately understand the latter two without detailed information on unit cell and exciton band structure, the latter being dependent on interactions between molecules belonging to different unit cells.

Whether or not excitons are important in an antenna system or protein–pigment complex contained therein depends on which aspect of excitonic behavior is being addressed; for example, manifestations of excitonic coupling in circular dichroism and linearly polarized spectra, the kinetics of downward energy cascading, the mechanism of transport between structurally distinct complexes and coherent exciton transport. For consideration of such, exciton level structure and bandwidth, pure dephasing frequencies of exciton levels, electron–phonon coupling, and diagonal energy disorder stemming from structural heterogeneity are important factors. Thus, the temperature of the system often needs to be specified when the above question is posed. For example, the unit cell excitonic interactions of crystals such as naphthalene, phenanthrene, and anthracene are sufficiently strong to result in the linear polarizations of the $S_1$ state Davydov components of the exciton band at room temperature being dictated by the unit-cell factor group (symmetry). However coherent transport, by which we mean that the coherence length (mean free path) of the exciton wavepacket is greater than the unit-cell length, is observed only at very low temperatures and for ultrapure "strain-free" crystals.

Research in photosynthesis on excitons has been largely limited to understanding the relationship between protein–pigment structure and elementary exciton level structure. As will be further illustrated[215,219] here, persistent nonphotochemical hole burning (NPHB) is an important frequency domain technique for probing exciton level structure and exciton relaxation/scattering processes.

The first application of NPHB to the problem of excitonic behavior in an antenna protein complex was for the base-plate BChl *a* (bacteriochlorophyll *a*) complex of *Prosthecochloris aestuarii* which is devoid of the reaction center. The results showed that[219] the structured $Q_y$ ($S_1$) absorption spectrum should be interpreted in terms of delocalized exciton levels of a $C_3$ trimer of subunits, each of which contains 7 symmetry inequivalent BChl *a* molecules.[260,261] The unstructured lowest energy absorption band at 824 nm was shown to be due to two states separated by ~40 $cm^{-1}$. It was concluded that they are trimer states polarized parallel and perpendicular to the $C_3$ symmetry axis. Fluorescence studies later confirmed these polarizations.[262] Furthermore, the zero-phonon hole profiles (4.2 K) obtained with a wide range of burn wavelengths ($\lambda_B$) led to ~200 fs total dephasing times for the higher energy exciton levels which were[219] interpreted in terms of ~100 fs downward inter-exciton level relaxation via phonon emission. Importantly, the ZPH widths for the lowest energy exciton level at 827 nm yielded a much longer dephasing time at 4.2 K of 40 ps, which in view of the results reviewed below for the antenna complex of *Rb. sphaeroides* and our understanding of exciton–defect scattering processes in organic crystals, can be given a physical interpretation. The above NPHB studies showed, for the first time, that inter-exciton level scattering via phonon emission (which we will refer to as the Davydov mechanism[250]) can lead to ultrafast downward energy cascading in a protein–Chl complex.

Following the studies of the above complex of *P. aestuarii*, NPHB was applied to the antenna of the purple bacterium *Rb. sphaeroides*. The antenna of *Rb. sphaeroides* is comprised of two main complexes, B800-B850 (LH II) and B875 (LH I), with the former peripheral to the latter, which surrounds the RC. Various structural models have been proposed for B800-B850.[263-272] The models have in common that the cornerstone of the structure is an $\alpha,\beta$-polypeptide pair[265] capable of binding 1 and 2 BChl at the cytoplasmic and periplasmic sides of the membrane, respectively. The $Q_y$ and $Q_x$ dipoles of the latter two are believed to lie approximately in and perpendicular to the membrane plane, respectively, while the $Q_x$ and $Q_y$ dipoles of the single BChl at the cytoplasmic side are both approximately parallel to the plane.[263] The center-to-center distance between the 2 BChl at the periplasmic side has been estimated to be no greater than 15 Å.[267] This distance can lead to an excitonic matrix element as large as about 100 $cm^{-1}$.[266] The distance between the center of either of these and the other BChl has been estimated to be no greater than 21 Å. However, it is the organization of the $\alpha,\beta$ pairs into a cyclic arrangement and the two-dimensional lattice commensurate with this arrangement that determine the optical absorption and CD properties.[266] There appears to be general agreement that an aggregate of the 2 BChl at the periplasmic side is associated with B850 and that its structure may be similar to that of B875. In the original Zuber model[268,269] the B800-B850 unit cell was taken to be a hexamer of $\alpha,\beta$ pairs $(\alpha,\beta)_6$ with $C_6$ symmetry. In a revised model,[265] which becomes apparent when a two-dimensional lattice of these hexamers is constructed, the unit cell is a trimer of $\alpha,\beta$ pairs with the two members of the pair belonging to adjacent hexamers of the original Zuber model. This means that the B850 unit cell is a trimer of BChl tetramers (12 BChl molecules/unit cell). Scherz and co-workers[270-272] have also proposed trimer of tetramer models which are distinctly different from the revised Zuber model. The reader is referred to the article by Pearlstein[266] for a detailed discussion. It seems unlikely that one will be able to determine which of the trimer of tetramer models for B850 is correct (if any) until a crystal structure is available. There are several reasons for this including: the difficulty in determining the relative contributions from excitonic and protein–BChl interactions to the red-shifts of B800, B850, and B875 relative to the energy of the $Q_y$ state of "isolated" (monomer) BChl *a* at ~780 nm the sensitivity of the CD spectrum to weak excitonic interactions.[266] We note that the models of Scherz and co-workers are based on the assumption that, in LH2, a strong pairwise exciton interaction between the BChl of the $\alpha,\beta$ pair is responsible for the red-shift of $Q_y$ transition to 850 nm.

Energy (singlet) transfer in the light harvesting (LH) antenna complex has been extensively studied by picosecond techniques. The B850 to B875 transfer time is 35 ps at room temperature,[273] whereas the B875 to RC (open) transfer time at $T$ = 77 K is about 60 ps[274] for chromatophores. The B800 to B850 transfer has been reported to be much faster, 2 ± 1 ps at 77 K.[273] More recently, experiments with femtosecond resolution have led to a transfer time of 0.7 ps at room temperature for the isolated B800-850 complex.[275]

Nonphotochemical hole burning of B800 established that the total dephasing time ($T_2$) of B800* is 4.8 ps at pumped helium temperatures,[229] which was later proven to be due to downward energy transfer to B850.[216] Contrary to the findings of van der Laan et al.,[229] NPHB of B850 is as facile as for B800.[213,214] Furthermore, the 4.2 K hole spectra of Reddy and Small yielded a B800 ZPH width of 4.2 ± 0.5 $cm^{-1}$ which leads to a lifetime of 2.4 ± 0.2 ps for B800*. Within experimental uncertainty this value for the hole width agrees with that determined by van der Laan et al.[229]

Thus, B800 to B850 transfer is weakly temperature dependent even though the ~170-$cm^{-1}$ bandwidth of B800 is predominantly due to site inhomogeneous broadening ($\Gamma_I$) and the $\lambda_B$-dependent hole spectra show that the excitonic interaction between B800 and B850 BChl *a* is weak. However, the hole profile of B850 obtained with $\lambda_B$ located in B850 (FWHM ≈ 280 $cm^{-1}$) is dominated by a broad hole possessing a width of 210 $cm^{-1}$ at 4.2 K which is invariant to $\lambda_B$. This proved that the homogeneous broadening ($\Gamma_H$) is ~210 $cm^{-1}$, which is comparable to $kT$ at room temperature. The weak temperature dependence could, as a consequence, be understood.[216] A dominant 750-$cm^{-1}$ vibronic hole, which builds on the broad B850 origin hole, was observed with a Franck–Condon factor of 0.05 and a width of *only* 60 $cm^{-1}$. This novel vibronic hole narrowing phenomenon is due to *Franck–Condon factor narrowing of the exciton bandwidth.*[215,216] In a straightforward manner it was determined that a *minimum* value for the B850* exciton bandwidth is ~210 $cm^{-1}$. Furthermore, the 750-$cm^{-1}$ vibration was assigned as the dominant mode for B800 to B850 Förster transfer. The results for B875 were similar to those for B850 and

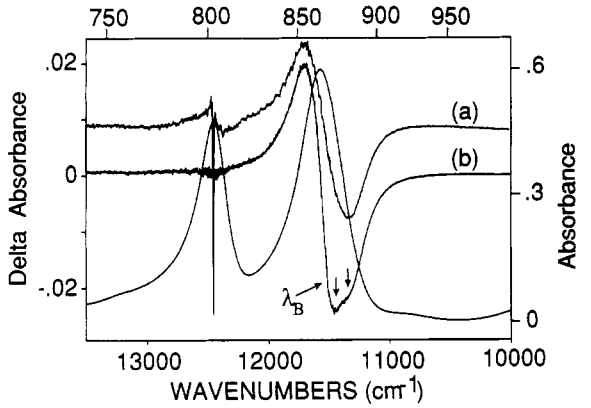


**Figure 19.** $Q_y$ region absorption and hole-burned spectra (4.2 K) of isolated B800-B850 complex of *Rhosopseudomonas acidophila* (strain 10050). At 4.2 K the B800 and B850 bands are at 803.2 and 864.3 nm, respectively. The burn frequencies, $\omega_B$, for the hole-burned spectra shown are (a) 12 450 cm$^{-1}$ and (b) 11 507 cm$^{-1}$. Burn conditions are 250 mW/cm$^2$ for 30 min and read resolution = 4 cm$^{-1}$. Reprinted from ref 218. Copyright 1992 American Society of Photobiology.

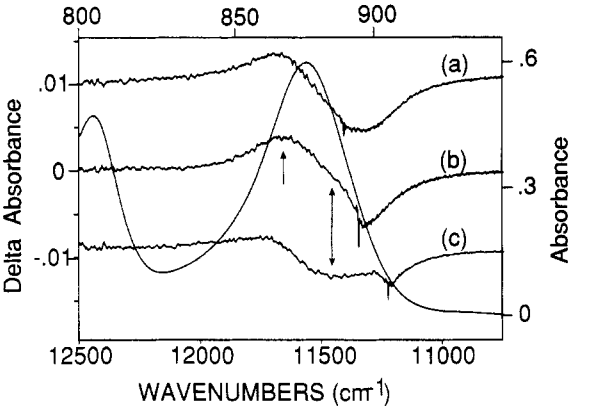


**Figure 20.** Hole-burned spectra (4.2 K) of *Rps. acidophila*. Burn conditions are 300 mW/cm$^2$ for 30 min and read resolution = 4 cm$^{-1}$. The burn frequencies are (a) 11 415, (b) 11 350, and (c) 11 229 cm$^{-1}$. Absorption spectrum is also shown for convenience. Reprinted from ref 218. Copyright 1992 American Society of Photobiology.

led to a *minimum* exciton bandwidth of ~210 cm$^{-1}$ for B875. For both B850 and B875 it was argued that $\Gamma_H$ is a consequence of exciton level structure and ultrafast inter-exciton level scattering.[216] The site inhomogeneous broadenings ($\Gamma_I$) for B850 and B875 were found to be 60 and 80 cm$^{-1}$, respectively.[215,216]

Very recently[217] NPHB was used to investigate B870 and B896, due to two additional states of the *Rb. sphaeroides* antenna which time-domain and other studies[276-280] have implicated as possible "shuttle" states for transfer from B850 to B875 and from B875 to P870 (primary electron donor of the reaction center), respectively. Although B870 and B896 are due to BChl *a* molecules, the nature of the B870* and B896* states is not understood. Novel NPHB action spectra were presented that allow for the resolution of the absorption profiles of the weakly absorbing B896 and B870 components and the determination of their underlying structure.[217] The results presented together with those for the base-plate antenna complex of *P. aestuarii* indicate that B870* and B896* states are the lowest energy exciton level of the B850* and B875* exciton bands, respectively. For B896* (and B870*) the ZPH widths yield a total dephasing time of 6.6 ps at 4.2 K. Interpretations for this dephasing were considered including one in which it is the result of exciton scattering in a lattice rendered imperfect by structural heterogeneity. This interpretation is suggested by data for excitons in doped organic crystals.

Because of the novelty and potential importance of the just-mentioned zero-phonon hole (ZPH) action spectroscopy we present some very recent results for the B800-850 complex of the purple bacteria *Rhodopseudomonas acidophila* (strain 10050).

The upper hole-burned spectrum of Figure 19 was obtained with $\omega_B$ (burn frequency) = 12 450 cm$^{-1}$. In addition to the sharp ZPH at $\omega_B$ (peak of B800), a broad satellite hole is observed in B850. This behavior is similar to that observed for *Rb. sphaeroides*.[216] The width of the satellite hole at 11 350 cm$^{-1}$ is ~320 cm$^{-1}$. The broad increase in absorption to the blue of the satellite hole is the antihole expected for NPHB. As discussed by Reddy et al.,[216] the B850 satellite hole is due to NPHB in B850* following B800 → B850 energy transfer. We return to a discussion of its large width later. High-resolution scans of the B800 ZPH obtained with burn wavelengths between 794 and 819 nm yielded a width of 6.0 ± 0.3 cm$^{-1}$, i.e. no dependence on $\omega_B$ was observed as was also the case for B800 of *Rb. sphaeroides*. The 6.0-cm$^{-1}$ width corresponds to a B800* lifetime of 1.8 ± 0.2 ps which is somewhat longer than the 1-ps lifetime measured in the time domain at 77 K for the type I complex. The ability to burn ZPH throughout the B800 profile proves that B800 is predominantly inhomogeneously broadened with $\Gamma_I \approx$ 240 cm$^{-1}$ ($\Gamma_I \approx$ 170 cm$^{-1}$ for B800 of *Rb. sphaeroides*).

The broad (~180 cm$^{-1}$) hole just to the right (red) of the B800 ZPH in the upper spectrum of Figure 19 has been attributed to downward energy transfer between B800 molecules.[218]

We turn now to the results obtained with $\omega_B$ located within the B850 band. For $\omega_B \gtrsim$ 11 500 cm$^{-1}$, no sharp ZPH of the type observed by burning in B800 were observed, only a broad hole similar to that shown in spectrum a of Figure 19. The lower spectrum (b) of Figure 19 was obtained with $\omega_B$ = 11 507 cm$^{-1}$. (The B850 absorption maximum is at 11 570 cm$^{-1}$.) The broad B850 hole is barely resolved into two components at ~11 470 and ~11 320 cm$^{-1}$. To explore the nature of this doubling, hole-burned spectra were obtained at constant burn fluence for a series of burn frequencies located on the low-energy side of B850. Three of the spectra are shown in Figure 20. The ZPH action spectrum for eight burn frequencies is shown in Figure 21. It is centered at 11 300 cm$^{-1}$ (885 nm) and carries an inhomogeneous width $\Gamma_I \approx$ 110 cm$^{-1}$. The analogous ZPH action spectrum for B850 of *Rb. sphaeroides* has its maximum at 870 nm and a $\Gamma_I$ value of 60 cm$^{-1}$. That B870 of *Rb. sphaeroides* is shifted to 885 nm in *Rps. acidophila* is consistent with the shift of B850 to 864 nm in *Rps. acidophila*. This provides additional support for the assignment of B870 of *Rb. sphaeroides* as the lowest exciton level of the B850 unit cell. Returning to the lower spectrum of Figure 19, for which the B850 hole is a doublet with components at ~11 470 and ~11 320 cm$^{-1}$, we observe that the latter component is, within experimental uncertainty, coincident with the maximum of the ZPH action spectrum (Figure 21),

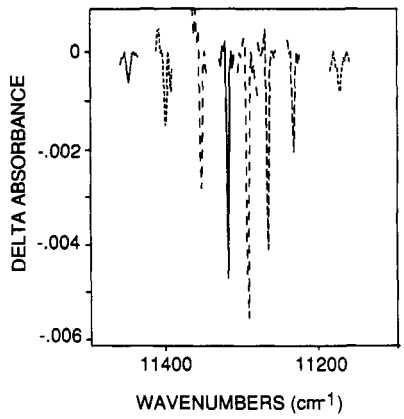


**Figure 21.** Constant fluence (250 mW/cm$^2$ for 30 min) hole-burned spectra in "B870" band. ZPHs are offset to have a common baseline and nonresonant holes accompanying the ZPHs are not shown. The maximum absorbance change shown is ~0.005. Reprinted from ref 218. Copyright 1992 American Society of Photobiology.

i.e. B870 of *Rps. acidophila*. The former component coincides with broad hole in spectrum c of Figure 20 which is indicated by the double-headed arrow. Spectrum c also shows that burning into the low-energy side of B870 produces a high-energy satellite hole in the main part of B850 near ~11470 cm$^{-1}$. This is consistent with B870 being the lowest exciton level of the B850 unit cell.[217] We note that in spectrum c of Figure 20 the real and pseudo-phonon sideband holes associated with the ZPH are discernible (displaced from the ZPH by ±18 cm$^{-1}$).

Finally, high-resolution scans of ZPH of the type shown in Figure 21 yielded a width of 2.0 ± 0.2 cm$^{-1}$, which corresponds to a total dephasing time of 5.3 ± 0.1 ps. As was the case for B870 and B896 of *Rb. sphaeroides*,[217] no significant dependence of the width on $\omega_B$ was observed.

To conclude we remark that NPHB may now be viewed as a powerful probe of exciton level structure and inter-exciton level relaxation processees in antenna complexes.

### 2. Conformational Relaxation Processes in Proteins at Low Temperatures

The structural order of protein crystals is only mesoscopic. As mentioned earlier, proteins are more glasslike on a microscopic scale. Frauenfelder et al.[214] showed that many properties of the motions of proteins and glasses can be discussed in terms of the features of rugged energy landscapes, which provides a unifying language. Very recently Friedrich and Vanderkooi and their co-workers[281] reported on interesting differences between configurational relaxation processes in a protein and glass for $T \lesssim 30$ K. The sensitive method of spectral diffusion of the ZPH produced by thermal cycling (cf. section IV.3) was applied to mesoporphyrin-substituted horseradish peroxidase and mesoporphyrin in glycerol. Holes were burned into the origin band of the mesoporphyrin at either 1.5 or 4.2 K ($T_B$) and read initially at $T_R = T_B$. Following a temperature cycle, $T_B \rightarrow T_{exc} \rightarrow T_B$, the hole was read again at $T_R = T_B$. The dependence of the ZPH width on the excursion temperature ($T_{exc} > T_B$) reflects the temperature dependence of thermally induced spectral diffusion. Up to $T_{exc} \sim 12$ K the spectral diffusion of the mesoporphyrin in the glass and protein are identical. However, for $T_{exc} > 12$ K there is a pronounced step in the diffusion for the small globular protein HRP. Zollfrank et al.[281] argue that the difference in behavior originates from finite size effects, i.e., since HRP is small (34 kDa), it may be characterized by a small number of TLS, and their distribution may be pseudo-discrete rather than continuous. This is an interesting possibility that can be checked by thermal cycle, pure dephasing, and time-resolved spectral diffusion measurements on proteins of different size and shape.

## *VII. Continuing Developments*

Hole burning remains an active, expanding area of spectroscopy. The applications discussed in section III continue to be developed and improved. Biological applications such as those discussed in section VI are very active areas of development. Both of these areas make use of the external field techniques of section V, and these techniques continue to be developed. In our own work, the effects of high pressure on hole burning of biologically important materials has begun. In complex, multichromophore systems such as reaction centers and antenna complexes dramatic effects on electron transfer and energy transfer and thereby on hole widths can be anticipated.

Regarding NPHB and the nature of the glassy state, little progress on determining the actual nature of the TLS has been made. Even for amorphous silicon dioxide, the most widely studied material, there is no microscopic description that has generally been agreed upon, although recent calculations[124,282] suggest that hindered rotations of several connected $SiO_4$ tetrahedra are reasonable candidates for the TLS excitations (or at least a fraction thereof). The structural model of Buchenau and co-workers[282] for the low-frequency excitations is associated with the concerted hindered rotation of five tetrahedra. The TLS asymmetric double-well potential associated with this motion exhibits a $\Delta$ of about 2 cm$^{-1}$ and a barrier height of several wave numbers.[124] This structural model has recently been shown to be consistent with low-temperature inelastic scattering measurements.[283] For the molecular systems on which much hole burning data has been accumulated, hole-growth studies (section IV.5) have shown that the kinetics are markedly slowed (couple orders of magnitude) by deuteration of the hydroxyl group. In sharp contrast, the magnitude and temperature dependence of the hole width and dephasing are unaffected. These findings are consistent with the previously discussed model that invokes two "types" of TLS, $TLS_{int}$ and $TLS_{ext}$. The latter, which are responsible for hole growth, have tunnel coordinates that involve considerable amplitude for the hydroxyl proton; however, the coordinates for the $TLS_{int}$, which are responsible for dephasing, do not. This in turn suggests that the $TLS_{int}$ are far more spatially extended than the $TLS_{ext}$. For polymers subtle and hindered cooperative motion of chains may be associated with the $TLS_{int}$. For the alcohol glasses, extended hydrogen-bonding networks may be the key to understanding the $TLS_{int}$ as may also be the case for amorphous water.

Our research on the nature of TLS is now aided by the development of a thermospray deposition appa-

ratus[284] which allows facile, reproducible formation of thin, hyperquenched films doped with visibly absorbing probe species. Hyperquenching[285] is a method of glass formation akin to "splat cooling"[286,287] in which cooling rates in excess of $10^6$ K $s^{-1}$ are achieved by projecting liquid droplets onto a cooled substrate. With such large cooling rates, glasses may be made even from materials which are difficult to vitrify. From the viewpoint of using hole burning to study glass properties, the thermospray device has two important qualities: (1) reproducible control over parameters of the glass formation process and (2) thin films are amenable to probing not only of electronic transitions in the visible, but also of vibrational transitions, in the infrared. It is our expectation that this latter attribute will allow us to further elucidate the role of TLS in hole burning as well as the nature of the TLS.

## VIII. Acknowledgments

This article was made possible by support from the Division of Materials Research of the National Science Foundation under grant no. DMR-8920515. The authors also wish to acknowledge the contributions of numerous co-workers whose efforts have made this review possible. Particular appreciation is extended to Raja Reddy, Paul Lyle, Steve Kolaczkowski, Lushuan Shu, and Mike Kenney, recent group members whose results are reviewed here.

## IX. References

(1) Kharlamov, B. M.; Personov, R. I.; Bykovskaya, L. A. *Opt. Commun.* **1974**, *12*, 191.
(2) Gorokhovskii, A. A.; Kaarli, R. K.; Rebane, L. A. *JETP Lett.* **1974**, *20*, 216.
(3) Moerner, W. E., Ed.; *Topics in Current Physics, Persistent Spectral Hole Burning: Science and Applications*; Springer-Verlag: New York, 1987; Vol. 44.
(4) Narasimhan, L. R.; Littau, K. A.; Pack, D. W.; Bai, Y. S.; Elschner, A.; Fayer, M. D. *Chem. Rev.* **1990**, *90*, 439.
(5) Johnson, S. G.; Lee, I.-J.; Small, G. J. In *Chlorophylls*; Scheer, H., Ed.; CRC Press: Boca Raton, 1991; p 739.
(6) Jankowiak, R.; Small, G. J. In *Photosynthetic Reaction Centers*; Deisenhofer, J., Norris, J., Eds.; Academic Press: Boston, in press.
(7) Reddy, N. R. S.; Lyle, P. A.; Small, G. J. *Photosynth. Res.* **1992**, *31*, 167.
(8) deVries, H.; Wiersma, D. A. *Phys. Rev. Lett.* **1976**, *36*, 91.
(9) deVries, H.; Wiersma, D. A. *Chem. Phys. Lett.* **1977**, *51*, 565.
(10) See, for example: *Optical Spectroscopy of Glasses*; Zschokke, I., Ed.; Reidel: Dordrecht, 1986.
(11) Sargeant, M., III; Scully, M. O.; Lamb, W. E., Jr. *Laser Physics*; Addison-Wesley: Reading, 1974.
(12) Levenson, M. D.; Kano, S. *Introduction to Nonlinear Laser Spectroscopy*; Academic Press: Boston, 1988.
(13) Hayes, J. M.; Jankowiak, R.; Small, G. J. In *Topics in Current Physics, Persistent Spectral Hole Burning: Science and Applications*; Moerner, W. E., Ed.; Springer-Verlag: New York, 1987; Vol. 44, p 153.
(14) Hayes, J. M.; Small, G. J. *J. Phys. Chem.* **1986**, *90*, 4928.
(15) Won, Y.; Friesner, R. A. *Proc. Natl. Acad. Sci. U.S.A.* **1987**, *84*, 5511.
(16) Hayes, J. M.; Gillie, J. K.; Tang, D.; Small, G. J. *Biochim. Biophys. Acta* **1988**, *932*, 287.
(17) Lee, I.-J.; Hayes, J. M.; Small, G. J. *J. Chem. Phys.* **1989**, *91*, 3463.
(18) Small, G. J. *J. Chem. Phys.* **1970**, *52*, 656 and references therein.
(19) Middendorf, T. R.; Mazzola, L. T.; Gaul, D. F.; Schenck, C. C.; Boxer, S. G. *J. Phys. Chem.* **1991**, *95*, 10142.
(20) Völker, S.; MacFarlane, R. M.; Genack, A. Z.; Trommsdorff, H. P.; van der Waals, J. H. *J. Chem. Phys.* **1977**, *67*, 1759.
(21) Dick, B. *Chem. Phys.* **1989**, *136*, 429.
(22) Kishii, N.; Asai, N.; Kawasumi, K.; Tamura, S.; Seto, J. *Appl. Phys. Lett.* **1988**, *52*, 16.
(23) Hori, K.; Mori, T.; Naito, T.; Mita, I. *Appl. Phys. Lett.* **1988**, *53*, 935.
(24) Van den Berg, R.; Visser, A.; Völker, S. *Chem. Phys. Lett.* **1988**, *144*, 105.
(25) Lee, I.-J.; Small, G. J.; Hayes, J. M. *J. Phys. Chem.* **1990**, *94*, 3376.
(26) Hayes, J. M.; Small, G. J. *Chem. Phys. Lett.* **1978**, *54*, 435.
(27) Hayes, J. M.; Small, G. J. *Chem. Phys.* **1978**, *27*, 151.
(28) Kenney, M. J.; Jankowiak, R.; Small, G. J. *Chem. Phys.* **1990**, *146*, 47.
(29) Berg, M.; Walsh, C. A.; Narasimhan, R.; Littau, K. A.; Fayer, M. D. *J. Chem. Phys.* **1988**, *88*, 1564.
(30) Fearey, B. L.; Stout, R. P.; Hayes, J. M.; Small, G. J. *J. Chem. Phys.* **1983**, *78*, 7013.
(31) Anderson, P. W.; Halperin, B. I.; Varma, C. M. *Philos. Mag.* **1972**, *25*, 1.
(32) Phillips, W. A. *J. Low Temp. Phys.* **1972**, *7*, 351.
(33) Hunklinger, S.; Raychaudhuri, A. K. In *Progress in Low Temperature Physics*; Brewer, D. F., Ed.; North Holland-Elsevier: Amsterdam, 1986; Vol. 9, p 265.
(34) Small, G. J. In *Molecular Spectroscopy*; Agranovich, V. M., Hochstrasser, R. M., Eds.; North Holland: Amsterdam, 1983; Chapter 9.
(35) Hayes, J. M.; Stout, R. P.; Small, G. J. *J. Chem. Phys.* **1981**, *74*, 4266.
(36) Gillie, J. K.; Small, G. J.; Golbeck, J. H. *J. Phys. Chem.* **1989**, *93*, 1620.
(37) Shu, L.; Small, G. J. *Chem. Phys.* **1990**, *141*, 447.
(38) Jankowiak, R.; Bässler, H. *J. Mol. Electron.* **1985**, *1*, 73.
(39) Childs, A. F.; Francis, A. H. *J. Phys. Chem.* **1985**, *89*, 466.
(40) Bogner, U.; Schwarz, R. *Phys. Rev. B* **1981**, *24*, 2846.
(41) Kokai, F.; Tanaka, H.; Brauman, J. I.; Fayer, M. D. *Chem. Phys. Lett.* **1988**, *143*, 1.
(42) Szabo, A. *Phys. Rev. Lett.* **1970**, *25*, 924.
(43) Erickson, L. E. *Phys. Rev. B.* **1975**, *11*, 4512.
(44) Shelby, R. M.; MacFarlane, R. M. *Chem. Phys. Lett.* **1979**, *64*, 545.
(45) Haarer, D. In *Topics in Current Physics, Persistent Spectral Hole Burning: Science and Applications*; Moerner, W. E., Ed.; Springer Verlag: New York, 1987; Vol. 44, p 79.
(46) Fearey, B. L. Ph.D. Thesis, Iowa State University, 1986.
(47) Optical Society of America, Persistent Spectral Hole Burning: Science and Applications, Monterey, CA, 1991.
(48) Optical Society of America, Spectral Hole-Burning and Luminescence Line Narrowing: Science and Applications, Ascona, Switzerland, 1992.
(49) Rebane, K. K.; Rebane, L. A. In *Topics in Current Physics Persistent Spectral Hole Burning: Science and Applications*; Moerner, W. E., Ed.; Springer-Verlag: New York, 1987; Vol. 44, p 17.
(50) Wild, U. P.; Bucher, S. E.; Burkhalter, F. A. *Appl. Opt.* **1985**, *24*, 1526.
(51) Bogner, U.; Beck, K.; Maier, M. *Appl. Phys. Lett.* **1985**, *46*, 534.
(52) Moerner, W. E.; Lenth, W.; Bjorklund, G. C. In *Topics in Current Physics Persistent Spectral Hole Burning: Science and Applications*; Moerner, W. E., Ed.; Springer-Verlag: New York, 1987; Vol. 44, p 251.
(53) Wild, U. P.; Renn, A. In *Photochromism: Molecules and Systems*; Dürr, H., Bouas-Laurent, H., Eds.; Elsevier: Amsterdam, 1990; p 930.
(54) Renn, A.; Wild, U. P. *Appl. Opt.* **1987**, *26*, 4040.
(55) Wild, U. P.; Renn, A.; Locher, R.; Meixner, A. J. *Jpn. J. Appl. Phys.* **1987**, *26*, 233.
(56) Wild, U. P.; Renn, A.; DeCaro, C.; Bernet, S. *Appl. Opt.* **1990**, *29*, 4329.
(57) Wild, U. P.; Renn, A. *J. Mol. Electron.* **1991**, *7*, 1.
(58) Bernet, S.; Renn, A.; Kohler, B.; Wild, U. P. In *Spectral Hole Burning and Luminescence Line Narrowing: Science and Applications, Technical Digest 1992*; Optical Society of America: Washington, DC, 1992; Vol. 22, p 218.
(59) Moerner, W. E.; Levenson, M. D. *J. Opt. Soc. Am. B* **1985**, *2*, 915.
(60) Winnacker, A.; Shelby, R. M.; Macfarlane, R. M. *Opt. Lett.* **1985**, *10*, 350.
(61) Zhang, L.; Yu, J.; Huang, S. *J. Lumin.* **1990**, *45*, 301.
(62) Iannone, M.; Scott, G. W.; Brinza, D.; Coulter, D. R. *J. Chem. Phys.* **1986**, *85*, 4863.
(63) Machida, S.; Horie, K.; Yamashita, T. *Appl. Phys. Lett.* **1992**, *60*, 286.
(64) Ambrose, W. P.; Moerner, W. E. *Chem. Phys.* **1990**, *144*, 71.
(65) Luo, B.; Tian, M.; Li, W.; Huang, S.; Yu, J. *J. Lumin.* **1992**, *53*, 247.
(66) Furasawa, A.; Horie, K. *J. Chem. Phys.* **1991**, *94*, 80.
(67) Holliday, K.; Wei, C.; Croci, M.; Wild, U. P. *J. Lumin.* **1992**, *53*, 227.
(68) Aizengendler, M.; Bogner, U.; Dolendo, I.; Kikas, J.; Sildos, I. *Chem. Phys. Lett.* **1991**, *183*, 245.
(69) Renn, A.; Meixner, A. J.; Wild, U. P.; Burkhalter, F. A. *Chem. Phys.* **1985**, *93*, 157.
(70) Levenson, M. D.; Macfarlane, R. M.; Shelby, R. M. *Phys. Rev. B* **1980**, *22*, 4915.
(71) Dick, B. *Chem. Phys. Lett.* **1988**, *143*, 186.
(72) Moerner, W. E.; Kador, L. *Phys. Rev. Lett.* **1989**, *62*, 2535.
(73) Kador, L.; Horne, D. E.; Moerner, W. E. *J. Phys. Chem.* **1990**, *94*, 1237.
(74) Ambrose, W. P.; Moerner, W. E. *Nature* **1991**, *349*, 225.
(75) Moerner, W. E.; Ambrose, W. P. *Phys. Rev. Lett.* **1991**, *66*, 1376.
(76) Ambrose, W. P.; Basché, Th.; Moerner, W. E. *J. Chem. Phys.* **1991**, *95*, 7150.
(77) Basché, Th.; Moerner, W. E. *Nature* **1992**, *355*, 335.

(78) Basché, Th.; Ambrose, W. P.; Moerner, W. E. *J. Opt. Soc. Am. B* **1992**, *9*, 829.
(79) Orrit, M.; Bernard, J. *Phys. Rev. Lett.* **1990**, *65*, 2716.
(80) Orrit, M.; Bernard, J. *Mod. Phys. Lett. B* **1991**, *5*, 747.
(81) Talon, H.; Fleury, L.; Bernard, J.; Orrit, M. *J. Opt. Soc. Am. B.* **1992**, *9*, 825.
(82) Bogner, U.; Schätz, P.; Maier, M. *Chem. Phys. Lett.* **1985**, *119*, 335.
(83) Basché, Th.; Bräuchle, C. *Chem. Phys. Lett.* **1991**, *181*, 179.
(84) Basché, Th.; Bräuchle, C. *J. Phys. Chem.* **1991**, *95*, 7130.
(85) Sauter, B.; Basché, Th.; Bräuchle, C. *J. Opt. Soc. Am. B.* **1992**, *9*, 804.
(86) Basché, Th.; Bräuchle, C. *J. Phys. Chem.* **1988**, *92*, 5069.
(87) Williams, D. W.; Fayer, M. D. *Chem. Phys. Lett.* **1990**, *168*, 371.
(88) Hirschmann, R.; Köhler, W.; Friedrich, J.; Deltrozzo, E. *Chem. Phys. Lett.* **1988**, *151*, 60.
(89) Hirschmann, R.; Friedrich, J.; Daltrozzo, E. *J. Chem. Phys.* **1989**, *91*, 7296.
(90) Hirschmann, R.; Friedrich, J. *J. Chem. Phys.* **1989**, *91*, 7988.
(91) Hirschmann, R.; Friedrich, J. *J. Opt. Soc. Am. B.* **1992**, *9*, 811.
(92) DeBoer, S.; Vink, K. J.; Wiersma, D. A. *Chem. Phys. Lett.* **1987**, *137*, 91.
(93) Trommsdorff, H. P.; Zeigler, J. M.; Hochstrasser, R. M. *J. Chem. Phys.* **1988**, *89*, 4440.
(94) Trommsdorff, H. P.; Zeigler, J. M.; Hochstrasser, R. M. *Chem. Phys. Lett.* **1989**, *154*, 463.
(95) Arnold, S.; Liu, C. T.; Whitten, W. B.; Ramsey, J. M. *Opt. Lett.* **1991**, *16*, 420.
(96) Arnold, S.; Comunale, J.; Whitten, W. B.; Ramsey, J. M.; Fuller, K. A. *J. Opt. Soc. Am. B.* **1992**, *9*, 819.
(97) Jankowiak, R.; Small, G. J.; Athreya, K. B. *J. Phys. Chem.* **1986**, *90*, 3896.
(98) Jankowiak, R.; Small, G. J.; Ries, B. *Chem. Phys.* **1987**, *118*, 223.
(99) Selzer, P. M.; Huber, D. L.; Hamilton, D. S.; Yen, W. M.; Weber, M. J. *Phys. Rev. Lett.* **1976**, *36*, 813.
(100) Avouris, P.; Campion, A.; El-Sayed, M. A. *J. Chem. Phys.* **1977**, *67*, 3397.
(101) Morgan, J. R.; El-Sayed, M. A. *Chem. Phys. Lett.* **1977**, *84*, 215.
(102) Hegarty, J.; Yen, W. M. *Phys. Rev. Lett.* **1974**, *33*, 1126.
(103) Hayes, J. M.; Stout, R. P.; Small, G. J. *J. Chem. Phys.* **1980**, *83*, 4129.
(104) Reinecke, T. L. *Solid State Commun.* **1979**, *32*, 1103.
(105) Lyo, S. K.; Orbach, R. *Phys. Rev. B* **1980**, *22*, 4223.
(106) Lyo, S. K. *Phys. Rev. Lett.* **1982**, *48*, 688.
(107) Phillips, W. A., Ed. *Amorphous Solids-Low Temperature Properties*; Springer: Berlin, 1981.
(108) MacFarlane, R. M.; Shelby, R. M. *J. Lumin.* **1987**, *36*, 179.
(109) Reinecker, P.; Kassner, K. In *Optical Spectroscopy of Glasses*; Zschokke, I., Ed.; Dordrecht: Reidel, 1986; p 65.
(110) See: Völker, S. In *Relaxation Processes in Molecular Excited States*; Fünfschilling, J., Ed.; Kluwer Academic Publisher: Dordrecht, 1989; p 113 and references therein.
(111) Boxer, S. G.; Gottfried, D. S.; Lockhart, D. J.; Middendorf, T. R. *J. Chem. Phys.* **1987**, *86*, 2439.
(112) Bai, Y. S.; Fayer, M. D. *Chem. Phys.* **1988**, *128*, 135.
(113) Littau, K. A.; Fayer, M. D. *Chem. Phys. Lett.* **1991**, *176*, 551.
(114) Littau, K. A.; Bai, Y. S.; Fayer, M. D. *J. Chem. Phys.* **1990**, *92*, 4145.
(115) Littau, K. A.; Elschner, A.; Fayer, M. D. *Chem. Phys. Lett.* **1990**, *175*, 149.
(116) Lyo, S. K. In *Optical Spectroscopy of Glasses*; Zschokke, I., Ed.; Reidel: Dordrecht, 1986; p 1.
(117) Molenkamp, L. W.; Wiersma, D. A. *J. Chem. Phys.* **1985**, *83*, 1.
(118) Jankowiak, R.; Small, G. J. *J. Phys. Chem.* **1986**, *90*, 5612.
(119) Jankowiak, R.; Small, G. J. *Chem. Phys. Lett.* **1986**, *128*, 377.
(120) Hunklinger, S.; Raychauduri, A. K. In *Progress in Low Temperature Physics*; Brewer, D. F., Ed.; North Holland: Amsterdam, 1986; Vol. IX, p 265.
(121) Jankowiak, J.; Hayes, J. M.; Small, G. J. *Phys. Rev. B* **1988**, *38*, 2084.
(122) Jankowiak, R.; Small, G. J. *Phys. Rev. B* **1988**, *37*, 8407.
(123) Lasjaunias, J. C.; Maynard, R.; Thoulouze, D. *Solid State Commun.* **1972**, *10*, 215.
(124) Guttman, L.; Rahman, S. M. *Phys. Rev. B* **1986**, *33*, 1506.
(125) Schilling, R. *Phys. Rev. Lett.* **1984**, *53*, 2258.
(126) Stephens, R. B. *Phys. Rev. B* **1975**, *14*, 754.
(127) Kassner, K.; Silbey, R. *J. Phys.: Condens. Matter* **1989**, *1*, 4599.
(128) Kassner, K. *Z. Phys. B: Condens. Matter* **1990**, *81*, 245.
(129) Friedrich, J.; Wolfrum, H.; Haarer, D. *J. Chem. Phys.* **1982**, *77*, 2309.
(130) Breinl, W.; Friedrich, J.; Haarer, D. *J. Chem. Phys.* **1984**, *81*, 3915.
(131) Müller, K. P.; Haarer, D. *Phys. Rev. Lett.* **1991**, *66*, 2344.
(132) Gruzdev, N. V.; Sil'kis, E. G.; Titor, V. D.; Vainer, Yu. G. *J. Opt. Soc. Am. B* **1992**, *9*, 941.
(133) Lasjaunias, J. C.; Ravex, A.; Vandorpe, M.; Hunklinger, S. *Solid State Commun.* **1975**, *17*, 1045.
(134) Zeller, R. C.; Pohl, P. O. *Phys. Rev. B* **1971**, *4*, 2029.
(135) Stephens, R. B. *Phys. Rev. B* **1973**, *8*, 289.
(136) van den Berg, R.; Völker, S. *Chem. Phys. Lett.* **1986**, *127*, 525.
(137) van den Berg, R.; Wisser, A.; Völker, S. *Chem. Phys. Lett.* **1988**, *144*, 105.
(138) Meijers, H. C.; Wiersma, D. A. *Phys. Rev. Lett.* **1992**, *68*, 381.
(139) Wannemacher, R.; Smorenburg, H. E.; Schmidt, Th.; Völker, S. In *Spectral Hole-Burning and Luminescence Line Narrowing: Science and Applications, Technical Digest 1992*; Optical Society of America: Washington, DC, 1992; Vol. 22, p 200.
(140) Meijers, H. C.; Wiersma, D. A. In *Spectral Hole-Burning and Luminescence Line Narrowing: Science and Applications, Technical Digest 1992*; Optical Society of America: Washington DC, 1992; Vol. 22, p 243.
(141) Jankowiak, R.; Small, G. J. *Chem. Phys. Lett.* **1990**, *166*, 217.
(142) Jankowiak, R.; Shu, L.; Kenney, M. J.; Small, G. J. *J. Lumin.* **1987**, *36*, 293.
(143) Silbey, R.; Kassner, K. *J. Lumin.* **1987**, *36*, 283.
(144) Joffrin, J.; Levelut, A. *J. Phys. (Paris)* **1975**, *36*, 811.
(145) Jankowiak, R.; Small, G. J. *Phys. Rev. B* **1993**, *47*, in press.
(146) Hu, P.; Walker, L. R. *Phys. Rev. B* **1978**, *18*, 1300.
(147) Mukamel, S. *Phys. Rev. A* **1983**, *28*, 3480; *Phys. Rev. Rep.* **1983**, *93*, 1.
(148) Mukamel, S.; Loring, R. F. *J. Opt. Soc. Am. B* **1986**, *3*, 595.
(149) Jankowiak, R.; Small, G. J. In preparation.
(150) Narasimhan, L. R.; Bai, Y. S.; Dugan, M. A.; Fayer, M. D. *Chem. Phys. Lett.* **1991**, *176*, 335.
(151) Shu, L.; Small, G. J. *J. Opt. Soc. Am. B* **1992**, *9*, 733.
(152) Shu, L. S.; Small, G. J. *J. Opt. Soc. Am. B.* **1992**, *9*, 724.
(153) Jankowiak, R.; Small, G. J. *Science* **1987**, *237*, 618.
(154) Breinl, W.; Friedrich, J.; Haarer, D. *Chem. Phys. Lett.* **1984**, *106*, 487.
(155) Köhler, W.; Meiler, J.; Friedrich, J. *Phys. Rev. B.* **1987**, *8*, 4031.
(156) Elschner, A.; Bässler, H. *Chem. Phys.* **1988**, *123*, 305.
(157) Fearey, B. L.; Small, G. L. *Chem. Phys.* **1986**, *101*, 269.
(158) Richter, W.; Sesselmann, Th.; Haarer, D. *Chem. Phys. Lett.* **1989**, *159*, 235.
(159) Gorokhovskii, A. A.; Zavt, G. S.; Pal'm, V. V. *JETP Lett.* **1988**, *48*, 369.
(160) Shu, L. S.; Small, G. J. *J. Opt. Soc. Am. B.* **1992**, *9*, 738.
(161) Fearey, B. L.; Carter, T. P.; Small, G. J. *Chem. Phys.* **1986**, *101*, 279.
(162) Maier, M. *Appl. Phys.* **1986**, *B41*, 73.
(163) Personov, R. I. *Izv. Akad. Nauk SSSR, Ser. Fiz.* **1988**, *52*, 628 (in Russian).
(164) Renn, A.; Bucher, S. E.; Meixner, A. J.; Meister, E. C.; Wild, U. P. *J. Lumin.* **1988**, *39*, 181.
(165) Marchetti, A. P.; Scozzafara, M.; Young, R. M. *Chem. Phys. Lett.* **1977**, *51*, 424.
(166) Meixner, A. J.; Renn, A.; Bucher, S. E.; Wild, U. P. *J. Phys. Chem.* **1986**, *90*, 6777.
(167) Kanaan, Y.; Attenberger, T.; Bogner, U.; Maier, M. *Appl. Phys.* **1990**, *B51*, 336.
(168) Bogner, U.; Schätz, P.; Seel, R.; Maier, M. *Chem. Phys. Lett.* **1983**, *102*, 267.
(169) Hanson, D. M.; Patel, J. S.; Winkler, I. C.; Morrobel-Sosa, A. In *Spectroscopy and Excitation Dynamics of Condensed Molecular Systems*; Agranovich, V. M., Hochstrasser, R. M., Eds.; North-Holland: Amsterdam, 1983; p 621.
(170) Schätz, P.; Bogner, U.; Maier, M. *Appl. Phys. Lett.* **1986**, *49*, 1132.
(171) Samoilenko, V. D.; Razumova, N. V.; Personov, R. I. *Opt. Spectrosc.* **1982**, *52*, 346.
(172) Kador, L.; Haarer, D.; Personov, R. I. *J. Chem. Phys.* **1987**, *86*, 5300.
(173) Schätz, P.; Maier, M. *J. Chem. Phys.* **1987**, *87*, 809.
(174) Renn, A.; Locher, R.; Meixner, A. J.; Wild, U. P. *J. Lumin.* **1987**, *38*, 37.
(175) Liptau, W. In *Excited States*; Lim, E. C., Ed.; Academic: New York, 1974; Vol. 1, p 129.
(176) Johnson, L. W.; Murphy, M.; Pope, C.; Foresti, M.; Lombardi, J. R. *J. Chem. Phys.* **1987**, *86*, 4335.
(177) Schwoerer, H.; Gygax, H.; Rebane, A.; Wild, U. P. In *Spectral Hole-Burning and Luminescence Line Narrowing: Science and Applications, Technical Digest 1992*; Optical Society of America: Washington, DC, 1992; Vol. 22, pp 135.
(178) Hartmannsgruber, N.; Bogner, U.; Maier, M. *Opt. Quantum Electron.* **1991**, *23*, 361.
(179) Renge, J. In *Spectral Hole-Burning and Luminescence Line Narrowing: Science and Applications Technical Digest 1992*; Optical Society of America: Washington, DC, 1992; Vol. 22, pp 122.
(180) Offen, H. W. In *Organic Molecular Photophysics*; Birks, J. B., Ed.; Wiley: London, 1973; Vol. 1, p 103.
(181) Drickamer, H. G. *Int. Rev. Phys. Chem.* **1982**, *2*, 171. In *High Pressure Chemistry and Biochemistry*; van Eldick, I., Jonas, I., Eds.; D. Reidel: Dordrecht, 1987; p 263.
(182) Kalinowski, J.; Jankowiak, R.; Bässler, H. *J. Lumin.* **1981**, *22*, 397.
(183) Kador, L.; Personov, R.; Richter, W.; Sesselman, Th.; Haarer, D. *Polym. J.* **1987**, *19*, 61.
(184) Ellervee, A.; Jaaniso, R.; Kikas, J.; Laisaar, A.; Suisalu, A.; Shcherbakov, V. *Chem. Phys. Lett.* **1991**, *176*, 472.
(185) Politis, T. G.; Drickamer, H. *J. Chem. Phys.* **1981**, *74*, 263.
(186) Zollfrank, J.; Friedrich, J. *J. Phys. Chem.* **1992**, *96*, 7889.
(187) Zollfrank, J.; Friedrich, J. *J. Phys. Chem.* **1992**, *96*, 7887.
(188) Personov, R. I. *J. Photochem. Photobiol. A: Chem.* **1992**, *62*, 321.
(189) Jankowiak, R.; Small, G. J. *Chem. Res. Toxicol.* **1991**, *4*, 256.

(190) Sesselmann, Th.; Richter, W.; Haarrer, D.; Morawitz, H. *Phys. Rev. B* **1987**, *B 36*, 7601.
(191) Haarer, D.; Kador, L. *Macromol. Chem., Macromol. Symp.* **1991**, *44*, 139.
(192) Friedrich, J.; Zollfrank, J.; Gafert, J. In *Spectral Hole-Burning and Luminescence Line Narrowing: Science and Applications Technical Digest 1992*, Optical Society of America: Washington, DC, 1992; Vol. 22, pp 70.
(193) Zollfrank, J.; Friedrich, J.; Parak, F. *Biophys. J.* **1992**, *61*, 716.
(194) Moerner, W. E.; Huston, A. L. *Appl. Phys. Lett.* **1986**, *48*, 1181.
(195) Laird, B. B.; Skinner, J. L. *J. Chem. Phys.* **1989**, *90*, 3274.
(196) Skinner, J. L.; Laird, B. B.; Root, L. *J. Lumin.* **1990**, *45*, 6.
(197) Kador, L. *J. Chem. Phys.* **1991**, *95*, 846.
(198) Macfarlane, R. M.; Shelby, R. M. In *Spectroscopy of Solids Containing Rare Earth Ions*; Kaplyanskii, A. A., Macfarlane, R. M., Eds.; North Holland: Amsterdam, 1987; p 51.
(199) Van den Berg, R.; van der Laan, H.; Völker, S. *Chem. Phys. Lett.* **1987**, *142*, 535.
(200) Ulitskii, N. I.; Kharlamov, B. M.; Pyndyk, A. M.; Personov, R. I. *Opt. Spectrosk.* **1985**, *59*, 560.
(201) Dicker, A. I. M.; Dobkowski, J.; Noort, M.; Völker, S.; van der Waals, J. H. *Chem. Phys. Lett.* **1982**, *88*, 135.
(202) Van den Berg, R.; van der Laan, H.; Völker, S. *Chem. Phys. Lett.* **1987**, *142*, 535.
(203) Dicker, A. I. M.; Noort, M.; Völker, S.; van der Waals, J. H. *Chem. Phys. Lett.* **1980**, *73*, 1.
(204) Ulitskii, N. I.; Kharlamov, B. M.; Personov, R. I. *Chem. Phys.* **1988**, *722*, 1; **1990**, *141*, 441.
(205) Lengfellner, H.; Gosnell, P. R.; Tkach, R. W.; Sievers, A. J. *Appl. Phys. Lett.* **1983**, *43*, 437.
(206) Beck, K.; Rõska, G.; Bogner, U.; Maier, M. *Solid State Commun.* **1986**, *57*, 703 and references therein.
(207) Bogner, U.; Rõska, G. *J. Lumin.* **1981**, *24/25*, 683.
(208) Angiolillo, P.; Leigh, J. S., Jr.; Vanderkooi, J. M. *Photochem. Photobiol.* **1982**, *36*, 133.
(209) Vanderkooi, J. M.; Moy, J. M.; Maniara, C.; Koloczek, H. *Biochemistry* **1985**, *24*, 7931.
(210) Kolaczek, H.; Fidy, J.; Vanderkooi, J. M. *J. Chem. Phys.* **1987**, *87*, 4388.
(211) Kaposi, A. D.; Vanderkooi, J. M. *Proc. Natl. Acad. Sci. U.S.A.*, in press.
(212) Singh, G. P.; Schink, H. J.; Lohneysen, H.; Parak, F.; Hunklinger, S. *Z. Phys.* **1984**, *B55*, 23.
(213) Yang, I.-S.; Anderson, A. C. *Phys. Rev. B* **1986**, *34*, 2942.
(214) Frauenfelder, H.; Sligar, S. G.; Wolynes, P. G. *Science* **1991**, *254*, 1598.
(215) Reddy, N. R. S.; Small, G. J. *J. Chem. Phys.* **1991**, *94*, 7545.
(216) Reddy, N. R. S.; Small, G. J.; Seibert, M.; Picorel, R. *Chem. Phys. Lett.* **1991**, *181*, 391.
(217) Reddy, N. R. S.; Picorel, R.; Small, G. J. *J. Phys. Chem.* **1992**, *96*, 6458.
(218) Reddy, N. R. S.; Cogdell, R. J.; Zhao, L.; Small, G. J. *Photochem. Photobiol.* **1993**, *57*, 35.
(219) Johnson, S. G.; Small, G. J. *J. Phys. Chem.* **1991**, *95*, 471.
(220) Johnson, S. G.; Tang, D.; Hayes, J. M.; Jankowiak, R.; Tiede, D. M.; Small, G. J. *J. Phys. Chem.* **1989**, *93*, 5953.
(221) Tang, D.; Jankowiak, R.; Small, G. J.; Tiede, D. M. *Chem. Phys.* **1989**, *131*, 99.
(222) Johnson, S. G.; Tang, D.; Jankowiak, R.; Hayes, J. M.; Small, G. J.; Tiede, D. M. *J. Phys. Chem.* **1990**, *94*, 5849.
(223) Tang, D.; Johnson, S. G.; Jankowiak, R.; Hayes, J. M.; Small, G. J.; Tiede, D. M. In *Twenty*-Second *Jerusalem Symposium: Perspectives in Photosynthesis*; Jortner, J., Pullman, B., Eds.; Kluwer Academic Publ.: Boston, 1990; pp 99.
(224) Gillie, J. K.; Lyle, P. A.; Small, G. J. *Photosyn. Res.* **1989**, *22*, 233.
(225) Jankowiak, R.; Tang, D.; Small, G. J. *J. Phys. Chem.* **1989**, *93*, 1649.
(226) Tang, D.; Jankowiak, R.; Seibert, M.; Small, G. J. *Photosyn. Res.* **1990**, *27*, 19.
(227) Tang, D.; Jankowiak, R.; Seibert, M.; Yocum, C. F.; Small, G. J. *J. Phys. Chem.* **1990**, *94*, 6519.
(228) Johnson, S. G.; Small, G. J. *Chem. Phys. Lett.* **1989**, *155*, 371.
(229) van der Laan, H.; Schmidt, Th.; Visschers, R. W.; Visscher, K. J.; van Grondelle, R.; Völker, S. *Chem. Phys. Lett.* **1990**, *170*, 231.
(230) Reddy, N. R. S.; Picorel, R.; Small, G. J. *J. Phys. Chem.* **1992**, *96*, 6458.
(231) Köhler, W.; Friedrich, J.; Fischer, R.; Scheer, H. *J. Chem. Phys.* **1988**, *89*, 871.
(232) Small, G. J.; Hayes, J. M.; Silbey, R. S. *J. Phys. Chem.* **1992**, *96*, 7499.
(233) Fleming, G. R.; Martin, J.-L.; Breton, J. *Nature* **1988**, *333*, 190.
(234) Jortner, J. *Biophys. Acta* **1980**, *594*, 193.
(235) Vos, M. H.; Lambry, J. C.; Robles, S.; Youvan, D. C.; Breton, J.; Martin, J. C. *Proc. Natl. Acad. Sci. U.S.A.* **1991**, *88*, 8885.
(236) Du, M.; Rosenthal, S. J.; Xie, X.; DiMagno, T. J.; Schmidt, M.; Shifter, M.; Hanson, D. K.; Norris, J. R.; Fleming, G. R. *Proc. Natl. Acad. Sci. U.S.A.* **1992**, *89*, 8517.
(237) Kolaczkowski, S. V.; Lyle, P. A.; Small, G. J. In *Structure, Function and Dynamics of the Bacterial Reaction Center*; Breton, J., Ed.; Plenum Press: New York, NY, in press.
(238) Lyle, P. A.; Kolaczkowski, S. V.; Small, G. J. *J. Phys. Chem.*, in press.
(239) Bixon, M.; Jortner, J. *Chem. Phys. Lett.* **1989**, *159*, 17.
(240) Sevian, H. M.; Skinner, J. L. *Theor. Chim. Acta* **1992**, *82*, 29.
(241) Reddy, N. R. S.; Kolaczkowski, S. V.; Small, G. J. *Science* **1992**, *260*, 68.
(242) Robinson, G. W. *Brookhaven Symp. Biol.* **1966**, *19*, 16.
(243) Pearlstein, R. M. In *Photosynthesis: Energy Conversion by Plants and Bacteria*; Govindjee, Ed.; Academic Press: New York, 1986; p 293.
(244) van Grondelle, R. *Biochim. Biophys. Acta* **1985**, *811*, 147.
(245) Pearlstein, R. M.; Zuber, H. In *Antennas and Reaction Centers of Photosynthetic Bacteria*; Michel-Beyerle, M. E., Ed.; Springer-Verlag: Berlin, 1985; Vol. 42, p 53.
(246) Knox, R. S. In *Encyclopedia of Plant Physiology*; Staehelin, L. A., Arntzen, C. J., Eds.; Springer-Verlag: Berlin, 1986; Vol. 19, p 286.
(247) McClure, D. S. In *Electronic Spectra of Molecules and Ions in Crystals*; Academic Press: New York, 1959; p 1.
(248) Craig, D. P.; Walmsley, S. H. In *Physics and Chemistry of Organic Solid State*; Fox, D., Labes, M. M., Weissberg, A., Eds.; John Wiley and Sons Inc.: New York, 1963; Vol. I, p 585.
(249) Craig, D. P.; Walmsley, S. H. *Excitons in Molecular Crystals*; Benjamin: New York, 1968.
(250) Davydov, A. S. *Theory of Molecular Excitons*; Plenum Press: New York, 1971.
(251) Philpott, M. R. *Adv. Chem. Phys.* **1973**, *23*, 227.
(252) Hochstrasser, R. M.; Li, T. Y.; Sung, H. N.; Wessel, J.; Zewail, A. H. *Pure Appl. Chem.* **1974**, *37*, 85.
(253) Ochs, F. W.; Kopelman, R. *J. Chem. Phys.* **1977**, *6665*, 1599.
(254) Port, H.; Rund, D.; Small, G. J.; Yakhot, V. *Chem. Phys.* **1979**, *39*, 175.
(255) Hochstrasser, R. M.; Prasad, P. N. In *Excited States*; Lim, E. C., Ed.; Academic Press: New York, 1974; Vol. 1, p 197.
(256) Dissado, L. A. *Chem. Phys.* **1975**, *8*, 289.
(257) Dissado, L. A.; Brillante, A. *J. Chem. Soc., Faraday Trans. 2* **1977**, *9*, 1262.
(258) Johnson, C. K.; Small, G. J. In *Excited States*; Lim, E. C., Ed.; Academic Press: New York, 1982; Vol. 6, p 97.
(259) Stevenson, S. H.; Connolly, M. A.; Small, G. J. *Chem. Phys.* **1988**, *128*, 157 and references therein.
(260) Matthews, B. W.; Fenna, R. E. *Acc. Chem. Res.* **1980**, *13*, 309.
(261) Tronrud, D. E.; Schmid, M. F.; Matthews, B. W. *J. Mol. Biol.* **1986**, *188*, 443.
(262) van Mourik, F.; Verwijst, R. R.; Mulder, J. N.; van Grondelle, R. *J. Lumin.* **1992**, *53*, 499.
(263) Kramer, H. J. M.; van Grondelle, R.; Hunter, C. M.; Westerhuis, W. H. J.; Amesz, J. *Biochim. Biophys. Acta* **1984**, *765*, 156.
(264) Breton, J.; Nabedryk, E. In *The Light Reactions*; Barber, J., Ed.; Elsevier: Amsterdam, 1987; p 159.
(265) Zuber, H.; Brunisholz, R. N. In *Chlorophylls*; Scheer, H., Ed.; CRC Press: Boca Raton, 1991; p 627.
(266) Pearlstein, R. N. In *Chlorophylls*; Scheer, H., Ed.; CRC Press: Boca Raton, 1991, p 1047.
(267) Bergstrom, H.; Sundstrom, V.; van Grondelle, R.; Akesson, E.; Gillbro, T. *Biochim. Biophys. Acta* **1986**, *852*, 279.
(268) Zuber, H. *Photochem. Photobiol.* **1985**, *42*, 821.
(269) Zuber, H.; Brunisholz, R. N.; Sidler, W. *New Compre. Biochem.* **1987**, *15*, 233.
(270) Scherz, A.; Parson, W. W. *Photosyn. Res.* **1986**, *9*, 21.
(271) Scherz, A.; Rosenbach-Belkin, V. *Proc. Natl. Sci. Acad. U.S.A.* **1989**, *86*, 1505.
(272) Braun, P.; Scherz, A. *Biochemistry* **1991**, *30*, 5177.
(273) van Grondelle, R.; Bergstrom, H.; Sundstrom, V.; Gillbro, T. *Biochim. Biophys. Acta* **1987**, *894*, 313.
(274) Freiberg, A.; Godik, V. I.; Pullerits, T.; Timpmann, K. *Chem. Phys.* **1988**, *128*, 227.
(275) Shreve, A. P.; Trautman, J. K.; Frank, H. A.; Owens, T. G.; Albrecht, A. C. *Biochim. Biophys. Acta* **1991**, *973*, 93.
(276) Bolt, J.; Sauer, K. *Biochim. Biophys. Acta* **1979**, *546*, 54.
(277) Borisov, A. Y.; Gadonas, R. A.; Danielius, R. V.; Piskarskas, A. S.; Razjivin, A. P. *FEBS Lett.* **1982**, *138*, 25.
(278) Kramer, H. J. M.; Pennoyer, J. D.; van Grondelle, R.; Westerhuis, W. H. J.; Neidermann, R. A.; Amesz, J. *Biochim. Biophys. Acta* **1984**, *767*, 335.
(279) Sundstrom, V.; van Grondelle, R.; Bergstrom, H.; Akesson, E.; Gillbro, T. *Biochim. Biophys. Acta* **1986**, *851*, 431.
(280) van Dorssen, R. J.; Hunter, C. N.; van Grondelle, R.; Korenhof, A. H.; Amesz, J. *Biochim. Biophys. Acta* **1988**, *932*, 179.
(281) Zollfrank, J.; Friedrich, J.; Vanderkooi, J. M.; Fidy, J. *Biophys. J.* **1991**, *59*, 305; *J. Chem. Phys.* **1991**, *95*, 3134.
(282) Buchenau, U.; Prager, M.; Nucker, N.; Dianoux, A. J.; Ahmad, N.; Phillips, W. A. *Phys. Rev. B* **1986**, *34*, 5665.
(283) Buchenau, U.; Zhou, H. M.; Nucker, N.; Gilroy, K. S.; Phillips, W. A. *Phys. Rev. Lett.* **1988**, *60*, 1318.
(284) Kim, W.-H.; Hayes, J. M.; Small, G. J. *Chem. Phys. Lett.*, in press.
(285) Hallbrucker, A.; Mayer, E.; Johari, G. P. *Phil. Mag. B.* **1989**, *60*, 179.
(286) Klement, W.; Willens, R. H.; Duwez, P. *Nature* **1960**, *187*, 169.
(287) Elliot, S. R. *Physics of Amorphous Materials*; Longman: London, 1983.